UNIVERSIDADE DE LISBOA

INSTITUTO SUPERIOR TÉCNICO

Design and Modeling of Therapeutic Ophthalmic Lenses for Controlled Drug Release

Andreia Filipa Relvas Pimenta

Supervisor: Doctor Rogério Anacleto Cordeiro Colaço

Co-supervisor: Doctor Ana Paula Valagão Amadeu do Serro

Thesis specifically prepared to obtain the PhD Degree in Bioengineering

Draft

December 2017

Abstract

One of the most often used methods of ocular medications delivery to the eye are topical drops. Nonetheless, patient compliance and administration are frequently problematic. Eye drops show low bioavailability and may cause side effects due to systemic absorption.

Therefore, the aim of the present thesis was to contribute to the development of alternative ocular drug delivery systems. The focus was kept on hydrogel contact and intraocular lenses as the choice platforms, since they are placed *in situ* and present worldwide acceptance for correction of refractive errors. Different aspects on the design of the drug eluting lenses were taken into account, for instance: the interactions for each particular pair drug/hydrogel; different strategies to increase the duration of release such as surface coating or hydrogel composition modifications; or the hydrodynamic *in vivo* environment were the lenses are placed.

Results show that hydrodynamic conditions, in particular those of the tear film, can influence the release kinetics resulting in slower and more gradual release when compare to the static conditions commonly used in laboratory experiments. Moreover, the interactions between a drug and a certain material greatly influence the release kinetics, which can be described through the partition and effective diffusivity coefficients. The correct assessment of these coefficients is essential for the construction of good mathematical models. Mathematical modeling was used in the present thesis as a tool for the design of lenses with tailored *in vivo* drug concentration profiles. The most promising system studied was a HEMA/MMA hydrogel loaded with an antibiotic and a nonsteroidal anti-inflammatory. In detail, the hydrogel was sequentially loaded with moxifloxacin and diclofenac, and presented the capability of releasing simultaneously both drugs with favorable kinetics. The drugs concentrations in the aqueous humor when released from an IOL made with this hydrogel were estimated. Effective concentrations are expected to be maintained *in vivo* up to 3 weeks for the antibiotic and over a period of time higher than 3 weeks for the anti-inflammatory.

Resumo

Os fármacos oftálmicos são usualmente administrados sob forma de colírios. Contudo, a administração frequente dos colírios e consequente adesão do paciente ao tratamento são muitas vezes problemáticas. Estas formulações apresentam também baixa biodisponibilidade e podem resultar em efeitos sistémicos indesejáveis.

A presente tese tem como objectivo o desenvolvimento de sistemas alternativos de libertação de fármacos oftálmicos baseados em lentes de contacto e lentes intra-oculares. Estes dispositivos de hidrogel foram escolhidos como veículos de libertação dado que são colocadas *in situ* e apresentam uma larga aceitação como correctores de erros refractivos. Diferentes aspetos do *design* destes sistemas de libertação foram investigados, tais como: as interacções entre cada fármaco e hidrogel, diferentes estratégias para o prolongamento do tempo de libertação (revestimentos superficiais e modificações na composição do hidrogel) e a influência do ambiente hidrodinâmico onde as lentes são colocadas.

Os resultados mostram que em condições hidrodinâmicas, especialmente do filme lacrimal, a libertação dos fármacos pode ocorrer de forma mais lenta e gradual do que nas condições estáticas habitualmente usadas em estudos laboratoriais, aproximando-se do que ocorre *in vivo*. Mais, verificou-se que as interacções entre o fármaco e o hidrogel influenciam a cinética de libertação, que pode ser descrita através dos coeficientes de partição e de difusividade efectiva. A correcta aferição destes coeficientes é essencial na construção de bons modelos matemáticos para representação do sistema de libertação. Estes modelos foram utilizados como ferramenta auxiliar no *design* de lentes com perfis de libertação adequados às aplicações desejadas. O sistema que apresentou resultados mais promissores foi obtido com um hidrogel baseado em hidroxietil-metacrilato (HEMA) e metil-metacrilato (MMA) para a libertação simultânea de um antibiótico (moxifloxacina, MFX) e de um anti-inflamatório não-esteroide (diclofenac, DCF). As concentrações no humor aquoso de MFX e DCF libertados a partir de uma lente intra-ocular fabricada com este hidrogel foram estimadas através de um modelo matemático. Concentrações efectivas de MFX e DCF foram estimadas por um período de 3 semanas para o antibiótico e um período superior a 3 semanas para o anti-inflamatório.

Keywords

CONTROLLED DRUG RELEASE

CONTACT LENSES

INTRAOCULAR LENSES

MATHEMATICAL MODELING

THERAPY/PROPHYLAXIS FOR OCULAR DISEASES

Palavras Chave

LIBERTAÇÃO CONTROLADA DE FÁRMACOS

LENTES DE CONTACTO

LENTES INTRAOCULARES

MODELAÇÃO MATEMÁTICA

TERAPIA/PROFILAXIA PARA DOENÇAS OCULARES

Acknowledgments

This dissertation gathers the results obtained during four years, but it would be an incomplete work if I did not began by expressing my gratitude to those that contributed to its improvement and completion.

First and foremost, I am grateful to my supervisor Doctor Rogério Colaço and my co-supervisor Doctor Ana Paula Serro for accepting me as their student, and for the guidance and support that has allowed me to develop as a researcher over the last years. I thank them for the trust, motivation, brainstorming and corrections provided during this journey, always accompanied with kindness and patience.

I would like to express my gratitude to Doctor Benilde Saramago for allowing me to work in her laboratory, but, most important, for always being available to share ideas, for the help throughout this work, and for being an example of work ethic, passion, and commitment to research. To Doctor José Mata I would like to thank his kindness, advices, and most appreciated technical support when it was most needed.

I would like to give special thanks to Doctor Anuj Chauhan, from the Chemical Engineer Department at the University of Florida, for welcoming me in his group and sharing his time and knowledge, a fruitful contribution for the final result of this dissertation. Doctor Anuj and all the Chauhan's Lab colleagues are among the top reasons for which I will always cherish the time spent in Gainesville.

A significant part of the work presented in this dissertation was developed within the scope of a collaborative M-ERA.NET ("Surflenses") project and a *thank you* is due to all the members of this project with whom I have had the privilege of working alongside. Special thanks to Ana Paula Vieira, Doctor António Jorge Guiomar and Doctor Helena Gil from University of Coimbra, to Doctor Dimitriya Bozukova from PhysIOL S.a., and last, but not least, Dr. Helena Filipe.

My gratitude to Doctor Helena Barroso from Instituto Superior de Ciências da Saúde Egas Moniz and all the laboratory technicians for the help during the microbiology

INDEX

List of Figures

List of Tables

List of Abbreviations

26Y	Hydrophilic acrylic material
AC	Anterior chamber
AFM	Atomic force microscopy
AIBN	2,20-azobis(2-methylpropionitrile)
AMD	Age-related macular degeneration
AMPS	2-acrylamido-2-methylpropane sulfonic acid
CDDS	Controlled drug delivery system
CEC	Corneal endothelial cells
CHX	Chlorhexidine
CL	Cross-linker
CME	Cystoid macular edema
CMV	Cytomegalovirus
DAA	Diacetone acrylamide
DCF	Diclofenac sodium salt
DD	Distilled and deionized water
DEF50	Definite50-Contamac®
DMA	n,n-dimethyl acrylamide
DNA	Deoxyribonucleic acid
ECCE	Extracapsular cataract extraction
EGDMA	Ethylene glycol dimethacrylate
EMA	European Medicines Agency
EWC	Equilibrium water content
FBS	Fetal bovine serum
FDA	Food and Drug Administration
GF	Hydrophobic acrylic glistening-free material
HBSS	Hank's balanced salt solution
HEMA	2-Hydroxyethyl methacrylate
HPLC	High performance liquid chromatograph
IC_{50}	Half maximal inhibitory concentration
IOL	Intraocular lens
KETO	Ketorolac tromethamine
LVF	Levofloxacin
MAA	Methacrylic acid
MEM	Minimum Essential Medium
MFX	Moxifloxacin hydrochloride
MH	Muller Hinton
MIC	Minimum inhibitory concentration
MMA	Methyl-methacrylate
mPDMS	Monofunctional polydimethylsiloxane
NCVE	n-carboxyvinyl ester
NMR	Nuclear Magnetic Resonance
NSAID	Nonsteroidal anti-inflammatory drug
NVP	n-vinyl pyrrolidone
PBS	Phosphate buffered saline
PBVC	Poly(dimethysiloxy) di (silylbutanol) bis (vinyl carbamate)
PC	Posterior chamber
PCO	Posterior lens capsule opacification

PDMAAm	Poly(N,N-dimethylacrylamide)
PGSE-NMR	Pulsed Gradient Spin-Echo
PHEMA	Poly 2-hydroxyethylmethacrylate
PMMA	Polymethylmethacrylate
POE	Postoperative endophthalmitis
PVP	Poly-(vinyl pyrrolidone)
SBMA	[2-(methacryloyloxy)ethyl]dimethyl-(3-sulfopropyl)ammonium hydroxide
SC	Swelling capacity
SCL	Soft contact lens
SEM	Scanning electron microscopy
STE	Stimulated echo sequence
TAC	Total absorption capacity
TPVC	Tris-(trimethyl siloxysilyl) propylvinyl carbamate
TRIS	3-tris(trimethylsilyloxy)silylpropyl2-methylprop-2-enoate
VEGF	Vascular endothelial growth factor
VP	1-vinyl-2-pyrrolidone

List of Symbols

A_{cornea}	Lateral corneal area
A_{IOL}	Lateral intraocular lens area
$A_{surface}$	Lateral lens area
C	Drug concentration
C_0	Initial drug concentration in the loading solution
C_{aq}	Drug concentration in the aqueous humor
C_F	Flory characteristic ratio
$C_{f,l}$	Equilibrium concentration in the loading solution
$C_{f,r}$	Final concentration of the release medium
C_{gel}	Hydrogel equilibrium drug concentration
C_i	Initial drug concentration in the lens
C_{in}	Drug concentration in the inner-loaded layer
C_{out}	Drug concentration in the outer layers
C_r	Concentration in the release medium
C_{sol}	Aqueous solution equilibrium drug concentration
$C_{MAA^-}^{gel}$	Molar concentration of charged MAA
C_{NaCl}^{bulk}	NaCl molar concentration
D	Diffusion coefficient
D_0	Bulk aqueous diffusion coefficients
D_e	Effective diffusion coefficient
D_{e_in}	Effective diffusion coefficient in the inner-loaded layer
D_{e_out}	Effective diffusion coefficient in the outer layers
E	Enhancement factor
E	Young's modulus
E_{ad}	Specific solute adsorption enhancement factor
E_{el}	Electrostatic interaction enhancement factor
E_{HS}	Hard-sphere size exclusion enhancement factor
F	Faraday constant
g	Gradient amplitude
$G´(0)$	Zero-frequency shear storage modulus
h	Lens half-thickness
I	Signal intensity
$I0$	Intensity in the absence of gradient pulse
j	Drug mass flux
K	Partition coeficient
k_B	Boltzmann constant
K_{cornea}	Corneal permeability
KH	Henry's constant
l	Coating layer thickness
$M(\infty)$	Total amount of drug released
$M(t)$	Amount of drug release at time t
M_r	Molecular weight of a repeating unit
M_W	Molecular weight
n	Number of moles of specifically adsorbed solute per unit polymer volume in the gel
pKa	Acid dissociation constant at logarithmic scale
q	Renovation rate of the aqueous humor

R	Gas constant
R_a	Average roughness
r_f	Radius of the polymer fiber
R_s	Hydrodynamic radius of the solute
STDV	Standard deviation
T	Temperature
t	Time
V_{aq}	Volume of the aqueous humor
V_{gel}	Volume of the hydrated sample
V_{load}	Loading volume
V_r	Volume of the release medium
$W(\infty)$	Hydrated equilibrium weight
W_0	Dry weight
w_{MMA-}	Copolymer weight fraction
y	Space coordinate
Z	Charge number of the solute
α	Experimentally adjustable mass transport related parameter
$\langle \xi \rangle$	Average mesh size
γ	Gyromagnetic ratio of the nucleus
δ	Duration of the applied NMR gradient
Δ	Diffusion time
$\Delta\phi_{don}$	Donnan potential
$\Delta\phi_{don}^{B}$	Donnan potentials at the interfaces of the hydrogel with the salt bridge
$\Delta\phi_{don}^{S}$	Donnan potentials at the interfaces of the hydrogel with the salt solution
$\Delta\phi_{liq}^{m}$	Liquid junction potentials of the hydrogel
$\Delta\phi_{liq}^{s}$	Liquid junction potentials of the solution
η	Viscosity
θ	Water volume fraction
ρ	Density of the dry polymer
φ	Polymer volume fraction
ψ	Donnan electric potential difference

1 State of the art

Table of Contents

1.1 Controlled drug delivery

Controlled drug delivery systems (CDDS) history began in the 1950's with the introduction by Smith Kline & French of the first formulation able to control the release rate of a drug [1]. Before 1950, all drugs were made into pill or capsule formulations that released the loaded drug immediately upon contact with water. The first generation of CDDS (1950 – 1980) were based mainly in dissolution and diffusion controlled mechanisms. Oral and transdermal dosage forms were the most explored routes of delivery during this first period of development of CDDS, where the basic foundations of controlled release were built. The second generation of CDDS (1980 – 2010) focused in the development of *smart* delivery systems, responsive to the surrounding environment. Triggers such pH, temperature or glucose levels were explored. Protein and peptide delivery were also introduced during this period. In the last decade of the so called second generation (2000 – 2010), attention was focused on the development of nanoscale approaches. The third generation of CDDS is expected to center the spotlight on overcoming the challenges presented by the biological environment, such as crossing of biological barriers or microenvironment navigation to reach target tissues, which are still not fully predictable or even understood mechanisms. [1, 2]

In the last 60 years, CDDS assumed different forms such as drug formulations or devices (microchips, biosensors and microfluidics) to deliver the drug. All aimed to achieve the primary goal of controlled release, "to enable the introduction of a therapeutic substance in the body and improve its efficacy and safety by controlling the rate, time, and place of release in the body" [3]. In opposition to traditional drug delivery systems, with a CDDS, release kinetics, toxicity or therapeutic level can be adjusted. In traditional systems, the concentration of drug reaches a maximum level and decreases to a low value sometime after administration (see Figure 1.1). It can be challenging to maintain concentration of drug above the therapeutic level without frequent administration, which could lead, if not properly monitored, to concentrations above the toxic level. [3] With traditional delivery it can also be difficult to attain the same drug concentrations for different administration points in time (see Figure 1.1).
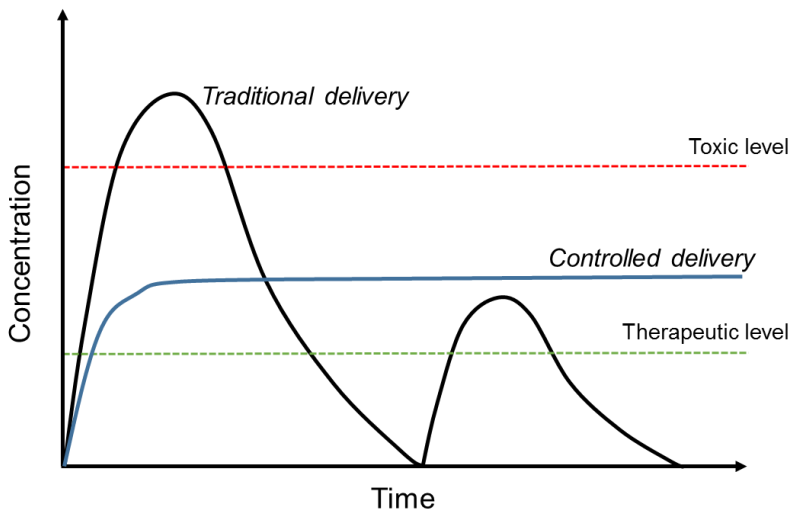
Figure 1.1 - Comparison between traditional and controlled drug release.

Accordingly with the biological application of the CDDS, different mechanisms to control the release can be chosen. Among these mechanisms, some of the most used are dissolution, diffusion, osmosis, swelling or erosion. In diffusion controlled systems, delivery is driven by the gradient of concentration between the inside of the device and the exterior environment. The diffusion coefficient (*D*), or diffusivity, is the parameter that describes the ability of the drug to diffuse from the higher drug concentration region to a lower concentration region. Fick's second law is widely used to describe the diffusion mechanism if diffusivity is independent of time, space, and drug concentration (*C*) [4]:

$$\frac{dC}{dt} = D \left(\frac{\partial^2 C}{dy^2} \right) \qquad \textbf{Equation 1.1}$$

This equation can be solved with adequate initial and boundary conditions.

Diffusion controlled drug release in polymers can be achieved through the polymer matrix, for monolithic systems, or through the polymer membrane for reservoir systems. Monolithic and reservoir systems can be further divided in two categories. Monolithic systems where the initial drug loading is below drug solubility limit = all drug is dissolved (solution), or where the initial drug loading is above the solubility limit = drug is partially dissolved and the remaining is in the form of solid drug crystals and/or amorphous particles (dispersion). Analogously, reservoir systems can have drug concentration in the

reservoir below its solubility limit, with non-constant activity, and have drug molecules in non-dissolved state, with constant activity (see Figure 1.2) [5].
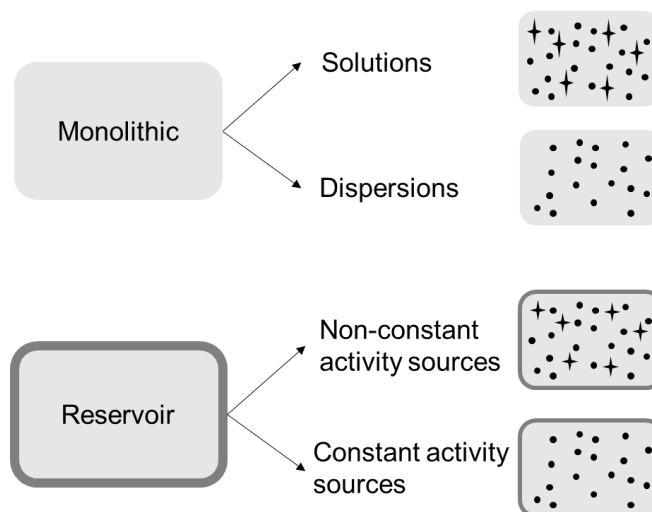
Figure 1.2 - Schematic classification of diffusion-controlled drug delivery systems. Circles represent individual drug molecules, crosses drug crystals and/or amorphous aggregates. Adapted from [6].

Swelling is defined as the uptake of water by a polymer system with consequent increase in volume. In controlled release through swelling the matrix swelling rate is slow when compared to the drug diffusivity and is, therefore, the controlling mechanism. In osmosis controlled systems, the drug is confined in a polymer reservoir (with a small orifice for drug diffusion) that allows water diffusion, but not drug diffusion. The rate of drug release is dependent on the osmotic pressure generated within the polymer reservoir upon contact with water. Erodible and degradable systems are used mainly for implantable or injectable devices, since they do not require retrieval after drug is fully released. Erosion occurs when components of the biological release medium attack chemical bonds in the polymer matrix [7].

1.2 Ocular drug delivery routes

The eye is an organ which detects and converts light into electro-chemical impulses in neurons. It is commonly divided into two segments: anterior and posterior. The anterior segment is constituted by tissues such as the cornea, the conjunctiva, the aqueous humor, the iris, the ciliary body and the lens, and occupies approximately one-third of the total

eye's volume. The remaining portion is occupied by the posterior segment which includes the sclera, the choroid, the retinal pigment epithelium, the neural retina, the optic nerve and the vitreous humor (see Figure 1.3). Most of these constituent parts allow to block external aggressions through different barrier layers, both static (different corneal, scleral and retinal layers including blood aqueous and blood–retinal barriers) and dynamic (choroidal and conjunctival blood flow, lymphatic clearance and tear dilution) [8, 9].
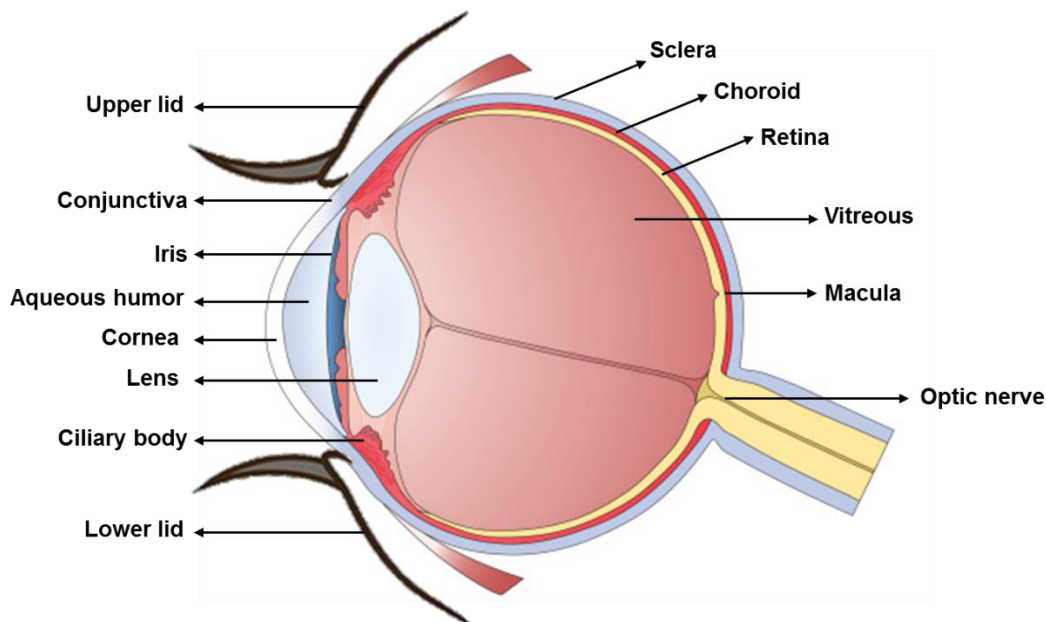
Figure 1.3 – Schematic representation of the most relevant eye constituents.

Due to these restrictions, delivery of drugs to specific ocular tissues has been one of major challenges for controlled drug release research. Four main routes can be used to deliver pharmaceuticals to the eye: topical, intravitreal, periocular and systemic [10].

Topical application of drugs is the most widely use route for ocular drug delivery [11]. Topical administration of pharmaceuticals is commonly used for medication of the anterior segment of the eye since, to reach deeper tissues, drug molecules must permeate the corneal barrier. The cornea is an avascular, thin, transparent and highly innervated tissue that helps to protect the eye from dust, germs, and other external aggressions. Histologically, the cornea is composed of three different layers: the corneal epithelium, the stroma, and the endothelium separated, by the Descemet's membrane and the Bowman's layer (see Figure 1.4) [12, 13]. Due to a dual nature, lipophilic and hydrophilic,

the cornea is very resistant to drug transport. Permeability of drugs through the cornea route will depend on the drug's permeability through its component layers. After permeation of the cornea, drug molecules reach the aqueous chamber and intraocular tissues. Only a small amount of drug is able to reach this point, and even an inferior amount is able to reach posterior tissues: only 1 to 5% of the delivered drug [14-16].
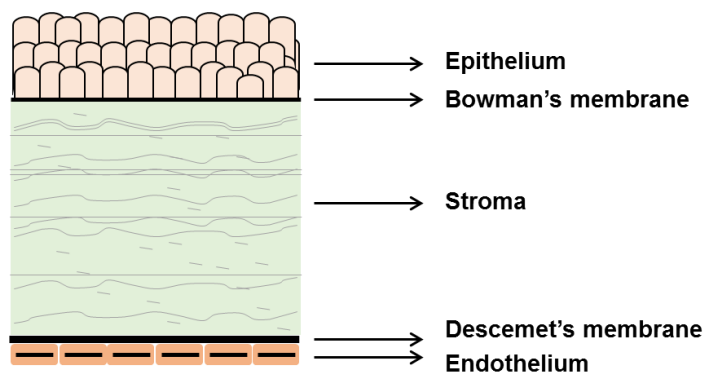
Figure 1.4 – Schematic representation of the corneal layers. Adapted from [9].

Intravitreal injections involve the direct delivery of pharmaceuticals to the posterior segment, providing high drug concentration, and allowing direct access of the drug molecules to the retina and the vitreous. This route presents major disadvantages, especially when frequent administration of drugs is required, since it can lead do retinal detachment, endophthalmitis or increased intraocular pressure [10, 11].

Periocular route is considered the least painful and the most efficient route of drug delivery to the posterior segment, and mainly involves retrobulbar, peribulbar, subtenon and subconjunctival deliver. Through this route, drug molecules are deposited against the external surface of the sclera, hence decreasing the risk of endophthalmitis, and retinal damage associated with the intravitreal route of administration. The sclera is also less resistant to permeation of molecules compared to the cornea [17].

Finally, drug delivery can also be achieved through systemic administration, but the blood–aqueous and blood–retinal barriers present themselves as the major obstacles for anterior segment, and posterior segment ocular drug delivery, respectively (only 1-2% reaches vitreous cavity) [17]. Towards a more efficient systemic delivery, specific oral or

intravenous targeting systems are needed [11, 18]. Intracameral injections and suprachoroidal devices are also used for drug delivery to the eye. In Figure 1.5, a schematic representation of the different drug delivery routes to the eye is shown.
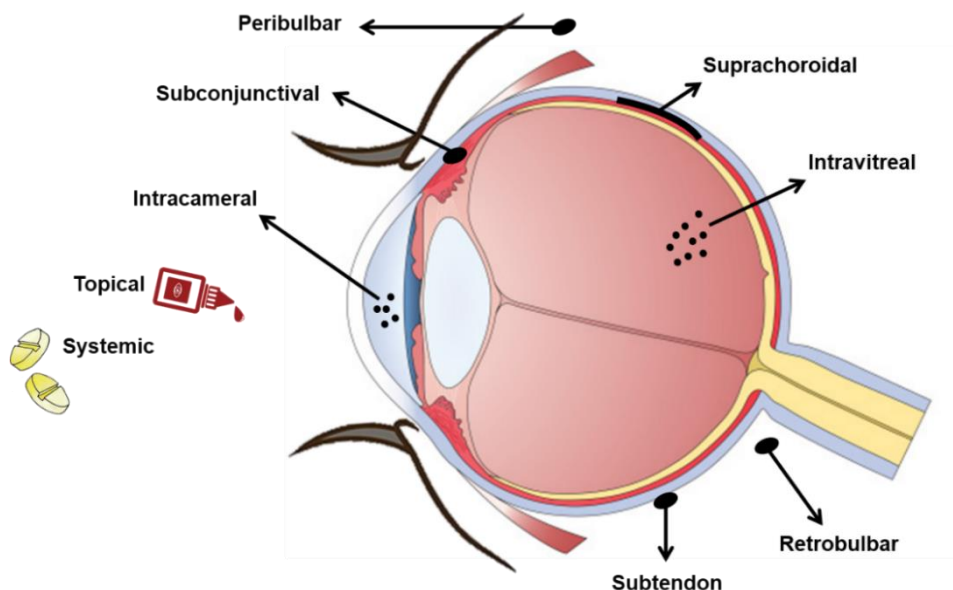
Figure 1.5 – Schematic representation of the drug delivery routes to the eye. Adapted from [10].

1.2.1 Eye disorders and treatment

Topical administration of drug is, as mentioned previously, the most straightforward approach to delivery medication to the eye. Diverse anterior segment conditions as dry eye disease, glaucoma, post-eye-surgery therapy or bacterial keratitis relay on this delivery route to achieve effective regimen, despite the low bioavailability of the drugs administered through eye drop instillations.

Keratitis, which can have fungal, bacterial or viral origin, is an inflammation of the cornea. Bacterial keratitis is characterized by its rapid progression (corneal destruction may be complete in 24-48 hours) and is generally caused by Gram-positive bacteria: *S. aureus*, *S. epidermidis* and several *Streptococcus* and *Bacillus* spp. Gram-negative bacteria such as *P. aeruginosa* or *S. marcescens* have been also associated to keratitis

[19]. Treatment of bacterial keratitis consists in topical application of antibiotic containing eye drops.

Dry eye disease manifests itself through symptoms such as dryness, burning, and irritation of the eye, resulting in increasing discomfort and sensitivity to bright light. Usually mild irritation associated to dry eye does not induce long-term effects. However, if left untreated it can become severe, with complications such as impaired vision [20, 21]. Depending on the population looked at, the incidence of dry eye range from 5 to 34% [22]. A high incidence rate justifies the demand for an effective treatment to dry eye, which, again, relies mainly in topical administration. Moderate cases can be treated with application of artificial tears every few hours, providing relief to patients with aqueous tear deficiency, but do not prevent the underlying inflammation or reserve conjunctival squamous metaplasia in chronic dry eye cases [23]. Inflammation can be tackled, for instance, with combinations of artificial tears, short-term steroids, and cyclosporine A [23-25].

Endophthalmitis is an intraocular infection that occurs most commonly as a complication of intraocular surgery, and often causes severe visual impairment or even the loss of the eye. Postoperative endophthalmitis (POE) incidence has been reported to range from 0.04 to 0.2% in the last decade [26-28]. Topical administration of antibiotics constitutes the most used form of prevention for endophthalmitis. It offers numerous advantages, namely ease of procedure and patient compliance. However, topical administration presents low bioavailability as mention previously. A cost-effectiveness analysis of POE prophylaxis reported that topical antibiotic were among the most expensive options for prophylaxis, compared with intracameral or subconjunctival delivery routes [29].

Cystoid macular edema (CME) is a painless disorder in which swelling develops in the macula. As the swelling increases, multiple fluid filled cysts develop in the macula, causing vision loss and distortion. Inflammation after cataract removal surgery is one of the mechanisms responsible for the development of CME [30]. Published studies suggest benefits to early visual recovery of topical application of nonsteroidal anti-inflammatory drugs (NSAIDs), and also in the decrease of likelihood of postoperative CME. Kessel and

co-workers performed a systematic literature search in four databases to identify randomized trials published from 1996 till 2014 comparing topical steroids with topical NSAIDs in controlling inflammation and preventing CME in patients undergoing cataract extraction. They found low to moderate evidence that topical NSAIDs are more effective in controlling postoperative inflammation after cataract surgery [31].

Glaucoma is a multifactorial optic neuropathy that can result in vision loss due to damage to the optic nerve, and it is the most frequent cause of irreversible blindness worldwide [32]. The two main types of glaucoma are open-angle and angle-closure, marked by an increase in intraocular pressure, and characterized by progressive destruction of retinal ganglion cells and their axons [33]. Glaucoma cannot be exclusively classified as an anterior segment disease, but medication aimed to lower intraocular pressure is usually applied via topical administration. Laser or surgical procedures are only seen as final options. Delivery to the eye of carbonic anhydrases, prostaglandins or beta-blockers can lead to intraocular pressure reduction, and alleviation of the disease process [33-35]. A major challenge in glaucoma treatment, especially when multiple drops are prescribed, is the patient compliance. Increase in the number of drop bottles to a patient's treatment regimen has been demonstrated to affect negatively the patient adherence to the treatment [36]. New alternatives for drug delivery to the eye, with the possibility of multiple drugs being delivered simultaneously, could benefit patient's compliance, and overall treatment results.

Topical route is not efficient for treatment of disorders in the back of the eye, since drug molecules are not able to permeate to deep ocular tissues. Unfortunately, the most direct methods to deliver drug to this eye region rely on invasive routes such as injections, as exposed in section 1.2, and subjecting the patient to periodical applications. Commercially available drug delivery technologies to treat the back of the eye are mainly based in the intravitreal route, either in the form of implants or in the form of solutions.

Wet age-related macular degeneration (AMD) can lead to irreversible vision loss, and occurs when the macula, the small center portion of the retina, deteriorates due to abnormal blood vessels growth from the underneath choroid. Anti-angiogenic agents are used to reduce the level of a protein called vascular endothelial growth factor (VEGF) that

stimulates blood vessels growth in the retina and the macula, leading to the development of wet AMD [37]. The management of cytomegalovirus (CMV) retinitis, an acquired immunodeficiency syndrome related opportunistic infection that can lead to blindness as also be attained through the use of non-degradable vitreal implants. Implants have also been used to deliver corticosteroids for management of posterior uveitis, an inflammation of the eye middle layer between the retina and the sclera named uvea [38].

Eye disorders/conditions presented in this section demand, in most cases, more effective vehicles of drug deliver to the eye. Conventional routes are able to achieve an immediate solution, but present heavy drawbacks such as dependence on patient compliance, invasive methods, and maintenance of therapeutic concentrations through high dose frequency or side effects consequence of systemic drug absorption. Patient's quality of life, therapeutic safety, and even the treatment economic costs could positively benefit from the introduction of local and controlled drug release systems.

1.2.2 Approved drugs for ophthalmology

In this section, a synthesis of the commercially available drugs for eye disorders treatment is presented.

Ophthalmologists prescribe a wide range of compounds currently approved by regulatory agencies such as the FDA (Food and Drug Administration, USA) or the EMA (European Medicines Agency). Topical formulations are prepared and delivered to the eye surface as solutions, emulsions, ointments or suspensions. In this work, we chose to focus in drugs already approved and commercialized, and study their potential to be delivered to the eye through therapeutic ophthalmic lenses. In Table 1.1, a list of antibiotics usually prescribed is presented.

Table 1.1 – Representative list of antibiotics prescribed for ophthalmic treatment [39-41].

Class	Drug	Brand name	Manufacturer	Use
Aminoglycosides	Tobramycin	Tobrex®	Alcon, and generic	Conjunctival or corneal bacterial infections
	Gentamicin	Garamycin®	Perrigo, and generic	
Flouroquinolones	Besifloxacin	Besivance®	Bausch + Lomb	Bacterial conjunctivitis
	Ciprofloxacin	Ciloxan®	Alcon, and generic	Bacterial conjunctivitis Corneal ulcers
	Gatifloxacin	Zymar™	Allergan	Bacterial conjunctivitis
	Levofloxacin	Quixin® and Iquix®	Vistakon	Bacterial conjunctivitis Corneal ulcers
	Moxifloxacin	Vigamox™	Alcon	Bacterial conjunctivitis
	Ofloxacin	Ocuflox®	Allergan, and generic	Bacterial conjunctivitis Corneal ulcers
Polymyxin B combinations	Polymyxin B /trimethoprim	Polytrim®	Allergan, and generic	Bacterial conjunctivitis Blepharoconjunctivitis Superficial ocular infections
	Polymyxin B /bacitracin	Polysporin®	Generic	Bacterial conjunctivits
	Polymycin B /neomycin /gramicidin	Neosporin®	Generic	Bacterial conjunctivitis Superficial ocular infections
Others	Azithromycin	AzaSite®	Akorn	Bacterial conjunctivitis
	Erythromycin	Ilotycin®	Perrigo, and generic	Conjunctival or corneal bacterial infections
	Bacitracin	Bacitracin	Perrigo	Bacterial infections

Among the antibiotics presented in Table 1.1, fluoroquinolones are the broad spectrum antibiotics most widely used for treatment of ocular infections, such as keratitis, and in perioperative prophylaxis in ophthalmic surgery [42]. The first quinolone was developed in the 1960's and since then further compounds, which have been divided into "generations", were synthesized and commercialized. Briefly, quinolones exert their antibacterial effect by prevention of bacterial DNA replication through inhibition of DNA unwinding events, and can be both bacteriostatic and bactericidal [43]. The most recent generation is the 4th, which includes moxifloxacin. These 4th generation fluoroquinolones

are characterized by an excellent aqueous penetration [44, 45] and higher activity against *S. aureus* [46]. Fluoroquinolones can be also prescribed in cases of persistent bacterial conjunctivitis.

Nonsteroidal anti-inflammatories use within nonsurgical eye care is limited, being used in perioperative rather than in primary eye care [39]. NSAIDs act as inhibitors in the synthetic pathway to the production of prostaglandins, one of the more significant contributors to the inflammatory process [47]. Topical NSAIDs are generally used as post-cataract surgery care for prevention of endophthalmitis, reduction of pain and swelling. Steroid anti-inflammatories are regarded as more effective treatment of ocular surface and intraocular inflammation [39]. In Table 1.2, a list of ophthalmic anti-inflammatories is presented.

Table 1.2 - Representative list of nonsteroidal and steroidal anti-inflammatories prescribed for ophthalmic treatments [39-41].

Nonsteroidal anti-inflammatories			
Drug	**Brand name**	**Manufacturer**	**Use**
Ketorolac tromethamine	Acular® LS	Allergan, and generic	Irritation due to allergies Swelling and pain after cataract surgery
	Acuvail®	Allergan	Swelling, pain, and burning or stinging after cataract surgery
Bromfenac	BromSite®	Sun Pharma	Prevent ocular pain after cataract surgery
	Prolensa®	Bausch + Lomb	Prevent inflammation and reduction of ocular pain after cataract surgery
Nepafenac	Ilevro®	Alcon	Swelling and pain after cataract surgery
	Nevanac®	Alcon	Prevent inflammation and reduction of ocular pain after cataract surgery
Diclofenac sodium	Voltaren®	Novartis, and generic	Swelling and pain after cataract surgery

Steroidal anti-inflammatories			
Drug	**Brand name**	**Manufacturer**	**Use**
Prednisolone acetate	Pred forte®	Allergan, and generic	Steroid responsive inflammation of the palpebral and bulbar conjunctiva, cornea, and anterior segment of the globe

Rimexolone	Vexol®	Alcon	Postoperative inflammation following ocular surgery and in the treatment of anterior uveitis
Loteprednol etabonate	Lotemax®	Bausch + Lomb	Swelling and irritation
Fluorometholone acetate	Flarex®	Alcon	Steroid responsive inflammation of the palpebral and bulbar conjunctiva, cornea, and anterior segment of the globe
Dexamethasone	OcuDex®	Generic	Inflammation caused by infections, injury, surgery, or other conditions.
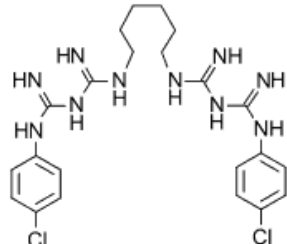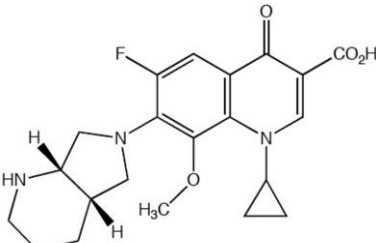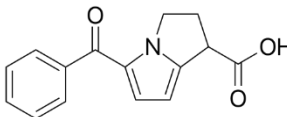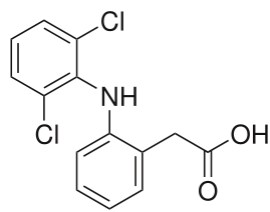
1.2.2.1 Ophthalmic drugs used in this thesis

Different drugs were used in this thesis, with main focus given to fluoroquinolones and nonsteroidal anti-inflammatory drugs.

Moxifloxacin is a 4th generation fluoroquinolone, whose molecular formula is $C_{21}H_{24}FN_3O_4$, with a molecular weight of 401.4 g.mol^{-1}. Moxifloxacin hydrochloride is used in ophthalmic formulations due to the higher aqueous solubility (24 mg.mL^{-1}) when compare to moxifloxacin [48]. As almost all fluoroquinolones, its zwitterionic form predominates at physiological pH (pKa$_1$=5.69, pKa$_2$=9.42). Levofloxacin is a 3th generation fluoroquinolone, whose molecular formula is $C_{18}H_{20}FN_3O_4$, and has a molecular weight of 361.4 g.mol^{-1} (pKa$_1$=6.24, pKa$_2$=8.74) and is soluble in water (40.4 mg.mL^{-1}) [49]. Both moxifloxacin and levofloxacin present a physical appearance of a yellowish white to yellow powder. Chlorhexidine is used as antibacterial agent and topical disinfectant [50] and has a molecular weight of 505.4 g.mol^{-1} and has the molecular formula $C_{22}H_{30}Cl_2N_{10}$, with more stable forms of salts e.g., the dihydrochloride, diacetate, and digluconate [51]. However, at physiological pH the salts dissociate and the cationic chlorhexidine ion is released (diacetate salt pKa=10.52). Diclofenac is a nonsteroidal, anti-inflammatory drug with analgesic activity [52], whose molecular formula is $C_{14}H_{11}Cl_2NO_2$, and has a molecular weight of 296.1 g.mol^{-1}. The sodium salt form is used in ophthalmic formulations, and has a reported solubility in water of 50 mg.mL^{-1} (pKa=4.15) [53]. The second NSAID used in this work was ketorolac with the molecular formula $C_{15}H_{13}NO_3$ and molecular weight of 255.3 g.mol^{-1}. Tromethamine salt is used in ophthalmic formulations with a reported solubility in water of 500 mg.mL^{-11} (pKa=3.54) [54]. NSAIDs exert their

action via inhibition of prostaglandin synthesis by inhibiting cyclooxygenase-1 (COX-1) and cyclooxygenase-2 (COX-2) [55]. In Table 1.3, the molecular structures of the drugs are presented.

Table 1.3 – Molecular structures of the drugs used in this thesis.

Drug	Structure
Chlorohexidine	
Moxifloxacin	
Levofloxacin	
Ketorolac	
Diclofenac	

1.3 The origin and evolution ophthalmic lenses

In this section, an outline over the history of contact and intraocular lenses (IOLs) will be given, followed by an overview of the research over ocular drug delivery by ophthalmic

lenses. Finally, the main challenges faced by ocular drug delivery through ophthalmic lenses will be briefly discussed, as the opportunities ahead for an innovative product as those herein studied.

The first contact lens was developed by Adolf Eugene Fick in 1888. According to his report "consists of a thin glass shell, bounded by concentric and parallel spherical segments. It is placed upon the eye, and the interspace between it and the eye ball is filled with a liquid having the same refractive index as the cornea." [56]. Eugene Kalt and August Müller, contemporaneous to Adolf Eugene Fick, also developed the so called "scleral" lenses, since they covered the entire front surface of the eye. These first lenses were made of glass and failed to be tolerated for more than a few hours [57]. In 1936, William Feinbloom introduced the first lenses made of a combination of glass and a clear plastic, polymethylmethacrylate (PMMA) [58]. PMMA is relatively impermeable to oxygen but presents advantages such as being lightweight, especially when compared to glass lenses, and more durable to the lathing and molding techniques needed for manufacture, in addition to its optimal light transmission [59]. Rigid contact lenses became gas permeable with the introduction of copolymers of PMMA with functionalized silicone and fluorine containing macromers. Hard contact lenses ride loosely on the cornea, as such they are good alternatives to patients with significant corneal astigmatism or non-spherical corneal surfaces [59]. Oppositely, soft hydrogel contact lens, due to the low modulus, conform to the cornea surface. Bausch & Lomb introduced the first commercially available soft contact lens in the USA in 1971 [60]. The breakthrough for the development of these new contact lens was the introduction of a hydrogel in the formulation, poly 2-hydroxyethylmethacrylate (PHEMA), based in on the work by Wichterle and Lim [61]. The improvement on the patient comfort brought by soft hydrogel contact lens helped to increase the worldwide acceptance of contact lens. More recently, in an effort to improve the oxygen permeability, while maintaining the comfort of standard hydrogel lens, siloxane-hydrogel contact lenses with high oxygen and water permeability were developed. Silicone lenses allow continuous wear for over two weeks, reducing the risks of hypoxia-related complications and retaining the comfort and clinical performance of the conventional hydrogel contact lenses [57, 59]. In Table 1.4, a representative summary of contact lens materials is shown.

Table 1.4 – Representative summary of the different types of commercialized contact lenses. Adapted from [59, 62].

Hard and Rigid Gas Permeable

Trade Name	USAN*	Manufacturer	Oxygen Permeability (Barrers)	Principal components
PMMA	-	-	0.5	PMMA
Silsoft	Siflufocon A	Bausch+Lomb	126	Silicone
Boston II	Itafocon A		12	TRIS, MMA, MAA
Boston Equalens II	Optifocon A		125	Co-Siloxy-fluoromethacrylate
Fluoroperm30	Paflufocon C	Paragon Vision Science	30	TRIS, MAA, MMA, VP
Fluoroperm151	Paflufocon D		151	TRIS, MAA, MMA, siloxy-based polyether macromer
MeniconSFP	Melafocon A	Menicon Co.	159	TRIS, VP, MAA
MeniconZ	Tisilfocon A		163-250	Co-Fluoro-siloxanylstyrene

Soft Hydrogel

Trade Name	USAN*	Manufacturer	Equilibrium Water Content (%)	Oxygen Permeability (Barrers)	Principal components
Soflens 38	Polymacon	Bausch+Lomb	38	9	HEMA
Softlens 59	Hilafilcon B		59	22	HEMA, VP
Hydrocurve II/45	Bufilcon A	CIBA Vision	45	12	HEMA, DAA, MAA
Focus Softcolors	Vilifilcon A		55	16	HEMA, VP, MMA
1 Day Acuvue	Etafilcon A	Johnson & Johnson	58	28	HEMA, MMA
Biomedics 55	Ocufilcon D	CooperVision	55	19.7	HEMA

Silicone Hydrogel

Trade Name	USAN*	Manufacturer	Equilibrium Water Content (%)	Oxygen Permeability (Barrers)	Principal components
Focus Night & Day	Lotrafilcon-A	CIBA Vision	24	140	DMA, TRIS, siloxane
AirOptix	Lotrafilcon-B		33	110	DMA, TRIS, siloxane
Acuvue Oasys	Senofilcon-A	Johnson & Johnson	38	103	mPDMS, DMA, HEMA
Acuvue Advance	Galyfilcon-A		47	60	mPDMS, DMA, HEMA, siloxane, PVP
Acuvue TruEye	Narafilcon-B		54	100	mPDMS, DMA, HEMA, siloxane

PureVision	Balafilcon-A	Bausch+Lomb	36	110	NVP, TPVC, NCVE, PBVC

*USAN stands for United States Adopted Names
PMMA: poly(methylmethacrylate), TRIS: 3-tris(trimethylsilyloxy)silylpropyl2-methylprop-2-enoate, MMA: methyl-methacrylate, MAA: methacrylic acid, VP: 1-vinyl-2-pyrrolidone, NVP: n-vinyl pyrrolidone, PVP: polyvinylpyrrolidone, DAA: diacetone acrylamide, DMA: n,n-dimethyl acrylamide, mPDMS: monofunctional polydimethylsiloxane, TPVC: tris-(trimethyl siloxysilyl) propylvinyl carbamate, NCVE: n-carboxyvinyl ester, PBVC: poly(dimethysiloxy) di (silylbutanol) bis (vinyl carbamate)

The first cataract surgery removal with implantation of an intraocular lens, made from PMMA, was performed in 1949 by Sir Harold Ridley [63]. Since then, intraocular lens implantation has emerged as a successful procedure with more than 10 million lenses implanted each year. PMMA remained as the dominant IOL material until the 1990's, when foldable IOLs of other materials emerged [64]. The evolution of IOLs materials and designs can be divided into six different generations, accordingly with the placement of the implanted IOL in the eye (see Figure 1.6).
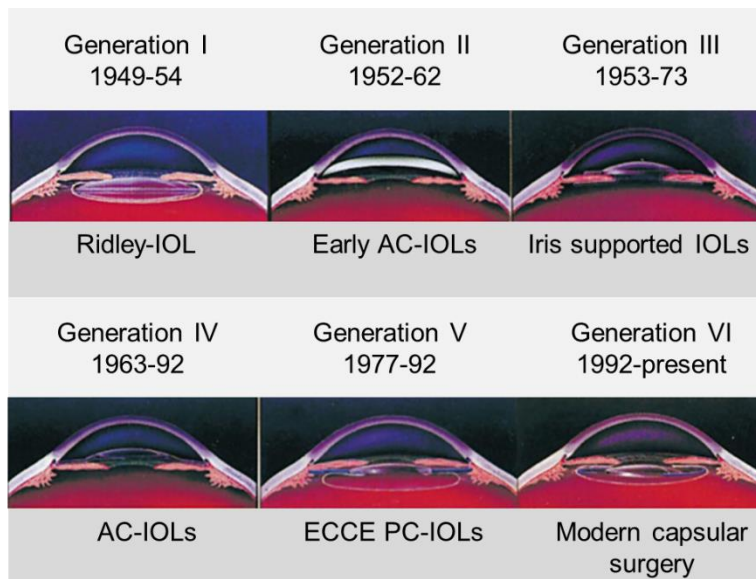
Figure 1.6 - Timeline showing the six major generations of IOLs. Adapted from [63].

Anterior chamber (AC) confinement was selected for fixation of IOLs (Generation II). Contact of these early AC-IOLs with the cornea, for instance by rubbing, lead to corneal endothelium damaging, and loss of corneal clarity [64]. This design was abandoned and

substituted by iris-fixated or –supported designs. Fixation structures (haptics) from various materials were first introduced with iris-supported IOLs. Erosion of the iris, IOL dislocation with dilation of the pupil, and difficulty of implantation discouraged iris-supported IOLs use [64]. New AC-IOL designs were introduced during this period with more evolved haptics for fixation, but long-term negative outcomes such as undesirable corneal decompensation, chronic uveal inflammation, and glaucoma lead to a definitive abandonment of the AC-IOLs [65]. Advances on surgical techniques allow the development of posterior chamber (PC) IOLs. Extracapsular cataract extraction (ECCE) is an eye surgery technique in which the lens of the eye is removed, while the elastic capsule that covers the lens is left partially intact. PC-IOL implantation required the ECCE cataract surgery method, and large numbers of IOLs were implanted with this method. Phacoemulsification in which the eye's internal lens is emulsified with an ultrasonic handpiece and aspirated from the eye allow the reduction of the incision length required to enter and remove the cataract. This surgical procedure evolution prompt the search for foldable IOLs ("capsular lenses") that could be inserted through the smaller incision, since postoperative results with this technique progressed positively towards safe, permanent, and secure in-the-bag fixation [63, 64]. In Table 1.5, a summary of types of biomaterials used for manufacturing of intraocular lens is shown.

Table 1.5 - Representative summary of the different biomaterials use for manufacturing of commercialized intraocular lenses. Adapted from [64].

Manufacturer	Trade Name	Principal components
Alcon	Aspheric AcrySof® IQ® Multiflocal ReSTOR®	Proprietary hydrophobic copolymer of acrylates with UV absorber only or with additional proprietary bonded yellow dye for blue-light filtering AcrySof® Natural® IOL material
Bausch+Lomb	Aspheric SoftPort® AO Aspheric Akreos™ AO Akreos™ MI-60 Crytalens® AT-50	PMMA with UV absorber Proprietary polysiloxane with UV and violet light absorber Proprietary hydrophilic copolymer of acrylates with UV absorber

Carl Zeiss Meditec	XL Stabi®, Hydromax® Aspheric Acri. Smart® Multifocal Acri.Lisa®	Proprietary hydrophilic and hydrophobic acrylates and polysiloxane materials with UV and optional violet filtering absorbers Polyvinylidene fluoride (PVDF) haptic material
Medenium	Foldable monofocal IOL Matrix®	Proprietary hydrophobic copolymer of acrylates with UV absorber Polyvinylidene fluoride (PVDF) haptic material

1.3.1 Therapeutic contact lenses

The ideal drug delivery system should broadly comply with two requirements: 1) deliver a majority of the drug to the target tissues at rates tailored for the specific indication and 2) ease of use. For ocular applications, it should also be ensure that the system is biocompatible, comfortable, and does not have any negative effect on vision or other functions such as blinking.

Contact lenses meet the requirements of being compatible and comfortable [15, 66, 67]. Due to the placement of the contact lens in the eye, concentration of drug delivered by the lens is expected to be higher near to the cornea compared to that near the conjunctiva, providing an increase on bioavailability up to 50% when compared to that delivery through eye drops [68]. A limitation of the bioavailability to about 5% is generally considered for eye drops instillation, since drug applied at the surface of the eye can permeate through the conjunctiva, or be washed away through the lacrimal system, diluting with tears. The product of the permeability and area for conjunctiva is at least 20 times that of the cornea [66].

When considering diseases that require multiple instillations each day, patient compliance is also expected to benefit from a drug eluting lens as substitute for eye drops. From an optimal drug eluting lens a controlled and sustained drug release profile can be expected, decreasing the probability of concentrations above toxic levels and eliminating the need for preservatives that are known to cause corneal toxicity [66, 69].

1.3.1.1 Drug loading strategies

Since the early 1960's contact lenses have been tested as drug delivery vehicles to the eye [61]. The most conventional and simple way to load drug into the lens is by soaking, which consists in the immersion of the contact lenses in the drug solution [70, 71]. The drug uptake will depend on the water content, thickness of the lens, molecular weight of the drug, soaking time period and concentration of drug in the soaking solution [72]. The drug uptake and afterwards the release are generally analyzed as a diffusional transport process and a partition phenomenon, and may depended on drug-polymer interactions [73]. Soluri and co-workers loaded 14 different commercially available contact lenses with ketotifen fumarate and found that lenses with charged surfaces [Balafilcon A, Etafilcon A, and Etafilcon A (daily disposable)] showed improved drug uptake and release duration, but, nonetheless, most lenses reached a plateaus concentration of drug quickly, and no lens was able to release drug for longer than 4 hours [74]. A similar strategy was chosen by Phan and co-workers that studied the performance of commercially available soft and silicone hydrogel contact lenses to release an antifungal ocular drug, natamycin. All contact lenses released clinically relevant concentrations of natamycin within 30 minutes, but this release reached a plateau after approximately 1 hour [75]. PHEMA based and silicone based hydrogels were investigated by Paradiso and co-workers as platforms for delivery of levofloxacin and chlorhexidine. The PHEMA based hydrogel demonstrated to be the best material to achieve a controlled release of levofloxacin. In the case of chlorhexidine, the silicone hydrogel led to better results. In both cases, results suggested that these materials were adequate only for the preparation of daily disposable therapeutic contact lenses, with delivery time periods inferior to one day [76]. Loading through soaking presents several limitations. High molecular weight drugs like hyaluronic acid, do not penetrate successfully into the lens and remain on the surface only, as demonstrated by Maulvi and co-workers [77]. Low affinity between drug molecules and polymer matrix can lead also to rapid release of the drug when release kinetics is only diffusion controlled.

Other strategies, besides the soaking method, have been attempted to decrease the initial burst release, and maintain the therapeutic levels for longer time periods. In molecular imprinting, the template drug is mixed with functional monomers, and the

mixture is polymerized. After polymerization, the drug is removed from the lens, which results in formation of tailored active sites due to the rearrangement and interaction between drug and polymer molecules. These molecular imprinted sites mimic the drug's receptors or its structurally similar analogy, which increase drug loading capacity (see Figure 1.7) [78, 79]. A key factor in this process is the affinity of the monomers to the template drug, which is potentiated if hydrogen bonds, hydrophobic or ionic interactions exists [80].
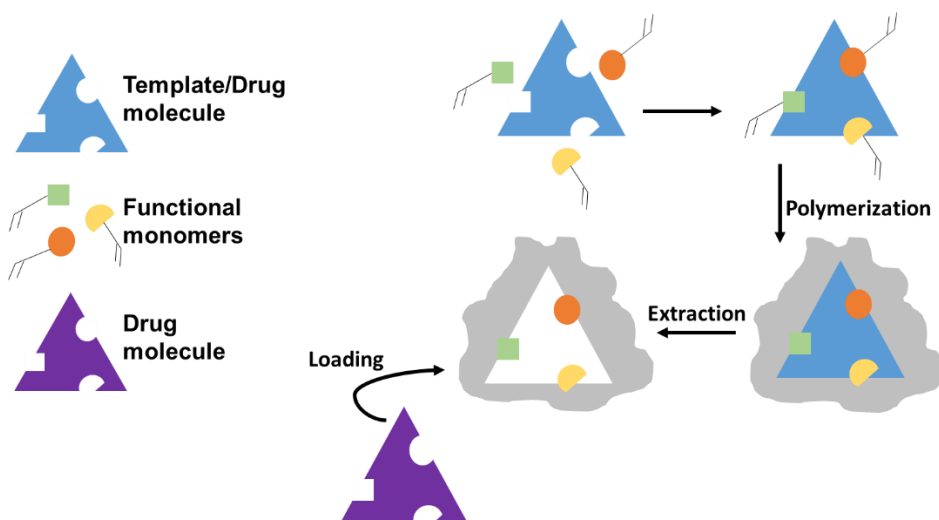
Figure 1.7 – Schematic representation of the molecular imprinting process.

Alvarez-Lorenzo and co-workers were among the firsts to identify the potential of the molecular imprinting technique for contact lenses drug loading. They enhanced norfloxacin loading ability of PHEMA hydrogels up to 300 times more than that shown by PHEMA conventional hydrogels [81]. Analogously, a *N,N*-dimethylacrylamid (DMA) tris(trimethylsiloxy)sililpropyl methacrylate (TRIS), and methacrylic acid (MAA) hydrogel showed a higher affinity for timolol, and a slower release rate than the non-imprinted hydrogels [82]. Some limitations of molecular imprinting have been identified, namely, the highly cross-linked hydrogel structure which influences the physical and optical performance of contact lenses [83], and a decrease in water content (decrease in swelling) that can lead to an insufficient ion and oxygen permeability, limiting the use of contact lenses for extended wear [84].

Partition of drug into the hydrogel can be increased by designing a matrix to capitalize on the absorption of the drug to the polymer chains. When drug molecules penetrate the hydrogel, they either dissolve in the aqueous phase or adsorb on the polymer matrix. Generally, the rates of adsorption-desorption are rapid compared to the diffusion rate of the drug, hence the bond and free drug concentrations are in equilibrium. The bounded drug can potentially diffuse along the polymer chains with a surface diffusivity which is typically lower than that of the free drug. In this case, an effective diffusivity (D_e) can be used to describe the overall drug transport, weighting both the bound and free drug fractions [66].

Due to the large number of ophthalmic drugs charged at physiological conditions, ionic interactions become a potential choice to increase drug affinity to polymer chains, as represented in Figure 1.8.
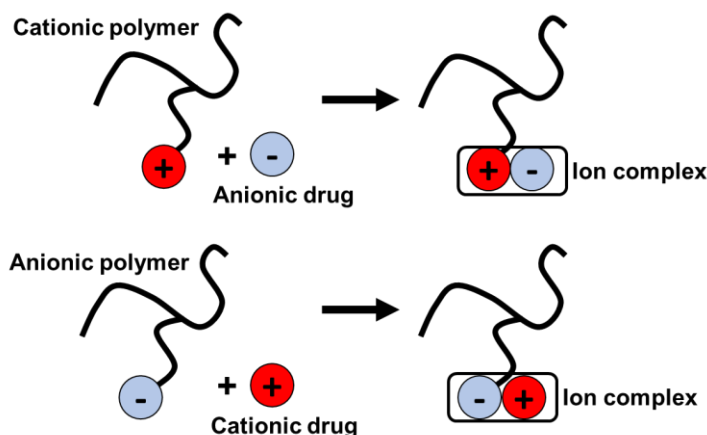
Figure 1.8 – Schematic representation of ionic interactions between charged drug molecules and polymer chains. Adapted from [85].

Bengani and Chauhan used a cationic surfactant (cetalkonium chloride) to increase an anionic drug (dexamethasone 21-disodium phosphate) release duration from in 1-day ACUVUE® contact lenses from 2 to 50 hours [86]. In this study, the ionic molecule was incorporated in the matrix after polymerization, assuring that no structural and material properties change. However, typically, the ionic molecules are already present before the polymerization. For instance, Yamazaki and co-workers explored the interaction between the antibiotic ofloxacin and the anionic HEMA based hydrogels whose composition

contained methacrylic acid, 2-methacryloyloxyethyl hydrogen succinic acid, and 3-methacryloxypropyl tris(trimethylsiloxy)silane. The increase on the release duration of ofloxacin was attributed to the reduction in transport of water, which is required for the solvation of the drug [85]. Kakisu and co-workers studied the release of two antibiotics (gatifloxacin and moxifloxacin) from PHEMA based hydrogels that also contained the anionic methacrylic acid. The uptake of both antibiotics was found to be proportional to the amount of MAA incorporated in the matrix, and presented an extended release of 2-3 days [87]. Through these ionic interactions approach is not, however, possible to deliver neutral drugs or a mixture of cationic and anionic drugs.

Another strategy that has been very popular in recent years, is the utilization of diffusion-blocking barriers inside the contact lens to increase the tortuosity for the drug transport. This approach was first proposed by Chauhan and co-workers (see Figure 1.9). They demonstrated that vitamin E barriers can be created in silicone-based contact lenses for extended wear without any impact on the transparency for vitamin E loading as high as 70% (w/w) [88-91].
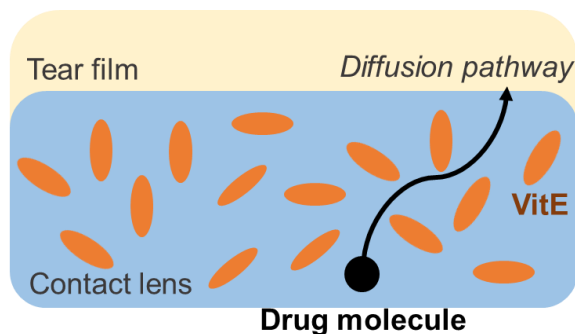
Figure 1.9 – Schematic representation the microstructure of vitamin E (VitE) contact lens and mechanism of drug transport.

Vitamin E barriers are easy to implement, with additional benefits such as UV blocking, and the possibility of attenuating transport of several drugs, even simultaneously. As disadvantages, the size increase on vitamin E incorporation and the decrease in ion permeability can limit the maximum amount of vitamin E that can be loaded into the lens [66].

Vitamin E acts as inner barrier for the drug transport, as alternative surface barriers can also increase the release time period, and potentially decrease the initial concentration burst. Contact lenses coatings are already used to improve the surface wettability and the lubricity. The most commonly used strategies to create these coatings are based on polyelectrolyte multilayers obtained by layer-by-layer deposition [92], on the adsorption/grafting of specific molecules [93, 94], and on the immobilization of liposomes at the lens surface [95, 96]. Silva and co-workers investigated the use of alginate/chitosan-based layers deposited by layer-by-layer technique to control the release of an antifungal (chlorhexidine), an antibiotic (moxifloxacin), and two anti-inflammatories (diclofenac and ketorolac) from different ophthalmic lenses materials. The initial burst of diclofenac released from a silicone hydrogel was significantly reduced, and the barrier effect of the coating revealed to be strongly affected by the characteristics of the pair hydrogel/drug [97]. A layered contact lens strategy has also been explored by different research groups. Guzman and co-workers proposed a three-layer system based on bimodal amphiphilic co-networks with hydrophilic poly(N,N-dimethylacrylamide) (PDMAAm) and hydrophobic polydimethylsiloxane (PDMS) networks that allow for high oxygen permeation and improved mechanical properties. The center layer contained high drug (moxifloxacin) loading, whereas the two outer layers contained no-drug, but were loaded with vitamin E. The two outer layers, due to the small drug diffusivity, slow down drug diffusion, and a constant-rate drug delivery was achieved without an initial burst. Obtained rates were consistent with potential several days of antibiotic release above the therapeutic level [98]. Ciolino and co-workers made a *sandwich* like structure where a fluorescein and ciprofloxacin loaded poly[lactic-co-glycolic acid] layer was placed between two PHEMA hydrogel layers [99]. With this approach, concerns about loss of transparency are present. Additionally, due to the inner layer nature, degradation may occur during sterilization and storage.

Other approaches have been used for incorporation of drugs into commercially or commercially like ophthalmic lenses. At this point, it must be referred that the currently available lenses were not developed with propose of being utilized as controlled drug release systems, but as devices for refractive correction. Thus, is reasonable to affirm that their compositions may not be optimal for drug release applications, and designing of new

materials with more adequate compositions is desirable and even recommended. Infinite combinations can be explore, having present that certain material properties, for suitable ophthalmic lenses, must always be attained, including transparency, ion permeability, and modulus.

1.3.1.2 Relevant material properties

All ophthalmic lenses materials must comply with the premise of not inferring with the user's visual performances, and they should safeguard the comfort and the preservation of the normal ocular physiology of the user. To assure this, first, the material must be biocompatible, which means that the material is nontoxic, not resulting in any immune response from the host biological system. Moreover, a material used for contact lens must be able to maintain a stable, continuous tear film, be permeable to oxygen to maintain normal corneal metabolism, be permeable to ions in order to maintain on-eye movement, and provide clear and stable vision [62].

Closely related with the later, optical transparency performance is described through the transmittance (%T), the percentage of visible light transmitted through the material, and is expressed as [100]:

$$\%T = 100 \times \frac{I}{I_0} \quad \textbf{Equation 1.2}$$

Where I_0 and I stand for the intensity of the incident light and of the transmitted light, respectively. The light transmittance properties of polymers can be divided in three categories: transparent, translucent, or opaque. Transparent are those that you can see through, translucent are those that you cannot see through but allow light to pass through, and opaque are those that neither permit you to see through nor allow light to pass through. Hydrogels which are useful as contact lens materials transmit over 90% of light in the visible part of the spectrum [62]. Ideally, an hydrogel should have a refractive index similar to that of the cornea, 1.37. The variance of the refractive index in conventional lenses with EWC is almost linear. For a 20% EWC the refractive indices range from 1.46 - 1.48 and for 75% EWC from 1.37 − 1.38. Silicone hydrogels do not follow this behavior due to their different nature [62].

The cornea receives most of its oxygen from the atmosphere, since it is one of the few avascularized tissues in the human body. Permeability to oxygen is, therefore, one of the most relevant properties of a contact lens. It can be described as the product of the oxygen diffusivity (D) and solubility (k) in the material, with unit Barrers defined as follows [101]:

$$Dk \ (barrers) = \frac{10^{-10}[cm \times cm^3(O_2)]}{sec \times cm^2 \times cmHg}$$ **Equation 1.3**

Where cm refers to the thickness of the material, $cm^3(O_2)$ to the volume of oxygen at standard temperature and pressure (STP) conditions, namely 0 ⁰C and 1 atm (101 325 Pa), cm^2 to the area of the lens, and $cmHg$ to the partial pressure of oxygen. The minimum oxygen permeability for ocular health maintenance is 35 Barrer/cm of lens thickness for the open eye, and 125 Barrer/cm of lens thickness for the closed eye [102].

The mechanical properties of contact lenses are important because they are directly related with comfort, fitting characteristics, physiological impact, durability, and handleability of the lenses [62]. The most important mechanical property is the tensile elastic modulus which determines the stiffness of the lens. Lower modulus lenses are more flexible, and easy to place in the eye, but they are more difficult to handle and prone to rupture. Conventional, soft hydrogel contact lenses have a lower modulus (0.2 – 0.6 MPa) when compared to silicone hydrogel lenses (1.1 - 1.4 MPa). Higher modulus silicone lenses due to their mechanical endurance, together with the higher oxygen permeability, are more suitable for extended wear, whereas conventional lenses for daily disposable lenses [62].

The equilibrium water content (EWC) is defined as follows [62]:

$$EWC = \frac{weight \ of \ water \ in \ polymer}{total \ weight \ of \ hydrated \ polymer} \times 100$$ **Equation 1.4**

In Figure 1.10, the relationship between oxygen permeability and EWC for soft hydrogel and silicone commercially available contact lenses is shown. In conventional soft hydrogels lenses, increased water content and oxygen permeability was achieved by adding hydrophilic monomers, such as MAA or NVP. Conventional lenses have the

potential to approach the oxygen permeability of pure water. However, high water content (>50%) has some disadvantages, for example, increased fragility due to low modulus [59]. In silicone lenses, the relationship between oxygen permeability and EWC is inversely proportional. The oxygen permeation in these lenses occurs mainly through the siloxane-rich zones, while water regions allow ion permeability [103].
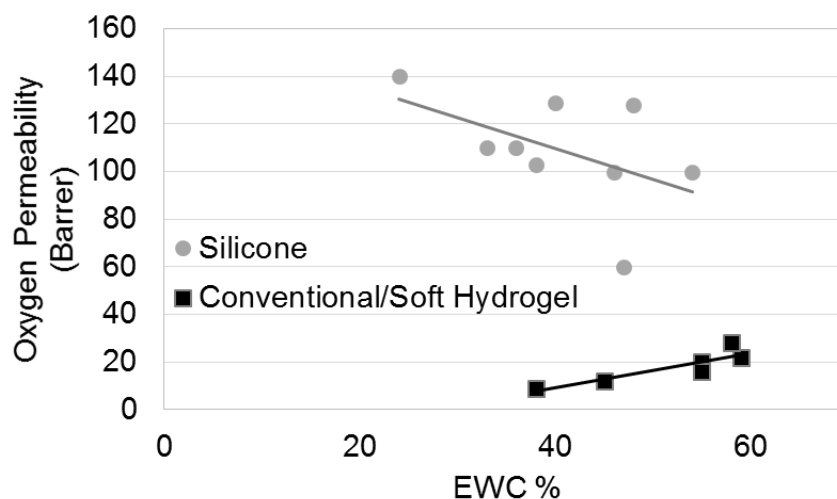
Figure 1.10 – Relationship between oxygen permeability versus equilibrium water content (EWC) of the silicone and conventional hydrogel lenses [59].

A minimum aqueous phase is necessary to permit on eye movement. For overnight wear, typically 24-28% EWC is necessary. For conventional hydrogels a minimum 38% EWC is reported to be necessary to maintain on eye movement [104]. Ionic permeability, which is a parameter related to the ability of Na^+ and Cl^- ions have to permeate through the polymeric matrix, should be regarded as important to ensure an adequate mobility od the lens in the eye. An ionic permeability bellow 2.4×10^{-7} cm^2s^{-1} was related with deficit on contact lens movement over the ocular surface [105].

Contact lens is placed in contact with the tear film while residing against the cornea. The tear film ensures important vital functions, namely the nutrients allocation to the eye tissues, and the lubrication and protection of the ocular surface. Thus, it is essential that the lens material has a wettable surface which allows a normal structure of the tear film, either above and below the lens [59]. Wettabilty is the ability of a liquid to spread over a surface, and it is based on equilibrium of the solid-liquid-vapor triple-phase contact line.

The most used way to characterize a surface regarding its wettability involves the measurement of contact angles, which indicate the degree of wetting when a solid and liquid interact. Small contact angles (< 90°) correspond to high wettability, while large contact angles (> 90°) correspond to low wettability [106]. The contact angle of a liquid drop on an ideal rigid and flat surface is defined by the Young equation [106]:

$$\gamma_{lv} cos\theta_Y = \gamma_{sv} - \gamma_{sl}$$ **Equation 1.5**

where γ_{lv}, γ_{sv}, and γ_{sl} represent the liquid-vapor, solid-vapor, and solid-liquid interfacial tensions, respectively, and θ_Y is the contact angle. Two types of techniques are commonly used for direct contact angle measurement: sessile drop and captive bubble (see Figure 1.11).

Sessile Drop   Captive Bubble
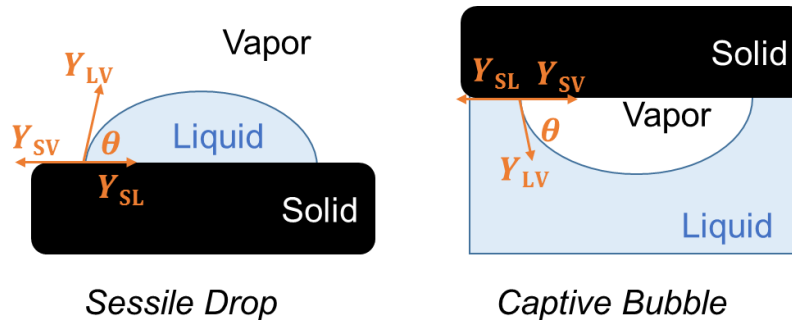
Figure 1.11 – Schematic representation of the two methods of goniometric analysis: sessile drop and captive bubble.

With the captive bubble technique the hydrogel sample is maintained hydrated, which is an advantage, since it is possible to simulate the tear film environment were the contact lens is placed. Small contact angles correspond to highly wettable surfaces.

1.3.2 Therapeutic intraocular lenses

When compared the number of research articles available on drug eluting contact lenses and drug eluting intraocular lenses, it becomes clear that less investment has been done in the later. IOLs are used as substitutes of the eye natural lens when a cataract is developed. Other type of implants are used, more or less successfully, to deliver medication to the back of the eye for diseases such as wet age-related macular degeneration or posterior uveitis (see section 1.2.1). Therefore, drug eluting intraocular

lens application seems to be restricted to cataract surgery prophylaxis only. Taking into account that every year more than 10 million IOLs are implanted, and that reports in the last decade point to a postoperative endophthalmitis incidence of 0.04 - 0.2% [26-28] it appears to exist economic and medical interest for the development of a therapeutic/prophylactic IOL.

1.3.2.1 Drug loading strategies

Since intraocular lenses are implanted *in situ*, were POE could potentially develop, several strategies have been proposed to use IOLs as drug carriers themselves or as support to other drug delivery devices. A PHEMA hydrogel device was developed by Garty and co-workers to deliver norfloxacin into the anterior chamber. The drug loaded PHEMA devices were attached to the IOL haptics and coated with a hydrophobic barrier. *In vivo* results from rabbits implanted with these IOLs shown that enough drug was released to maintain the concentration of norfloxacin above the minimum inhibitory concentration for 4 weeks [107]. Acrylic IOLs loaded with antibiotic by soaking in solution for 24 hours of gatifloxacin were implanted in rabbit eyes and antibiotic concentrations in the aqueous humor, and effects against bacterial proliferation were evaluated. Drug was detected until day 5 after implantation. Gatifloxacin concentrations in rabbit aqueous humor after administration by two different routes, antibiotic-loaded IOLs and intracameral injection, were compared. Concentration of gatifloxacin was higher after 4 hours and 8 hours for injection but comparable after 1 day. [108]. Due to the simplicity of the process, other authors also tested impregnation of IOLs with drugs through soaking. Kleinmann and co-workers choose loaded acrylic IOLs with moxifloxacin and gatifloxacin that were afterwards implanted in rabbits. In this study, the concentration of antibiotic in aqueous humor after implantation of presoaked IOLs was compared with that from eye drops topical application. The topical prophylaxis protocol chosen combined the pre-operative application of 1 drop every 5 minutes for 15 minutes an hour before the operation, 1 drop of antibiotic and prednisolone acetate 1% (corticosteroid) at the end of surgery, and every 2 hours until 2 hours before aqueous humor sampling. Concentration of drug released from IOLs was above the concentration of antibiotic measured after the eye drops administration at 4, 8 and 12 hours [109].

Other strategies described in section 1.3.1.1 could be also adapted and applied to the preparation of therapeutic intraocular lenses.

1.3.2.2 Relevant material properties

As for contact lenses, materials used for intraocular lenses manufacturing must not, as for contact lenses materials, affect the user's visual performance, and they should safeguard the comfort and the preservation of the normal ocular physiology.

The refractive index for IOLs should lie within the optimal interval of 1.42 to 1.55 [110], and the light transmittance higher than 90% above 500 nm [111, 112].

Cataract surgery and IOL implantation has become a common medical practice, but even with a success rate of 98% and with IOLs extended lifespan, complications may occur [113]. Some patients regain vision difficulties, due to the thickening of the back of the lens capsule, this is called posterior lens capsule opacification (PCO). PCO is a result from the growth and abnormal proliferation of lens epithelial cells on the posterior capsule, and is affected by the lens material [114]. Surface roughness and material hydrophobicity influence cell adhesion, migration, cellular inflammatory response, and the development of PCO [115]. Correlation of materials surface properties and biological interactions is not simple, since surface properties can be influenced by numerous factors. Atomic force microscopy (AFM), a high-resolution scanning probe microscopy at a nanoscale level, can be used to provide information about IOLs surface characteristics. Higher incidence of POC has been related with higher surface roughness [116], and different average roughness values have also be found for the same material with different dioptric powers [117].

Miyake and co-workers found in a comparative between hydrophobic and hydrophilic IOLs study that postoperative inflammation, and more rapid anterior capsule opacification, was seen in the eyes with hydrophobic IOLs [118]. Hollick and co-workers described a reduced inflammatory cell response in hydrophilic IOLs, when compared with silicone and PMMA IOLs, but with more epithelial cells on their anterior surface [119].

31

Contact angle measurements can be done to found the material hydrophobicity and facilitate the understanding of how the material might induce biological responses. Cunanan and co-workers analyzed different commercially available IOLs using both the sessile drop and the captive bubble method. They found that the contact angle measurements differed depending on the test conditions. Through sessile drop method, with dry IOL samples, common classification of the materials as hydrophobic or hydrophilic was possible. The captive bubble method, with hydrated IOL samples, differentiated materials based on their polar and dispersive forces [120].

When designing new materials for IOLs, one should take into account the glass transition temperature, the temperature at which an amorphous material passes from its rigid glassy state to its soft rubbery state [121]. This is a very important property for IOLs since it determines their ability to fold upon implantation in the eye. The lower the glass-transition temperature of the material, the more foldable the IOL [122].

1.3.3 Challenges and opportunities

Despite the promising results for the use of ophthalmic lenses as drug delivery systems, no commercial product is available after decades of research. One of the possible justifications for this fact, relies in early results that fail to obtain long release durations (see section 1.3.1.1). The ratio between the production costs of the drug eluting lenses and the benefit could be, for short release duration lenses, not viable, especially if more than one lens may need to be used each day. New extended wear lenses and advances in the area of control release, can potentially present innovative opportunities for the development of these devices. Studies on the effect of sterilization and packaging processes on the stability of therapeutic ophthalmic lenses have not been extensively explored. Thus, a lack of knowledge about the long term drug behavior of loaded lenses exists, and must be overcome for the general acceptance of such devices. The sterilization and packaging processes currently used in the industry may interfere with the release kinetics of the drug eluting lenses. For instance, sterilization of contact lenses is generally done inside the blister package, which is filled with buffered solution, and lenses are maintained in that solution until the moment of use. The storage period can go up to months, and during this period, if not accounted for, total release of drug may occur. One

possible solution could pass by having drug in the storage solution, maintaining the drug loaded lens in equilibrium, but this could potentially increase the production costs. Utilization of hydrogels that not require storage in solution could also be an alternative.

Topical administration of drug for ocular treatment is currently well stablish and is expected to retain its leading share of about 50% in revenue till 2025 [123]. Disruption of the market by a new product is not easy, and requires interest from the pharmaceutical industry, physicians, and patients. Regulatory processes are often pointed as burdens for the development of new medicinal or medical devices products, due to their costs, and prolonged time till requirements total fulfillment. In Table 1.6, a synthesis of the regulatory procedures for new drug delivery device in the US and Europe is presented.

Table 1.6 - Regulatory procedures in the US and Europe [124].

US, FDA

Primary mode of action:	Regulatory procedures:
Drug part	- Pre-investigational new drug (IND) phase - IND review phase - New drug application (NDA)
Biological part	- Pre-IND phase - IND review phase - Biologic License Application
Device part	- Pre-investigational device exemption (IDE) - IDE review phase

Europe

Product:	Regulatory procedures:
Drug, Marketing authorization application (MAA) *Therapeutic action is achieved principally via a metabolic, pharmacological or immunological mode of action*	- Clinical trial application for medicinal product (national) - Medicinal product MAAs (centralised, decentralised, mutual recognition procedures)
Medical device, CE marking *Therapeutic action is achieved principally via other means and in particular a mechanical/physical mode*	- Clinical trial application for medical devices (national) (new medical devices or in case devices are used outside already CE marked intended use) - CE marking valid for all of Europe and medical devices (except class I) certified by notified body

In the US, a drug with its delivery system will fall under the definition of a combination product: "drug/device, biologic/device, drug/biologic, or drug/device/biologic, that are physically, chemically, or otherwise combined or mixed and produced as a single entity". The regulatory procedure will depend on the primary mode of action: "the single mode of action of a combination product that provides the most important therapeutic action of the combination product" [124]. In Europe, products are either considered medicinal or medical devices, taking into account their principal mode of action, with the "combination product" concept being inexistent [124]. The timeline for approval of the new product will depended on different factors. Let's take as example the average timeline and costs for FDA approval process: Class I devices are deemed to be low risk (example: dental floss) will take 1 month with estimated costs of US$10000; Class II devices higher risks when compared to Class I (example: condoms) will take 3 – 6 months with estimated costs of US$22500; Class III devices (example: replacement heart valves) will take 18 – 30 months with estimated costs of over US$50000 [125]. Since contact and intraocular lenses are well accepted for biomedical applications, and a wide range of ophthalmic drugs are already available, a combination of both in a new ocular drug delivery device could help to reduce the time period, and costs to achieve a commercial product.

1.4 Thesis objective and outline

As becomes evident from the above exposed, the design of a controlled ophthalmic drug delivery system is a complex task. Different factors shall be taken into account to obtain a final optimal product, such as: the desired application, and consequentially the target ocular tissue; the type of biomaterial to be used as drug carrier; or the drug/combination of drugs necessary for therapeutic success.

In this thesis, it is aimed to study diverse and useful aspects that could positively contribute as an advance in this research field. Different strategies for drug release control were attempted, having always present that for a rational solution design, an understanding of the interactions between the drug molecules and the polymer matrix, and of the *in vivo* environment, where the device is expected to perform, must never

be neglected. In Chapter 2, the partition and diffusion aspects of drug molecules in the polymer matrix were studied using three drugs of different nature, and PHEMA and silicone based hydrogels. In Chapter 3, attention to the *in vivo* environment was given by employing a microfluidic cell to experimentally simulate the tear film in drug eluting contact lenses testing. In Chapter 4, an antibiotic was loaded on coated commercial IOLs, these coatings were obtained through a plasma-assisted grafting technique. In Chapter 5, a multi-layer lens strategy for release control was employed. In this chapter, it was also shown that a diffusion based mathematical model could help to choose the characteristics of lens, and to achieve a tailored release profile. In Chapter 6, a mathematical model to estimate the *in vivo* concentration in the aqueous humor for drug eluting intraocular lenses. In Chapter 7, different PHEMA base hydrogel compositions were tested to obtain the material with the best expected *in vivo* performance for the release of an antibiotic, and an anti-inflammatory.

1.5 References

1.   Park, K., *Controlled drug delivery systems: past forward and future back.* J Control Release, 2014. **190**: p. 3-8.
2.   Yun, Y.H., B.K. Lee, and K. Park, *Controlled Drug Delivery: Historical perspective for the next generation.* J Control Release, 2015. **219**: p. 2-7.
3.   Jain, K.K., *Drug delivery systems - an overview.* Methods Mol Biol, 2008. **437**: p. 1-50.
4.   Crank, J., *The Mathematics of Diffusion.* Second Edition ed. 1975, Oxford: Clarendon Press.
5.   Hoffman, A.S., *CHAPTER II.5.16 - Drug Delivery Systems*, in *Biomaterials Science (Third Edition)*. 2013, Academic Press. p. 1024-1027.
6.   Siepmann, J. and F. Siepmann, *Mathematical modeling of drug delivery.* Int J Pharm, 2008. **364**(2): p. 328-43.
7.   Siegel, R.A. and M.J. Rathbone, *Overview of Controlled Release Mechanisms*, in *Fundamentals and Applications of Controlled Release Drug Delivery*, J. Siepmann, R.A. Siegel, and M.J. Rathbone, Editors. 2012, Springer US: Boston, MA. p. 19-43.
8.   Patel, A., et al., *Ocular drug delivery systems: An overview.* World journal of pharmacology, 2013. **2**(2): p. 47-64.
9.   Gaudana, R., et al., *Ocular drug delivery.* Aaps J, 2010. **12**(3): p. 348-60.
10.   Thrimawithana, T.R., et al., *Drug delivery to the posterior segment of the eye.* Drug Discov Today, 2011. **16**(5-6): p. 270-7.
11.   Urtti, A., *Challenges and obstacles of ocular pharmacokinetics and drug delivery.* Adv Drug Deliv Rev, 2006. **58**(11): p. 1131-5.
12.   Eghrari, A.O., S.A. Riazuddin, and J.D. Gottsch, *Overview of the Cornea: Structure, Function, and Development.* Prog Mol Biol Transl Sci, 2015. **134**: p. 7-23.
13.   DelMonte, D.W. and T. Kim, *Anatomy and physiology of the cornea.* J Cataract Refract Surg, 2011. **37**(3): p. 588-98.
14.   Hughes, P.M., et al., *Topical and systemic drug delivery to the posterior segments.* Adv Drug Deliv Rev, 2005. **57**(14): p. 2010-32.
15.   Prausnitz, M.R. and J.S. Noonan, *Permeability of cornea, sclera, and conjunctiva: a literature analysis for drug delivery to the eye.* J Pharm Sci, 1998. **87**(12): p. 1479-88.
16.   Edward, A. and M.R. Prausnitz, *Predicted permeability of the cornea to topical drugs.* Pharm Res, 2001. **18**(11): p. 1497-508.
17.   Janoria, K.G., et al., *Novel approaches to retinal drug delivery.* Expert Opin Drug Deliv, 2007. **4**(4): p. 371-88.
18.   Gaudana, R., et al., *Ocular Drug Delivery.* The AAPS Journal, 2010. **12**(3): p. 348-360.
19.   Bremond-Gignac, D., F. Chiambaretta, and S. Milazzo, *A European perspective on topical ophthalmic antibiotics: current and evolving options.* Ophthalmol Eye Dis, 2011. **3**: p. 29-43.
20.   Meadows, M. *Dealing with Dry Eye*. FDA Consumer Magazine 2005 August 15, 2017].

21.   Conlon, R., H. Saheb, and Ahmed, II, *Glaucoma treatment trends: a review.* Can J Ophthalmol, 2017. **52**(1): p. 114-124.
22.   Messmer, E.M., *The pathophysiology, diagnosis, and treatment of dry eye disease.* Dtsch Arztebl Int, 2015. **112**(5): p. 71-81.
23.   Lin, H. and S.C. Yiu, *Dry eye disease: A review of diagnostic approaches and treatments.* Saudi J Ophthalmol, 2014. **28**(3): p. 173-81.
24.   Tatlipinar, S. and E.K. Akpek, *Topical ciclosporin in the treatment of ocular surface disorders.* Br J Ophthalmol, 2005. **89**(10): p. 1363-7.
25.   Barber, L.D., et al., *Phase III safety evaluation of cyclosporine 0.1% ophthalmic emulsion administered twice daily to dry eye disease patients for up to 3 years.* Ophthalmology, 2005. **112**(10): p. 1790-4.
26.   Miller, J.J., et al., *Acute-onset Endophthalmitis After Cataract Surgery (2000–2004): Incidence, Clinical Settings, and Visual Acuity Outcomes After Treatment.* American Journal of Ophthalmology, 2005. **139**(6): p. 983-987.
27.   Durand, M.L., *Endophthalmitis.* Clin Microbiol Infect, 2013. **19**(3): p. 227-34.
28.   Taban, M., et al., *Acute endophthalmitis following cataract surgery: a systematic review of the literature.* Arch Ophthalmol, 2005. **123**(5): p. 613-20.
29.   Sharifi, E., T.C. Porco, and A. Naseri, *Cost-effectiveness analysis of intracameral cefuroxime use for prophylaxis of endophthalmitis after cataract surgery.* Ophthalmology, 2009. **116**(10): p. 1887-96.
30.   *Cystoid Macular Edema.*   [cited 2017 December 4]; Available from: http://www.rvscny.com/cystoidmacularedema.html.
31.   Kessel, L., et al., *Post-cataract Prevention of Inflammation and Macular Edema by Steroid and Nonsteroidal Anti-inflammatory Eye Drops: A Systematic Review.* Ophthalmology, 2014. **121**(10): p. 1915-1924.
32.   Jonas, J.B., et al., *Glaucoma.* Lancet, 2017. **31**(17): p. 31469-1.
33.   Greco, A., et al., *Emerging Concepts in Glaucoma and Review of the Literature.* Am J Med, 2016. **129**(9): p. 26.
34.   Chidlow, G., J.P. Wood, and R.J. Casson, *Pharmacological neuroprotection for glaucoma.* Drugs, 2007. **67**(5): p. 725-59.
35.   Schuettauf, F., et al., *Effects of anti-glaucoma medications on ganglion cell survival: the DBA/2J mouse model.* Vision Res, 2002. **42**(20): p. 2333-7.
36.   Hollo, G., F. Topouzis, and R.D. Fechtner, *Fixed-combination intraocular pressure-lowering therapy for glaucoma and ocular hypertension: advantages in clinical practice.* Expert Opin Pharmacother, 2014. **15**(12): p. 1737-47.
37.   Tobin, K.A., *Macugen treatment for wet age-related macular degeneration.* Insight, 2006. **31**(1): p. 11-4.
38.   Bourges, J.L., et al., *Intraocular implants for extended drug delivery: therapeutic applications.* Adv Drug Deliv Rev, 2006. **58**(11): p. 1182-202.
39.   Thomas, R. and R. Melton. *Clinical Guide to Ophthalmic Drugs.*   [cited 2017 August]; Available from: https://www.reviewofoptometry.com/CMSDocuments/2016/5/dg0516i.pdf.
40.   [cited 2017 August]; Available from: https://www.drugs.com.
41.   Paradiso, P., *Strategies to improve the drug release performance of hydrogels for therapeutic soft contact lenses.* 2015, PhD thesis in Materials Engineering, University of Lisbon: Lisbon.

42.   Watanabe, R., et al., *Fluoroquinolone antibacterial eye drops: effects on normal human corneal epithelium, stroma, and endothelium.* Clin Ophthalmol, 2010. **4**: p. 1181-7.

43.   Hooper, D.C., *Emerging mechanisms of fluoroquinolone resistance.* Emerg Infect Dis, 2001. **7**(2): p. 337-41.

44.   Chang Lin, J.E. and D. Welty, *Ocular pharmacokinetics of moxifloxacin after topical treatment of animals and humans.* Survey of Ophthalmology, 2006. **51**(5).

45.   Hwang, D.G., *Fluoroquinolone resistance in ophthalmology and the potential role for newer ophthalmic fluoroquinolones.* Surv Ophthalmol, 2004. **49**(2): p. S79-83.

46.   Dajcs, J.J., et al., *Effectiveness of ciprofloxacin, levofloxacin, or moxifloxacin for treatment of experimental Staphylococcus aureus keratitis.* Antimicrob Agents Chemother, 2004. **48**(6): p. 1948-52.

47.   Ricciotti, E. and G.A. FitzGerald, *Prostaglandins and Inflammation.* Arteriosclerosis, thrombosis, and vascular biology, 2011. **31**(5): p. 986-1000.

48.   *Moxifloxacin Hydrochloride.* Available from: https://www.lktlabs.com/product/moxifloxacin-hydrochloride/.

49.   *Levofloxacin.* Tuberculosis, 2008. **88**(2): p. 119-121.

50.   Mathers, W., *Use of higher medication concentrations in the treatment of acanthamoeba keratitis*: Arch Ophthalmol. 2006 Jun;124(6):923.

51.   Zeng, P., et al., *Solubility properties of chlorhexidine salts.* Drug Dev Ind Pharm, 2009. **35**(2): p. 172-6.

52.   Goa, K.L. and P. Chrisp, *Ocular diclofenac. A review of its pharmacology and clinical use in cataract surgery, and potential in other inflammatory ocular conditions.* Drugs Aging, 1992. **2**(6): p. 473-86.

53.   *Diclofenac sodium salt* Available from: https://www.sigmaaldrich.com/catalog/product/sigma/d6899?lang=pt&region=PT.

54.   Young, P. *KETOROLAC.*   [cited 2017 December]; Available from: http://www.inchem.org/documents/ukpids/ukpids/ukpid06.htm.

55.   Gan, T.J., *Diclofenac: an update on its mechanism of action and safety profile.* Curr Med Res Opin, 2010. **26**(7): p. 1715-31.

56.   Fick, A.E., *A contact lens. 1888.* Arch Ophthalmol, 1997. **115**(1): p. 120-1.

57.   Phillips, A.J. and L. Speedwell, *Contact Lenses.* 1997: Butterworth-Heinemann.

58.   William, F., *Contact lens.* 1940, Google Patents.

59.   Jacob, J., *A - Biomaterials: Contact Lenses A2 - Ratner, Buddy D*, in *Biomaterials Science (Third Edition)*, A.S. Hoffman, F.J. Schoen, and J.E. Lemons, Editors. 2013, Academic Press. p. 909-917.

60.   Gupta, H. and M. Aqil, *Contact lenses in ocular therapeutics.* Drug Discov Today, 2012. **17**(9-10): p. 522-7.

61.   Wichterle, O. and D. Lim, *Hydrophilic Gels for Biological Use.* Nature, 1960. **185**(4706): p. 117-118.

62.   Efron, N. and C. Maldonado-Codina, *6.633 - Development of Contact Lenses from a Biomaterial Point of View – Materials, Manufacture, and Clinical Application A2 - Ducheyne, Paul*, in *Comprehensive Biomaterials.* 2011, Elsevier: Oxford. p. 517-541.

63.   *Evolution of Cataract Surgery and Intraocular Lenses (IOLs).* Survey of Ophthalmology, 2000. **45**(Supplement 1): p. S53–S69

64. Patel, A.S., *B - Intraocular Lens Implants: A Scientific Perspective A2 - Ratner, Buddy D*, in *Biomaterials Science (Third Edition)*, A.S. Hoffman, F.J. Schoen, and J.E. Lemons, Editors. 2013, Academic Press. p. 917-930.

65. Apple, D.J., et al., *Anterior chamber lenses. Part I: Complications and pathology and a review of designs.* J Cataract Refract Surg, 1987. **13**(2): p. 157-74.

66. Hsu, K.H., S. Gause, and A. Chauhan, *Review of ophthalmic drug delivery by contact lenses.* Journal of Drug Delivery Science and Technology, 2014. **24**(2): p. 123-135.

67. Del Amo, E.M. and A. Urtti, *Current and future ophthalmic drug delivery systems. A shift to the posterior segment.* Drug Discov Today, 2008. **13**(3-4): p. 135-43.

68. Li, C.-C. and A. Chauhan, *Modeling Ophthalmic Drug Delivery by Soaked Contact Lenses.* Industrial & Engineering Chemistry Research, 2006. **45**(10): p. 3718-3734.

69. Baudouin, C., et al., *Preservatives in eyedrops: the good, the bad and the ugly.* Prog Retin Eye Res, 2010. **29**(4): p. 312-34.

70. Hehl, E.M., et al., *Improved penetration of aminoglycosides and fluorozuinolones into the aqueous humour of patients by means of Acuvue contact lenses.* Eur J Clin Pharmacol, 1999. **55**(4): p. 317-23.

71. Peterson, R.C., et al., *Clinical performance of daily disposable soft contact lenses using sustained release technology.* Cont Lens Anterior Eye, 2006. **29**(3): p. 127-34.

72. Xinming, L., et al., *Polymeric hydrogels for novel contact lens-based ophthalmic drug delivery systems: a review.* Cont Lens Anterior Eye, 2008. **31**(2): p. 57-64.

73. Pimenta, A.F.R., et al., *Controlled drug release from hydrogels for contact lenses: Drug partitioning and diffusion.* Int J Pharm, 2016. **515**(1-2): p. 467-475.

74. Soluri, A., A. Hui, and L. Jones, *Delivery of ketotifen fumarate by commercial contact lens materials.* Optom Vis Sci, 2012. **89**(8): p. 1140-9.

75. Phan, C.M., L.N. Subbaraman, and L. Jones, *In vitro uptake and release of natamycin from conventional and silicone hydrogel contact lens materials.* Eye Contact Lens, 2013. **39**(2): p. 162-8.

76. Paradiso, P., et al., *Comparison of two hydrogel formulations for drug release in ophthalmic lenses.* J Biomed Mater Res B Appl Biomater, 2014. **102**(6): p. 1170-80.

77. Maulvi, F.A., T.G. Soni, and D.O. Shah, *Extended release of hyaluronic acid from hydrogel contact lenses for dry eye syndrome.* J Biomater Sci Polym Ed, 2015. **26**(15): p. 1035-50.

78. Alvarez-Lorenzo, C. and A. Concheiro, *Molecularly imprinted polymers for drug delivery.* J Chromatogr B Analyt Technol Biomed Life Sci, 2004. **804**(1): p. 231-45.

79. White, C.J. and M.E. Byrne, *Molecularly imprinted therapeutic contact lenses.* Expert Opin Drug Deliv, 2010. **7**(6): p. 765-80.

80. Byrne, M.E., K. Park, and N.A. Peppas, *Molecular imprinting within hydrogels.* Advanced Drug Delivery Reviews, 2002. **54**(1): p. 149-161.

81. Alvarez-Lorenzo, C., et al., *Imprinted soft contact lenses as norfloxacin delivery systems.* Journal of Controlled Release, 2006. **113**(3): p. 236-244.

82.   Hiratani, H., Y. Mizutani, and C. Alvarez-Lorenzo, *Controlling Drug Release from Imprinted Hydrogels by Modifying the Characteristics of the Imprinted Cavities.* Macromolecular Bioscience, 2005. **5**(8): p. 728-733.

83.   White, C.J., A. Tieppo, and M.E. Byrne, *Controlled drug release from contact lenses: a comprehensive review from 1965-present.* Journal of Drug Delivery Science and Technology, 2011. **21**(5): p. 369-384.

84.   Byrne, M.E. and V. Salian, *Molecular imprinting within hydrogels II: progress and analysis of the field.* Int J Pharm, 2008. **364**(2): p. 188-212.

85.   Yamazaki, Y., et al., *Effect of anionic/siloxy groups on the release of ofloxacin from soft contact lenses.* Journal of Applied Polymer Science, 2013. **127**(6): p. 5022-5027.

86.   Bengani, L.C. and A. Chauhan, *Extended delivery of an anionic drug by contact lens loaded with a cationic surfactant.* Biomaterials, 2013. **34**(11): p. 2814-2821.

87.   Kakisu, K., et al., *Development and efficacy of a drug-releasing soft contact lens.* Invest Ophthalmol Vis Sci, 2013. **54**(4): p. 2551-61.

88.   Kim, J., C.C. Peng, and A. Chauhan, *Extended release of dexamethasone from silicone-hydrogel contact lenses containing vitamin E.* J Control Release, 2010. **148**(1): p. 110-6.

89.   Peng, C.C., J. Kim, and A. Chauhan, *Extended delivery of hydrophilic drugs from silicone-hydrogel contact lenses containing vitamin E diffusion barriers.* Biomaterials, 2010. **31**(14): p. 4032-47.

90.   Peng, C.C. and A. Chauhan, *Extended cyclosporine delivery by silicone-hydrogel contact lenses.* J Control Release, 2011. **154**(3): p. 267-74.

91.   Paradiso, P., et al., *Controlled Release of Antibiotics From Vitamin E-Loaded Silicone-Hydrogel Contact Lenses.* J Pharm Sci, 2016. **105**(3): p. 1164-72.

92.   Qiu, Y., et al., *Method for applying an LbL coating onto a medical device.* 2004, Google Patents.

93.   Willis, S.L., et al., *A novel phosphorylcholine-coated contact lens for extended wear use.* Biomaterials, 2001. **22**(24): p. 3261-3272.

94.   Vieira, A.P., et al., *Surface modification of an intraocular lens material by plasma-assisted grafting with 2-hydroxyethyl methacrylate (HEMA), for controlled release of moxifloxacin.* Eur J Pharm Biopharm, 2017. **16**(16): p. 30923-7.

95.   Danion, A., I. Arsenault, and P. Vermette, *Antibacterial activity of contact lenses bearing surface-immobilized layers of intact liposomes loaded with levofloxacin.* J Pharm Sci, 2007. **96**(9): p. 2350-63.

96.   Paradiso, P., et al., *Drug release from liposome coated hydrogels for soft contact lenses: the blinking and temperature effect.* J Biomed Mater Res B Appl Biomater, 2017. **105**(7): p. 1799-1807.

97.   Silva, D., et al., *Chitosan/alginate based multilayers to control drug release from ophthalmic lens.* Colloids and Surfaces B: Biointerfaces, 2016. **147**: p. 81-89.

98.   Guzman, G., et al., *Zero-Order Antibiotic Release from Multilayer Contact Lenses: Nonuniform Drug and Diffusivity Distributions Produce Constant-Rate Drug Delivery.* Adv Healthc Mater, 2017. **6**(3): p. 7.

99.   Ciolino, J.B., et al., *A drug-eluting contact lens.* Invest Ophthalmol Vis Sci, 2009. **50**(7): p. 3346-52.

100. Walsh, J.E., et al., *Novel method for determining hydrogel and silicone hydrogel contact lens transmission curves and their spatially specific ultraviolet radiation protection factors.* Eye Contact Lens, 2007. **33**(2): p. 58-64.

101. Stern, S.A., *The "barrer" permeability unit* Journal of Polymer Science: Part A-2, 1968. **6**.

102. Harvitt, D.M. and J.A. Bonanno, *Re-evaluation of the oxygen diffusion model for predicting minimum contact lens Dk/t values needed to avoid corneal anoxia.* Optom Vis Sci, 1999. **76**(10): p. 712-9.

103. Nicolson, P.C. and J. Vogt, *Soft contact lens polymers: an evolution.* Biomaterials, 2001. **22**(24): p. 3273-3283.

104. Austin, D. and R.V. Kumar, *Ionic conductivity in hydrogels for contact lens applications.* Ionics, 2005. **11**(3): p. 262-268.

105. Ana Rita Ferreira da, S., C. Vicente, and M.G.-M. José, *Reduction in ionic permeability of a silicone hydrogel contact lenses after one month of daily wear.* Materials Research Express, 2015. **2**(6): p. 065007.

106. Yuan, Y. and T.R. Lee, *Contact Angle and Wetting Properties*, in *Surface Science Techniques*, G. Bracco and B. Holst, Editors. 2013, Springer-Verlag Berlin Heidelberg.

107. Garty, S., et al., *Sustained antibiotic release from an intraocular lens-hydrogel assembly for cataract surgery.* Invest Ophthalmol Vis Sci, 2011. **52**(9): p. 6109-16.

108. Tsuchiya, Y., et al., *Preventive effect against post-cataract endophthalmitis: drug delivery intraocular lens versus intracameral antibiotics.* Curr Eye Res, 2008. **33**(10): p. 868-75.

109. Kleinmann, G., et al., *Hydrophilic acrylic intraocular lens as a drug-delivery system for fourth-generation fluoroquinolones.* J Cataract Refract Surg, 2006. **32**(10): p. 1717-21.

110. Bellucci, R., *An introduction to Intraocular Lenses: Material, Optics, Haptics, Design and Aberration*, in *Cataract*, G. J.L., Editor. 2013, S. Karger AG: Basel. p. 38-55

111. Artigas, J.M., et al., *Spectral Transmittance of Intraocular Lenses under Natural and Artificial Illumination.* Ophthalmology, 2011. **118**(1): p. 3-8.

112. Tanito, M., et al., *Measurements of transmission spectrums and estimation of retinal blue-light irradiance values of currently available clear and yellow-tinted intraocular lenses.* Japanese Journal of Ophthalmology, 2012. **56**(1): p. 82-90.

113. Beiko, G.H.H. and A. Grzybowski, *Intraocular lens implants: Do they come with a life time guaranty?* Saudi Journal of Ophthalmology, 2015. **29**(4): p. 247-248.

114. Jung, G.B., K.-H. Jin, and H.-K. Park, *Physicochemical and surface properties of acrylic intraocular lenses and their clinical significance.* Journal of Pharmaceutical Investigation, 2017. **47**(5): p. 453-460.

115. Yang, N., et al., *Topography, Wettability, and Electrostatic Charge Consist Major Surface Properties of Intraocular Lenses.* Current Eye Research, 2017. **42**(2): p. 201-210.

116. Lombardo, M., et al., *Analysis of intraocular lens surface properties with atomic force microscopy.* J Cataract Refract Surg, 2006. **32**(8): p. 1378-84.

117. Lombardo, M., et al., *Surface roughness of intraocular lenses with different dioptric powers assessed by atomic force microscopy.* J Cataract Refract Surg, 2010. **36**(9): p. 1573-8.

118. Miyake, K., et al., *Correlation between intraocular lens hydrophilicity and anterior capsule opacification and aqueous flare.* J Cataract Refract Surg, 1996. **1**: p. 764-9.

119. Hollick, E.J., D.J. Spalton, and P.G. Ursell, *Surface cytologic features on intraocular lenses: Can increased biocompatibility have disadvantages?* Archives of Ophthalmology, 1999. **117**(7): p. 872-878.

120. Cunanan, C.M., et al., *Contact-angle analysis of intraocular lenses.* J Cataract Refract Surg, 1998. **24**(3): p. 341-51.

121. Moynihan, C.T., et al., *Dependence of the glass transition temperature on heating and cooling rate.* The Journal of Physical Chemistry, 1974. **78**(26): p. 2673-2677.

122. Bozukova, D., C. Pagnoulle, and C. Jérôme, *Biomechanical and optical properties of 2 new hydrophobic platforms for intraocular lenses.* Journal of Cataract & Refractive Surgery, 2013. **39**(9): p. 1404-1414.

123. [cited 2017 September]; Available from: https://www.aboutpharma.com/blog/2017/07/03/ocular-drug-delivery-market-to-be-worth-us18-124-billion-by-2025-manufacturers-collaborating-with-hospitals-to-bolster-positions/.

124. Fournier, M. and A. Dupraz-Poiseau. *US and EU regulations for drug-delivery systems: development considerations for innovative products.* 2012 [cited 2017 September]; Available from: http://voisinconsulting.com/sites/default/files/2012_Scrip%20Regulatory_Anne_Marielle.pdf.

125. *US: The regulatory process for medical devices* [cited 2017 September]; Available from: https://its.utmb.edu/documents/FDA-Medical-Device-Regulatory-Process-Timeline.pdf.

2 Controlled drug release from hydrogels for contact lenses: Drug partitioning and diffusion

The following results were published in the peer-reviewed International Journal of Pharmaceutics:

Table of Contents

2.1 Introduction

Understanding the mechanisms of drug release for each particular pair drug/hydrogel membrane is very important for the optimization of the release kinetics from the delivery devices, and also for the construction of good mathematical models, which allow correct predictions of the release profiles. In this chapter, an investigation of the loading and release process of ophthalmic drugs in hydrogels used as contact lens materials is presented. The partition and diffusion coefficients were determined, and the interpretation of the obtained results at the light of the existing theories was attempted. Diffusion coefficients of the studied drugs in water and PBS were determined by NMR (Nuclear Magnetic Resonance) at the IST-UL NMR facility, housed in Centro de Química Estrutural – University of Lisbon, in collaboration with Professor José Ascenso. The Donnan potential measurements were obtained in collaboration with Professor João Fernandes, member of Grupo de Estudos de Corrosão e Efeitos Ambientais, also housed in Centro de Química Estrutural – University of Lisbon.

The controlled drug release from hydrogels is an important issue for medical applications that has been under intensive investigation in the last decades, both experimentally [1, 2] or through mathematical modelling [3, 4], including empirical∕semi-empirical models, as well as mechanistic realistic ones [5-8]. The simplest mechanistic model is based on the assumption of a mass transfer process controlled by drug diffusion. However, in many cases, the drug transport through polymeric membranes depends on polymer swelling and drug-polymer interactions, and it should be considered as a diffusional transport process and as a partition phenomenon. Thus, an important feature of the delivery system is the equilibrium partition coefficient, K, of the drug which depends on the relative strength of the interactions of the drug with both the hydrogel, and the solvent. It is defined as the ratio between C_{gel} and C_{sol} which are, respectively, the equilibrium drug concentrations in the hydrogel, and in the aqueous solution at the end of the drug loading step. The partition coefficient may be related to the polymer volume fraction in the hydrogel, φ, through the introduction of an enhancement factor, E, as follows [9]:

$$K = E\,(1 - \varphi) \qquad\qquad \textbf{Equation 2.1}$$

Following the reasoning of Dursch and co-workers [10], this enhancement factor for a solute in a dilute solution may be decomposed as the product of three individual enhancement factors E_{HS}, E_{el} and E_{ad}. E_{HS} accounts for the hard-sphere size exclusion, E_{el} refers to electrostatic interaction, and E_{ad} considers specific solute adsorption on polymer fibers. The hard-sphere solute enhancement factor was calculated in Kotsmar *et al.* [9], based on the theoretical mesh size distribution of Ogston for a random assembly of infinitely long fibers, to be:

$$E_{HS} = \exp\left\{-4\varphi\left[\left({}^{r_s}\!/r_f\right)\left(1 + {}^{r_s}\!/r_f\right)\right]\right\} \qquad \textbf{Equation 2.2}$$

where r_s is the hydrodynamic radius of the solute and r_f is the radius of the polymer fiber. $E_{HS} < 1$ reflects partial rejection due to size exclusion, while $E = 0$ indicates that the solute is too large to penetrate the hydrogel network. The electrostatic enhancement factor was introduced by Dursch and co-workers [10], based on the Donnan theory [11], as:

$$E_{el} = \exp\left(-\frac{ZF\psi}{RT}\right) \qquad \textbf{Equation 2.3}$$

where Z is the charge number of the solute, F is the Faraday constant, ψ is the Donnan electric potential difference between the hydrogel and the bulk aqueous solution, R is the gas constant and T is the temperature. For nonionic solutes $E_{el} = 1$, while $E_{el} > 1$ indicates electrostatic attractions between the solute and the polymer and $E_{el} < 1$ reflects electrostatic repulsions.

The specific solute adsorption enhancement factor, E_{ad}, may be calculated, assuming that the solutes are dilute, by:

$$E_{ad} = [1 + K^H\varphi/(1-\varphi)] \qquad \textbf{Equation 2.4}$$

where K^H is Henry's constant for solute adsorption on the polymer chains [9].

At dilute concentration, solute diffusion in a nonadsorbing gel follows Fick's second law with a constant diffusion coefficient, D. This law may be extended to account for the solute specifically adsorbed to the polymer which is different from that diffusing in the liquid-filled spaces [12]. The resulting equation involves the number of moles of non-adsorbed solute

in the liquid-filled voids per liquid volume, C, and the number of moles of specifically adsorbed solute per unit polymer volume in the gel, n:

$$\frac{\partial C(t,x)}{\partial t} + \left(\frac{\varphi}{1-\varphi}\right)\left(\frac{\partial n(t,x)}{\partial t}\right) = D\left(\frac{\partial^2 C(t,x)}{\partial x^2}\right) \qquad \textbf{Equation 2.5}$$

This equation is valid under the following assumptions: 1) hydrogel swelling is not affected by the presence of the solute in dilute conditions; 2) diffusion occurs within the liquid phase of the hydrogel; 3) surface diffusion along the polymer chains is negligible. If n is given by Henry's law $n = K^H C$ (K^H is Henry's adsorption constant), an effective diffusion coefficient, D_e, describing solute transport in the gel may be defined [12]:

$$D_e = D/[1 + K^H\varphi/(1-\varphi)] \qquad \textbf{Equation 2.6}$$
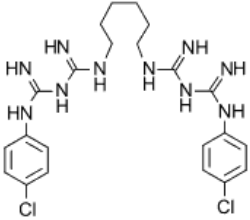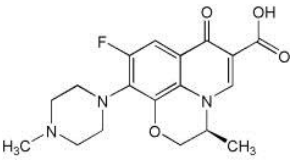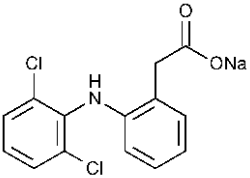
Equation 2.6 together with Equation 2.4 yields:

$$D = D_e E_{ad} \qquad \textbf{Equation 2.7}$$

As E_{ad} > 1, $D > D_e$, which means that the drug diffusion inside the hydrogel is retarded by drug adsorption on the polymer chains.

Three drugs, namely chlorhexidine (CHX), levofloxacin (LVF) and diclofenac (DCF), and two hydrogels which were recently investigated by our group [13]: a poly-hydroxyethylmethacrylate (PHEMA) based hydrogel and a silicone based hydrogel, were considered for this study. Chlorhexidine is used as antibacterial agent and topical disinfectant [14], levofloxacin is an antibiotic that is widely used both in the prophylaxis and treatment of ocular infections [15], and diclofenac is a nonsteroidal, anti-inflammatory drug with analgesic activity [16]. The characteristics of the drugs are given in Table 2.1.

Table 2.1 - Chlorhexidine, levofloxacin and diclofenac characteristics.

Drug	Structure	Ionicity	Solubiliy in water at 20ºC (mg/mL)	M$_W$ (g/mol)	pKa
CHX		Cationic	19	643.57	10.52
LVF		Zwitterionic	25	361.37	6.24 8.74
DCF		Anionic	2.37	318.13	4.15

The hydrodynamic radii (r_s) of the solutes were determined from measurements of the bulk aqueous diffusion coefficients, D_0, in water and in PBS, using Pulsed Gradient Spin-Echo (PGSE-NMR) and Stokes−Einstein theory [17]:

$$r_s = \frac{k_B T}{6\pi\eta D_o}$$ **Equation 2.8**

where k_B is the Boltzmann constant and, η, is the viscosity of the solvent. The volume polymer fraction in the hydrogel, φ, was determined from measurements of the swelling capacity. Thus, the enhancement factor, E, was obtained from Equation 2.1 and experimental determination of the partition coefficient. The value for E_{HS} was estimated from Equation 2.2, considering estimated values for the fiber radius of each hydrogel. The value of E_{el} was calculated using Equation 2.3 and experimentally determined values of ψ. The measurement of ψ was based on the method described by Higa and co-workers [18] which is described in section 2.2.4. Finally, $E_{ad} = E/(E_{HS}E_{el})$ may be obtained.

The effective diffusion coefficient, D_e, was obtained from fitting the experimental drug release profiles to an appropriate mathematical solution for the diffusion problem. Then, Equation 2.7 allows the calculation of, D, the Fick's second law diffusion coefficient of the drug if no interactions would occur between the solute and polymer. The diffusion coefficients of the non-adsorbed solutes, D, were correlated with the size of the solutes using two theories for hindered solute diffusion in hydrogels: the simplified steric model of Ogston and co-workers [19] and the model of Phillips and co-workers [20] which takes into account hydrodynamic and steric effects.

2.2 Experimental Part

2.2.1 Materials

2-Hydroxyethyl methacrylate, ≥99%, (HEMA), ethylene glycol dimethacrylate, 98% (EGDMA), 2,20-azobis(2-methylpropionitrile), 98% (AIBN), 3-tris(trimethylsilyloxy)silylpropyl 2-methylprop-2-enoate, 98% (TRIS), diclofenac sodium (DCF) and 0.01 M phosphate buffered saline (PBS) (NaCl 0.138 M; KCl - 0.0027 M; pH 7.4) were all purchased from Sigma-Aldrich. Poly(vinylpyrrolidone) (PVP K30, Kollidon®30) was kindly provided by BASF. N-Vinyl pyrrolidone, 98% (NVP), potassium chloride and sodium chloride were obtained from Merck, chlorhexidine diacetate monohydrate, 98% (CHX) from AppliChem, carbon tetrachloride from Riedel-de Haën, and dimethyldichlorosilane from Fluka. Distilled and deionized (DD) water was prepared in a Millipore Milli-Q system and had pH 5.6.

2.2.2 Hydrogel preparation, drug loading and release experiments

Two types of HEMA based hydrogels were prepared: HEMA/PVP (98/2, w/w) and TRIS/NVP/HEMA (40/40/20, w/w/w). The hydrogel preparation was described in previous works [13, 21]. In short, in the first case, an appropriate amount of the crosslinker EGDMA was dissolved in HEMA and the mixture was degassed before the addition of AIBN (initiator) and PVP. In the case of TRIS/NVP/HEMA hydrogel, TRIS (silicone monomer), NVP, HEMA and EGDMA were added to prepare a mixture which was degassed before the final addition of AIBN. Both mixtures were injected into a mold consisting of two silanized glass plates separated by a spacer of polyurethane or Teflon®. Thermo-polymerization was done at 60° for 1 h. For HEMA/PVP the free radical polymerization of

HEMA in the presence of PVP K30 is known to lead to semi-interpenetrating networks of PHEMA with PVP [22]. From ^{13}C solid-state NMR spectra, the molar ratio of the three monomers in the TRIS/NVP/HEMA hydrogel was determined to be 1.0/3.8±0.7/2.5±0.2. The presence of the crosslinker agent EGDMA was not taken into account.

The obtained hydrogel sheets were washed over 5 days, with DD water renewed three times a day, to remove unreacted monomers and to facilitate the cutting of the samples. The hydrated samples (10 mm in diameter and 0.25 or 0.30 mm in thickness for TRIS/NVP/HEMA and HEMA/PVP, respectively) were then dried, overnight, in an oven at 40 °C and stored dried.

The polymer volume fraction, φ, of the hydrogels was determined, as follows. Dry samples of each composition (three replicates each) were placed in DD water at 37ºC after determination of their dry weight, W_0. The samples were weighed at different times after careful wiping of their surface with absorbent paper and, when equilibrium was achieved, the constant weight, W_∞, was measured and the equilibrium water content, EWC, was calculated as follows:

$$EWC = \frac{W_\infty - W_0}{W_\infty}$$
Equation 2.9

Considering that the density of the dry and the hydrated hydrogels is close to 1000 kg/m3, EWC is equal to the water volume fraction, θ. The polymer volume fraction is $\varphi = 1 - \theta$.

The hydrogel samples were loaded with the drugs by soaking in the drug dissolved in PBS or water (V_{load} = 1 mL) with concentration of 1 mg/mL, until equilibrium was attained, at ambient temperature and under light protection. The equilibrium partition coefficient, K, was determined through the measurement of the drug concentration in the loading solution, before (C_0) and after (C_{sol}) the loading process:

$$K = \frac{C_{gel}}{C_{sol}} = \frac{V_{load}(C_0 - C_{sol})}{V_{gel}C_{sol}}$$
Equation 2.10

where V_{gel} is the volume of the hydrated sample ($V_{gel_{HEMA/PVP}}$= 23.6 mm3 and $V_{gel\_TRIS/NVP/HEMA}$ = 19.6 mm3). However, it holds also for partially reversible processes as

demonstrated on Dursch *et al.* [10] when studying partitioning of specifically adsorbed drugs in HEMA/ methacrylic acid (MAA) hydrogels.

Drug release was done in sink conditions by soaking each drug loaded lens in 3 ml of PBS or water, at 37 °C, in a closed vessel, under stirring (180 rpm). At pre-determined time intervals, aliquots of 0.2 mL of the supernatant were collected and replaced by the same volume of fresh PBS solution or water. At the end of the experiment, 1.8 mL of the release solution have been substituted by fresh medium. The drug concentration values were quantified using a spectrophotometer UV–VIS MultiscanGO from ThermoScientific® at wavelengths of 255 nm for CHX, 275 nm for DCF, and 290 nm for LVF. All measurements were done, at least, in triplicate.

Effective diffusion coefficients, D_e, were determined assuming the effective drug diffusivity independent of time and space, taking the space coordinate, x, with $x = 0$ at the center of the lens with total thickness of $2l$ $(-l < x < l)$, and describing the mass transfer from the material with a certain concentration of drug $(C(t,x))$, with the following equation:

$$\frac{\partial C(t,x)}{\partial t} = D_e \left(\frac{\partial^2 C(t,x)}{dx^2}\right)$$

Equation 2.11

The initial concentration in the lens $(C_{o,x})$ was assumed to be uniform and the concentration in the release medium was considered negligible since the release was done in sink conditions with replacement of the withdrawn aliquots by fresh solvent. A solution for this diffusion problem can be obtained from [23]:

$$\frac{M_t}{M_\infty} = 1 - \sum_{i=0}^{\infty} \frac{8}{(2i+1)^2\pi^2} \exp(-D_e(2i+1)^2\pi^2 t/4l^2)$$

Equation 2.12

where M_t denotes the total amount of drug that has diffused out of the lens at time t while M_∞ is the corresponding quantity after infinite time, and i is a dummy index. The ratio $M_\infty/Vgel$ defines the initial concentration in the lens $(C_{o,x})$. The experimental data was fitted to equation 12 using TableCurve® 2D software.

2.2.3 Determination of bulk diffusion coefficients using PGSE-NMR

Diffusion coefficients of the studied drugs in water and PBS were determined by the PGSE method in a NMR Bruker Avance III 500 MHz spectrometer with a 5 mm BBO probe

with a z-gradient shielded coil. This combination gives a maximum possible gradient of 0.55 Tm-1. A bipolar stimulated echo sequence (STE) with smoothed square gradients and WATERGATE solvent suppression was used [24]. The signal intensity (I) was monitored as a function of the square of the gradient amplitude (g) and the resulting self-diffusion coefficients (D_0) were calculated according to the echo attenuation equation for STE sequence:

$$I = I_0 exp\left[-D_0(\gamma\delta g)^2\left(\Delta - \frac{\delta}{3}\right)\right]$$

Equation 2.13

where I_0 is the intensity in the absence of gradient pulses, δ is the duration of the applied gradient, γ is the gyromagnetic ratio of the nucleus and Δ is the diffusion time.

The duration of the gradient pulses (δ) and the diffusion time (Δ) were optimized in order to obtain a residual signal of 2-5 % at the maximum gradient strength. The values used were 2.2 ms for the duration of the gradient pulses and 80 ms for the diffusion time. The gradient strength was incremented from 2% to 98% in a linear ramp with 16 steps. A delay of 15 s between echoes was used. The gradients were previously calibrated using 99.9 % pure D_2O as a standard. Each diffusion experiment produces a pseudo array of 16 spin echoes that were first FT processed in the t2 dimension using a LB of 0.2 Hz to generate a series of 1 D spectra that were phased and baseline corrected prior to extraction of the diffusion coefficient by Gaussian fittings using the T1/T2 relaxation module of Topspin 3.1. For each drug the areas of three or four single proton peaks were used in the fittings and the average D_0 value was taken.

Solutions of the drugs in water and PBS (~ 1 mg/ml) with 10% of D_2O for locking were poured in 5 mm NMR tubes to a total volume of 0.4 ml. To guarantee reproducibility of the results this geometry was kept in all the samples. Temperature was controlled at 37 °C by a BCU05 Bruker unit with an air flow of 521 Lh-1 and measured to within 0.1 K.

2.2.4 Measurement of Donnan potential of the hydrogels

The Donnan potential, $\Delta\phi_{don}$, at the interface between a charged polymer and a salt solution may be experimentally determined according to the method described by Higa co-workers [18]. In that method, two salt bridges are used: one connects the salt solution to one reference cell and the other connects the surface of the membrane to another

reference cell. The potential difference between the two cells is the sum of four contributions:

$$\Delta\phi = \Delta\phi_{don}^{B} + \Delta\phi_{don}^{S} + \Delta\phi_{liq}^{m} + \Delta\phi_{liq}^{s} \qquad \textbf{Equation 2.14}$$

where $\Delta\phi_{don}^{B}$ and $\Delta\phi_{don}^{S}$ are the Donnan potentials at the interfaces of the hydrogel with the salt bridge and the salt solution, respectively; $\Delta\phi_{liq}^{m}$ and $\Delta\phi_{liq}^{s}$ are, respectively, the liquid junction potentials of the hydrogel and the solution. The experimental apparatus used was similar to that described in Higa *et al* [18] and is sketched in Figure 2.1
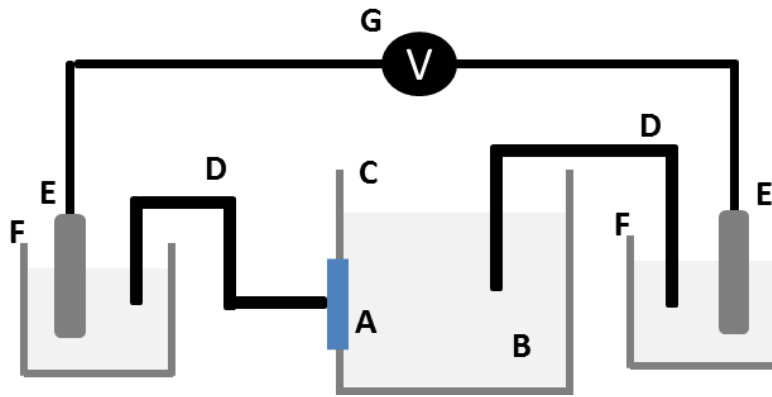
Figure 2.1 - Apparatus for the measurement of Donnan potential: A – Hydrogel; B – Water or PBS; C – Cell; D – salt bridges; E – saturated calomel reference electrode; F – reference cells; G – Sefram 7240 multimeter.

The salt bridges contained agar and 3 mol dm^{-3} KCl in glass tubes with total diameter of 0.6 cm. Under the condition that the hydrogel charge density is much smaller than the KCl concentration of the salt bridge, $\Delta\phi_{don}^{B}$ may be considered negligible. The liquid junction potentials were neglected following the reasoning by Higa and co-workers [18]. Eventual asymmetries between the two reference cells were corrected after calibration for the experimental conditions used. Thus, the total potential difference, $\Delta\phi$, gives a fairly good approximation for the Donnan potential at the interface between the hydrogel and the liquid medium. Prior to measurement, the hydrogels were immersed in water or PBS and the potential was continuously measured since the salt bridge contacted with the hydrogel surface. The value obtained after 1 minute of contact was considered in order to avoid long time interference of the highly concentrated KCl, which diffuses between the

salt bridge and the hydrogel, on the measured potential. The measurements were done, in duplicate, at room temperature (25ºC).

2.2.5 Determination of the mesh size of the hydrogels

To estimate the value of r_f, it is necessary to obtain the average mesh size of the hydrogels. The average mesh size $\langle \xi \rangle$ may be estimated from the zero-frequency shear storage modulus G´(0), using the rubber elastic theory, through the following equation [9]:

$$\langle \xi \rangle = l_{C-C} \sqrt{\frac{2C_F \rho RT}{M_r G´(0)}} \; \varphi^{-1/6} \qquad \qquad \textbf{Equation 2.15}$$

where IC-C is the length of the carbon-carbon bond in the backbone (0.154 nm), C_F is the Flory characteristic ratio = 6.9 for PHEMA [25], ρ is the density of the dry polymer and Mr is the molecular weight of a repeating unit.

The zero-frequency shear storage modulus G´(0) may be obtained from the experimental value of the Young's modulus, E, through the relation G´(0) =E/3, assuming a Poisson ratio of ½ for these materials [9]. The Young's modulus was determined from the slope of linear dependence of the stress–strain curves obtained during tensile tests performed on hydrogels swollen in PBS. The tests were made with a TA.XTplus Texture Analyser equipment, at room temperature, using a test speed of 0.3 mm/s, and making sure that the samples were kept well hydrated at all times during the experiment.

The parameters used in Equation 2.15 for both hydrogels are: ρ of dry HEMA/PVP equal to 1.14 g/mL and ρ of dry TRIS/NVP/HEMA equal to 1.04 g/mL; M_r of HEMA/PVP = 130.15 g/mol and M_r of TRIS/NVP/HEMA = 153.6 g/mol. In the absence of the value of C_F for TRIS /NVP/HEMA, the value of 6.9 was adopted.

2.3 Results and Discussion

The diffusion coefficients of the drugs measured in water and PBS, at 37 °C, are presented in Table 2.2 (except for CHX which is only slightly soluble in PBS) together with the hydrodynamic radii, r_s, calculated by substituting these diffusion coefficients in Equation 2.8.

Table 2.2 - Diffusion coefficients, D0, at 37 °C, and hydrodynamic radii, r_s, of the drugs. The uncertainties in Do values are less than 20%.

Drug	D$_0$ in water (m^2 s^{-1})	D$_0$ in PBS (m^2 s^{-1})	r_s in water (nm)	r_s in PBS (nm)
CHX	0.6 x10^{-9}	-	0.55	-
LVF	1.0 x10^{-9}	0.8 x10^{-9}	0.33	0.41
DCF	1.1 x10^{-9}	1.3 x10^{-9}	0.30	0.25

As expected, the diffusion coefficients decrease and the hydrodynamic radii, r_s, increase with increasing molecular weight (M_W) of the drugs. For charged molecules, the increase in ionic strength may lead to a decrease of electrostatic repulsions which is responsible for a higher tendency for aggregation with the consequent reduction of diffusivity; however, several authors found no effect of the ionic strength on the diffusion coefficients [26]. This is the case of anionic diclofenac where the difference between the values of the diffusion coefficients in water and in PBS lies within the analytical precision of the technique. The composition, the polymer volume fraction, the zero-frequency shear storage modulus G´(0) and the Donnan potential (in water and in PBS) of both materials are shown in Table 2.3. Assuming that the impurity present in HEMA/PVP is MAA [27], the amount of this impurity which should be responsible for a Donnan potential of -12.5 mV in PBS was calculated using [10]:

$$\frac{F\psi}{RT} = ln\left(\sqrt{\frac{E_{HS}^{Na^+}}{E_{HS}^{Cl^-}} + \alpha^2} - \alpha\right)$$

Equation 2.16

where F is the Faraday constant, ψ is the Donnan electric potential difference between the hydrogel and the bulk aqueous solution, R is the gas constant , T is the temperature, $E_{HS}^{Na^+}$ and $E_{HS}^{Cl^-}$ are the hard-sphere enhancement factors of ions Na+ and Cl- respectively, and $\alpha = C_{MAA^-}^{gel} / (2C_{NaCl}^{bulk} E_{HS}^{Cl^-} \theta)$. $C_{MAA^-}^{gel}$ is the molar concentration of charged MAA per total swollen hydrogel volume, C_{NaCl}^{bulk} is the NaCl molar concentration in PBS and θ is the water volume fraction in the hydrogel. $C_{MAA^-}^{gel}$ may be calculated from $C_{MAA^-}^{gel} = w_{MAA^-} f_{[-]}(1-$

$\theta)\rho_{dry}/M_{MAA^-}$, where w_{MAA^-} is the copolymer weight fraction, $f_{[-]} = 10^{-pKa}/(10^{-pH} + 10^{-pKa})$, pKa of MAA is 5.2, $\rho_{dry} = 1.15 \text{ g mol}^{-1}$ is the mass density of the dry polymer and M_{MAA^-} is the molecular weight of the monomer $M_{MAA^-} = 86.06 \text{ g mol}^{-1}$.

The Donnan potential is slightly lower in PBS due to the increased charge screening. Other measurements in PBS acidified to pH 2 with HCl led to ψ = -2.64 mV for HEMA/PVP, thus confirming that the MAA impurity became not ionized. Calculation of the amount of MAA which should be present in HEMA immersed in PBS to ensure ψ = -12.5 mV, led to a mass percentage of 0.425% which is compatible with the reported purity of 99% for HEMA. For TRIS/NVP/HEMA in PBS, the potential changed from slightly positive to slightly negative at pH 2 (-0.54 mV) which is difficult to explain, but, in any case, these values are close to zero and not meaningful.

Table 2.3 - Composition (w/w), polymer volume fraction,φ, zero-frequency shear storage modulus G′(0), Young's modulus (E) and Donnan potential, ψ, of the hydrogels.

	HEMA Hydrophilic	TRIS Hydrophobic	PVP Nonionic, hydrophilic	NVP Nonionic, hydrophilic	φ	G′(0) (MPa)	E (MPa)	ψ (mV)
HEMA/PVP	98	-	2	-	0.66	0.5	1.52 ± 0.08	In water: -14.6 In PBS: -12.5
TRIS/NVP/ HEMA	20	40	-	40	0.60	2.5	7.7 ± 0.9	In water: 7 In PBS: 1.13

From the G´(0) values, the average mesh sizes of both hydrogels were calculated by Equation 2.15 to be $\langle\xi\rangle$=4.0nm for HEMA/PVP and $\langle\xi\rangle$=1.6nm for TRIS /NVP/HEMA. The mesh size values reported in the literature for PHEMA depend on the cross-linking ratio and on the polymer volume fraction. Canal and Peppas [28] determined $\langle\xi\rangle$=2.6nm for PHEMA hydrogel with parameters $\varphi = 0.66$ and cross-linking ratio of 0.01 mol %, which are similar to those of our HEMA/PVP samples. Métrailler [29] obtained $\langle\xi\rangle$=2 nm for PHEMA samples with 40% of water and 2 wt.% EGDMA. The discrepancy between our value and those reported in the literature may be attributed to small differences in composition (e.g. the presence of PVP) and to the different methods used to determine the mesh size. The partition coefficients of the three drugs dissolved in water and in PBS (except CHX) with respect to both materials, HEMA/PVP and TRIS/NVP/HEMA, are given in Table 2.4. Comparison of the partition coefficients in water and PBS reveals that increasing ionic strength and pH significantly increases the partition coefficients of the anionic DCF. From the values of K and the volume polymer fraction in the hydrogel, φ, the enhancement factors, E, were calculated using Equation 2.1 and are presented in Table 2.4. All the enhancement factors are greater than unity, suggesting that drugs interact with the polymer chains through specific adsorption and/or electrostatic attraction.

Table 2.4 - Partition coefficients of the drugs, K, with standard deviations, and enhancement factors, E, calculated with Eq.1. Effective diffusion coefficients, De, calculated from the fitting of Eq. 12 to the experimental points shown in Figures 1 and 2, and r2 for De fittings.

		HEMA/PVP				TRIS/NVP/HEMA			
		K	E	D_e (m² s⁻¹)	r²	K	E	D_e (m² s⁻¹)	r²
In water	CHX	15.1±4.1	44.3	1.2 x10⁻¹²	0.9842	13.2±0.5	32.9	1.3 x10⁻¹²	0.9057
	LVF	13.5±6.5	39.8	6.1 x10⁻¹³	0.9947	6.1±0.6	15.3	5.5 x10⁻¹³	0.9973
	DCF	4.2±1.0	12.4	4.7 x10⁻¹³	0.9665	12.0±1.7	29.9	4.7 x10⁻¹³	0.8026
In PBS	CHX	-	-	-	0.9780	-	-	-	
	LVF	3.0±1.1	8.9	4.4 x10⁻¹³	0.9817	3.9±1.4	9.6	5.5 x10⁻¹³	0.9915
	DCF	34.2±1.0	100.6	5.5 x10⁻¹³	0.9830	37.4±2.4	93.4	4.1 x10⁻¹³	0.9594

The plots of the fraction release, $\frac{M_t}{M_\infty}$, of CHX, LVF and DCF in water as a function of time, t, from the HEMA/PVP and the TRIS /NVP/HEMA lenses, at 37 °C, are shown in Figure 2.2. In Figure 2.3, similar plots are presented for LVF and DCF in PBS. Experimental values of M_∞ varied with each system: drug/hydrogel/release medium: between 30 and 98 µg for chlorhexidine; between 15 and 60 µg for levofloxacin; between 75 and 675 µg for diclofenac.
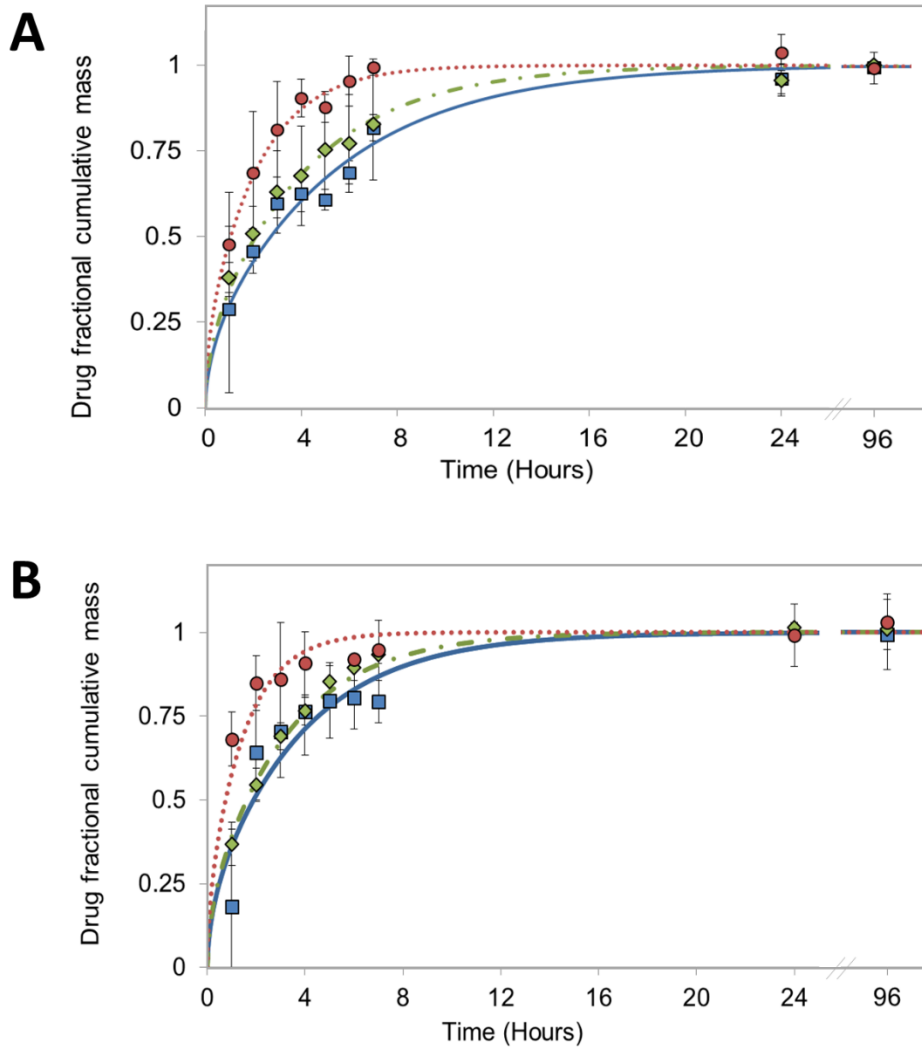
Figure 2.2 - CHX (red ·····), LVF (green — ·) and DCF (blue ——) fractional mass cumulative profiles for a) HEMA/PVP and b) TRIS/NVP/HEMA in water. Symbols represent the experimental results (□ DCF; ◊ LVF; ○ CHX) and lines, the fittings to Eq.12. The error bars represent ± standard deviations.
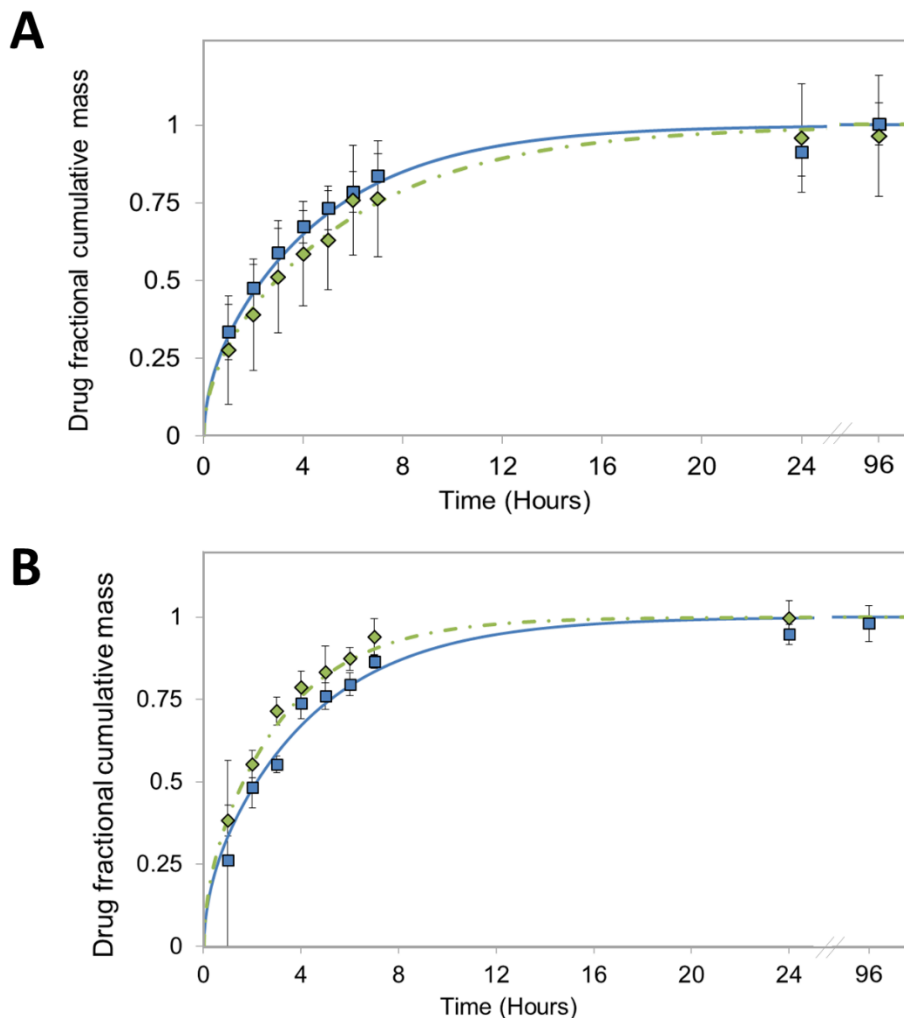
Figure 2.3 - LVF (green — ·) and DCF (blue ——) fractional mass cumulative profiles for a) HEMA/PVP and b) TRIS/NVP/HEMA in PBS. Symbols represent the experimental results (□ DCF; ◊ LVF) and lines, the fittings to of Eq.12. The error bars represent ± standard deviations.

The effective diffusion coefficients, D_e, were then calculated from the fitting of Equation 2.12 to the experimental points and are included in Table 2.4. Only one term was considered (i=0) since fitting with i= 0, 1 and 2 terms led to similar results. The effective diffusion coefficients of the drugs in the hydrogels immersed in both media do not reveal any correlation with the molecular weight of the molecules. We should stress here that the polymer volume fraction did not reveal to be sensitive to small changes in pH and ionic strength. Changing the medium from water to PBS led to an increase in EWC of both

61

hydrogels smaller than 3% which is in agreement with the findings of other authors relative to PHEMA [30]. Thus, the difference in the results obtained in water and in PBS must be attributed to the behavior of the drugs in solution and to their interactions with the polymeric membranes.

To understand the diffusion mechanism of the different drugs through the studied hydrogels, we tried to correlate the measured effective diffusion coefficients, D_e, with the diffusion coefficients, D, of the same solutes if they had not adsorb on the hydrogel chains and then, would follow Fick's second law. With this objective, the hard-sphere solute enhancement factors, E_{HS}, and the electrostatic enhancement factors, E_{el} were required to calculate E_{ad} from $E_{ad} = {E}/{(E_{HS}E_{el})}$, since Equation 2.6 could not be used without knowing the Henry's constants for adsorption on the polymer chains. The value of r_f, which was needed for the calculation of E_{HS} using Equation 2.2, was obtained from the average mesh size. According to the Ogston theory for the mesh size distribution [9], the average mesh size $\langle \xi \rangle$ is related with rf and φ, through the following equation [9]:

$$\frac{\langle \xi \rangle}{r_f} = \sqrt{\frac{\pi}{\varphi}} \, exp(\varphi) erfc \sqrt{\varphi} \qquad \textbf{Equation 2.17}$$

Using the values of $\langle \xi \rangle$ previously calculated, the following values for the fiber radius were obtained: r_f = 3.8 nm for HEMA/PVP and r_f =1.4 nm for TRIS /NVP/HEMA.

The electrostatic enhancement factors, E_{el}, were obtained substituting the measured values of Donnan potential in Equation 2.3. Then, the adsorption enhancement factors, E_{ad}, were calculated as explained above. The three calculated enhancement factors for the three drugs diffusing in both hydrogels, immersed in water and in PBS, are presented in Table 2.5.

Table 2.5 - Hard-sphere solute enhancement factors, E_{HS}, electrostatic interaction enhancement factors, E_{el}, and adsorption enhancement factors, E_{ad}, for the three studied drugs diffusing through HEMA/PVP and TRIS /NVP/HEMA hydrogels.

		HEMA/PVP			TRIS/NVP/HEMA		
		E_{HS}	E_{el}	E_{ad}	E_{HS}	E_{el}	E_{ad}
In water	CHX	0.65	3.15	21.81	0.27	0.56	219.41
	LVF	0.78	1	51.01	0.50	1	30.79
	DCF	0.80	0.56	27.45	0.54	1.34	41.75
In PBS	CHX	-	2.49	-	-	0.9	-
	LVF	0.73	1	12.16	0.40	1	23.92
	DIC	0.83	0.63	190.93	0.60	1.05	147.18

$E_{HS} < 1$ indicate partial rejection due to size exclusion [1] which is higher in TRIS/NVP/HEMA due to the smaller mesh size of this hydrogel. As expected, E_{HS} increases towards 1 as the hydrodynamic radius of the solutes decreases. E_{el} are < 1 when the solutes and the hydrogels repel each other and >1 in the opposite situation. In PBS the values of E_{el} are closer to 1 than in water due to charge screening. E_{el} >>1 for CHX in HEMA/PVP because CHX is a strong base at pH 6-9, presenting two positively charged amine groups which interact favorably with the negatively charged polymer. In water, E_{ad} is maximal for CHX in TRIS/NVP/HEMA, indicating a strong specific interaction between CHX and the TRIS monomers. Hydrogen bonding between the H bond donor amine groups in CHX and the H-bond acceptor silyloxy groups of TRIS may be responsible for this preferential interaction. In PBS, it was not possible to obtain E_{HS} and E_{ad} for CHX due to the solubility problems above referred and the most striking values refer to DCF. Once DCF is negatively charged, the reduction of the electrostatic repulsion between the adsorbed molecules, in the presence of PBS, should favor an increase in the adsorbed amount. The strong adsorption of DCF on HEMA monomers may be attributed, not only to hydrogen bonding between the three H bond acceptors in DCF and the hydroxyl groups in HEMA, but also to interactions between PVP chains and the aromatic rings in the DCF molecules. In fact, Molyneux and Frank [31] reported significant

interactions of PVP and aromatic compounds in aqueous solution through hydrophobic bonding and interactions between PVP and the aromatic π electrons of the solutes.

The diffusion coefficients of nonadsorbing solute, D, were calculated substituting the values of E_{ad} in Equation 2.7. They may be correlated with the size of the solutes using theories that describe hindered diffusion of macromolecules in nonadsorbing hydrogels [19, 20, 30, 32, 33]. Based on the assumption of Brady [34] that the relative diffusivity, defined as the ratio between the diffusion coefficients in the gel and in the dilute, bulk solution, is given by $D/D_0 = F \cdot S$, where F is a hydrodynamic-resistance factor and S is a steric factor, several diffusion models that have been proposed. In the simplest approach of Ogston et al. [19], the hydrodynamic-resistance is neglected (F = 1), and the relative diffusivity is given by:

$$D/\boldsymbol{D_0} = \boldsymbol{exp}(-\sqrt{\alpha})$$
<div align="right">**Equation 2.18**</div>

where $\alpha = \varphi\left(1 + \frac{r_s}{r_f}\right)^2$.

According to Phillips [20], both factors are taken into account and:

$$D/\boldsymbol{D_0} = \boldsymbol{exp}(-\boldsymbol{0.84}\alpha^{1.09})\,\boldsymbol{exp}(-a\varphi^b)$$
<div align="right">**Equation 2.19**</div>

where $a = 3.727 - 2.460\frac{r_f}{r_s} + 0.822\left(\frac{r_f}{r_s}\right)^2$ and $b = 0.358 + 0.366\frac{r_f}{r_s} - 0{,}0939\left(\frac{r_f}{r_s}\right)^2$.

The values of the diffusion coefficients of nonadsorbing solute, D, and of relative diffusivity (D/D0) as well as the values of α, for each solute in both hydrogels, immersed in water and in PBS, are given in Table 2.6. In water, the diffusion coefficients for the nonadsorbing solutes are 2 orders of magnitude greater than the corresponding effective diffusion coefficients, D_e, showing that the adsorption of the solutes on the polymeric fibers greatly retards the diffusion. In PBS, there is no data for CHX but, for DCF, the retardation of diffusion is even more accentuated (around 3 orders of magnitude in HEMA/PVP).

Table 2.6 - Diffusion coefficients of the nonadsorbing drugs, D, parameters $\alpha = \varphi \left(1 + \frac{r_s}{r_f} \right)^2$, and experimental values of the relative diffusivity (D/D0) of the drugs CHX, LVF and DCF in HEMA/PVP and TRIS/NVP/HEMA.

		HEMA/PVP			TRIS/NVP/HEMA		
		D	α	D/D_0 Exp.	D	α	D/D_0 Exp.
In water	CHX	2.62×10^{-11}	0.86	0.0436	2.85×10^{-10}	1.16	0.4754
	LVF	3.11×10^{-11}	0.78	0.0311	1.69×10^{-11}	0.92	0.0169
	DCF	1.29×10^{-11}	0.77	0.0177	1.96×10^{-11}	0.88	0.0178
In PBS	CHX	-	-	-	-	-	-
	LVF	5.35×10^{-12}	0.81	0.0067	1.32×10^{-11}	1.00	0.0164
	DCF	1.05×10^{-10}	0.75	0.0808	6.03×10^{-11}	0.83	0.0464

Comparison between the relative diffusivities, D/D_0, based on measured values and the relative diffusivities predicted with the models of Ogston and Phillips for each solute in each hydrogel, immersed in water and in PBS, is presented as a function of the fiber radius in Figure 2.4.
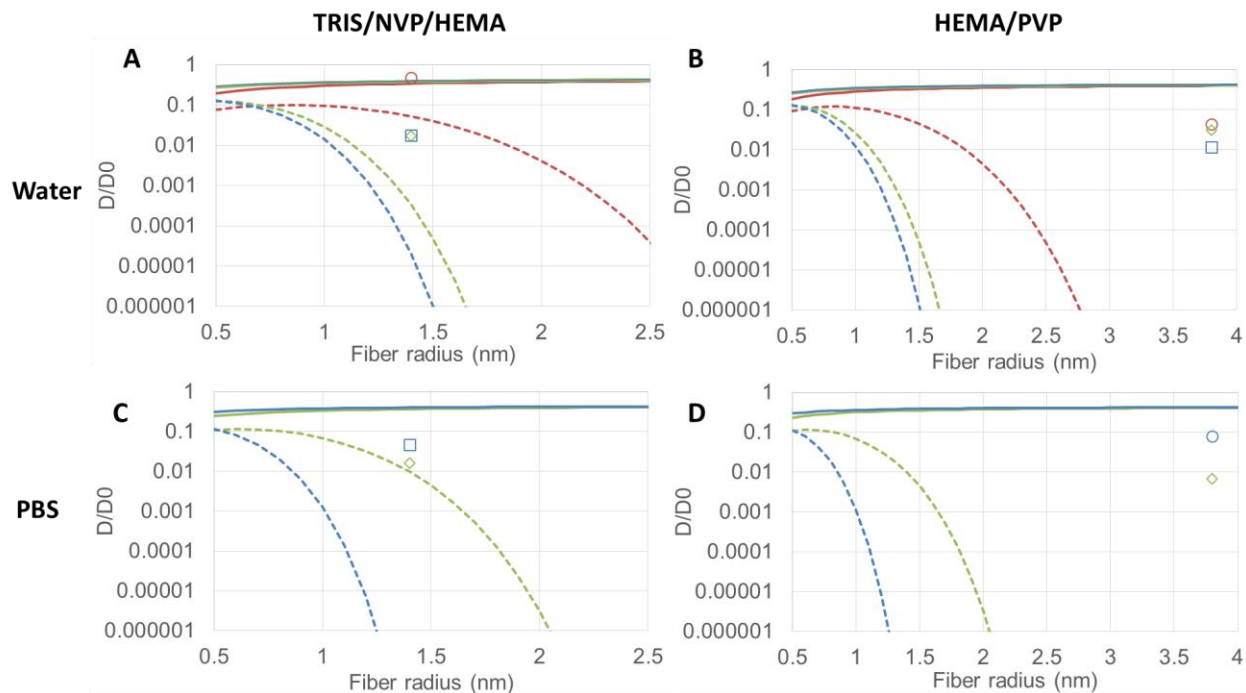
Figure 2.4 - Experimental relative diffusivity (symbols), D/D_0, and theoretical values obtained with the Ogston model - Equation 2.18 – (full lines) and the Phillips model - Equation 2.19 – (dashed lines) for CHX (○ red), LVF (◊ green) and DCF (blue □) in HEMA/PVP and TRIS/NVP/HEMA, immersed in water and in PBS, as a function of the fiber radius.

From this figure, we may conclude that the Ogston model yields values of D/D_0 almost independent of the fiber radius and much higher than the Phillips model. This latter model predicts null values for D when the radius of the fiber is considerably larger than the radius of the solute, which means that, in this case, the Phillips model is no longer applicable. Thus, in HEMA/PVP hydrogel characterized by a large fiber radius (3.8 nm), the experimental D/D_0 values are smaller than those predicted with the Ogston model, and cannot be described by the Phillips model.

For TRIS/NVP/HEMA with a small fiber radius (1.4 nm), the experimental D/D_0 of our larger solute (CHX) is in good agreement with the value predicted by the Ogston model. For the smaller molecules (DCF and LVF), the experimental D/D_0 values lie between those predicted by the Ogston and the Phillips models, meaning that some contribution of the effect of hydrodynamic drag must be considered. From this analysis, it is possible to

conclude that the relative diffusivity of CHX in TRIS/NVP/HEMA is mostly controlled by the steric factor which is the only factor taken into account by the Ogston model. In all other cases, the Ogston model underestimates the hindering in the diffusion inside the hydrogel while the Phillips model largely overestimates this hindering. This tendency in the Phillips model was recognized by the author who considered that it is not surprising that "a physical model that consists of a monomodal, homogeneous distribution of immobile, rigid fibers tends to yield a lower bound for D/D_0 [20]. Furthermore, the model of Phillips was found to give better agreement with experimental values for large solutes ($r_s > r_f$) which are not the conditions of our systems [35]. Even more sophisticated models did not reproduce the experimental values of diffusivity of other solutes through similar hydrogels. Liu and co-workers [12] studied the diffusion of dextrans with molecular masses of 4, 10, and 20 kDa and the cationic avidin protein in a HEMA/MAA (70/30,w/w) anionic hydrogel. They found that for dextrans, although being size excluded, the measured diffusivities were in good agreement with those predicted from a new effective-medium model which considered solute transport only in the accessible liquid-filled voids. In contrast, the protein strongly adsorbs to the polymer leading to quantitative disagreement between the calculated and measured effective diffusion coefficients. In our case, this effective-medium model was not applied because its application relies on the values of the hydraulic permeability of the aqueous solvent in the hydrogels which we do not know. Besides, the effective-medium theory underestimates the dynamic drag and obstruction of small solutes [12], .e. solutes smaller than the average mesh size, which is the case of the studied drugs.

We must refer at this point that, as the results are strongly dependent on the value of the fiber radius, different methods should be applied to measure this parameter, in order to achieve a reliable value. It would also be important to have experimental values for K^H in order to calculate E_{ad} independently, and to be able to further check the consistency of the applied models. The important conclusion from our experimental values of diffusion coefficients and partition coefficients is that the three studied drugs CHX, LVF and DCF adsorb on the polymeric strands of both hydrogels, independently of its charge or hydrophilicity.

67

2.4 Conclusions

Solute partitioning and diffusion in soft contact lens materials provide valuable information on the drug release mechanism of therapeutic contact lenses. In this work, we measured equilibrium partitioning and diffusion coefficients of several ophthalmic drugs, namely, chlorhexidine, levofloxacin and diclofenac in two contact lens materials: a PHEMA based hydrogel (HEMA/PVP) and a silicone based hydrogel (TRIS/NVP/HEMA). The diffusion coefficients, D_e, were experimentally determined from the drug release profiles from samples loaded in sink conditions. The hydrodynamic radii of the solutes were determined from measurements of diffusion coefficients in solution, D_0, with PGSE-NMR. From the values of the partitioning coefficients and the volume polymer fraction in the hydrogel, φ, the enhancement factors, E, were calculated following the approach developed by the group of C.J. Radke. As E > 1 in all cases, specific adsorption and/or attractive electrostatic interactions between the drugs and the polymeric chains are expected. In order to understand the causes for hindered diffusion of the solutes in the hydrogels, the hard-sphere solute, the electrostatic and the adsorption enhancement factors were calculated. E_{HS}< 1 indicated partial rejection of the solutes. E_{el} > 1 when the charges of the solutes and the hydrogels had opposite signs and E_{el} <1 in the opposite case. $E_{ad} \gg 1$ suggested that the three studied drugs specifically adsorb on both hydrogels, independently of their hydrophilicity. Adsorption was maximal for CHX on TRIS/NVP/HEMA due to strong hydrogen bonding. The relative diffusivity, D/Do, where D represents the diffusion coefficient of the nonadsorbing solutes, was compared with the predictions of the theoretical approaches of Ogston and Phillips for hindered diffusion of solutes in hydrogels. Good agreement was only found for the largest molecule (CHX) when using the Ogston model which considers exclusively the obstruction effect. The Phillips model whose applicability seems to be limited to large solute diffusion greatly underestimates the relative diffusivities of our small solutes.

2.5 References

1. Ratner, B.D. and A.S. Hoffman, *Synthetic Hydrogels for Biomedical Applications*, in *Hydrogels for Medical and Related Applications*, J. Andrade, Editor. 1976, American Chemical Society: Washington, D.C. p. 1-36.
2. Hoare, T.R. and D.S. Kohane, *Hydrogels in drug delivery: Progress and challenges.* Polymer, 2008. **49**(8): p. 1993-2007.
3. Siepmann, J. and F. Siepmann, *Mathematical modeling of drug delivery.* Int J Pharm, 2008. **364**(2): p. 328-43.
4. Peppas, N.A. and A.R. Khare, *Preparation, structure and diffusional behavior of hydrogels in controlled release.* Advanced Drug Delivery Reviews, 1993. **11**(1): p. 1-35.
5. Kaunisto, E., et al., *A mechanistic modelling approach to polymer dissolution using magnetic resonance microimaging.* J Control Release, 2010. **147**(2): p. 232-41.
6. Lamberti, G., I. Galdi, and A.A. Barba, *Controlled release from hydrogel-based solid matrices. A model accounting for water up-take, swelling and erosion.* International Journal of Pharmaceutics, 2011. **407**(1): p. 78-86.
7. Caccavo, D., et al., *Controlled drug release from hydrogel-based matrices: Experiments and modeling.* Int J Pharm, 2015. **486**(1-2): p. 144-52.
8. Caccavo, D., et al., *Modeling the Drug Release from Hydrogel-Based Matrices.* Molecular Pharmaceutics, 2015. **12**(2): p. 474-483.
9. Kotsmar, C., et al., *Aqueous Solute Partitioning and Mesh Size in HEMA/MAA Hydrogels.* Macromolecules, 2012. **45**(22): p. 9177-9187.
10. Dursch, T.J., et al., *Water-soluble drug partitioning and adsorption in HEMA/MAA hydrogels.* Biomaterials, 2014. **35**(2): p. 620-629.
11. Overbeek, J.G., *Colloid Science Vol. I Irreversible Systems*, ed. H.R. Kruyt. 1952, London: Elsevier Pub Co.
12. Liu, D.E., et al., *Macromolecule Sorption and Diffusion in HEMA/MAA Hydrogels.* Industrial & Engineering Chemistry Research, 2013. **52**(50): p. 18109-18120.
13. Paradiso, P., et al., *Comparison of two hydrogel formulations for drug release in ophthalmic lenses.* J Biomed Mater Res B Appl Biomater, 2014. **102**(6): p. 1170-80.
14. Mathers, W., *Use of higher medication concentrations in the treatment of acanthamoeba keratitis.* 2006. **124**(6): p. 923.
15. Dajcs, J.J., et al., *Effectiveness of ciprofloxacin, levofloxacin, or moxifloxacin for treatment of experimental Staphylococcus aureus keratitis.* Antimicrob Agents Chemother, 2004. **48**(6): p. 1948-52.
16. Goa, K.L. and P. Chrisp, *Ocular diclofenac. A review of its pharmacology and clinical use in cataract surgery, and potential in other inflammatory ocular conditions.* Drugs Aging, 1992. **2**(6): p. 473-86.
17. R. Byron Bird, W.E.S., Edwin N. Lightfoot *Transport Phenomena*. Revised 2nd Edition ed. 2007, New York: John Wiley & Sons.
18. Higa, M., A. Tanioka, and A. Kira, *A novel measurement method of Donnan potential at an interface between a charged membrane and mixed salt solution.* Journal of Membrane Science, 1998. **140**(2): p. 213-220.

19. Ogston, A.G., B.N. Preston, and J.D. Wells, *On the Transport of Compact Particles Through Solutions of Chain-Polymers.* Proceedings of the Royal Society of London. A. Mathematical and Physical Sciences, 1973. **333**(1594): p. 297-316.

20. Phillips, R.J., *A hydrodynamic model for hindered diffusion of proteins and micelles in hydrogels.* Biophysical Journal, 2000. **79**(6): p. 3350-3353.

21. Paradiso, P., et al., *Effect of plasma treatment on the performance of two drug-loaded hydrogel formulations for therapeutic contact lenses.* J Biomed Mater Res B Appl Biomater, 2015. **103**(5): p. 1059-68.

22. Yanez, F., A. Concheiro, and C. Alvarez-Lorenzo, *Macromolecule release and smoothness of semi-interpenetrating PVP-pHEMA networks for comfortable soft contact lenses.* Eur J Pharm Biopharm, 2008. **69**(3): p. 1094-103.

23. Crank, J., *The Mathematics of Diffusion.* Second Edition ed. 1975, Oxford: Clarendon Press.

24. Price, W.S., et al., *PGSE-WATERGATE, a new tool for NMR diffusion-based studies of ligand–macromolecule binding.* Magnetic Resonance in Chemistry, 2002. **40**(6): p. 391-395.

25. Peppas, N.A., H.J. Moynihan, and L.M. Lucht, *The structure of highly crosslinked poly(2-hydroxyethyl methacrylate) hydrogels.* Journal of Biomedical Materials Research, 1985. **19**(4): p. 397-411.

26. Gendron, P.O., F. Avaltroni, and K.J. Wilkinson, *Diffusion coefficients of several rhodamine derivatives as determined by pulsed field gradient-nuclear magnetic resonance and fluorescence correlation spectroscopy.* J Fluoresc, 2008. **18**(6): p. 1093-101.

27. E. Eckstein, L.P., M. Van de Mark, *A responsible hydrogel as a means of preventing classification in urological prostheses*, in *Polymers as Biomaterials*, W. Shalaby, Editor. 1984, Springer US: New York. p. 323-332.

28. Canal, T. and N.A. Peppas, *Correlation between mesh size and equilibrium degree of swelling of polymeric networks.* Journal of Biomedical Materials Research, 1989. **23**(10): p. 1183-1193.

29. Métrailler, S., *Measuring the mesh size of hydrogels*, in *Semester Proj. École Polytech. Fédérale Lausanne.* 2012.

30. Tomić, S.L., et al., *Swelling and drug release behavior of poly(2-hydroxyethyl methacrylate/itaconic acid) copolymeric hydrogels obtained by gamma irradiation.* Radiation Physics and Chemistry, 2007. **76**(5): p. 801-810.

31. Molyneux, P. and H.P. Frank, *The Interaction of Polyvinylpyrrolidone with Aromatic Compounds in Aqueous Solution. Part I. Thermodynamics of the Binding Equilibria and Interaction Forces1.* Journal of the American Chemical Society, 1961. **83**(15): p. 3169-3174.

32. Kim, J. and A. Chauhan, *Dexamethasone transport and ocular delivery from poly(hydroxyethyl methacrylate) gels.* Int J Pharm, 2008. **353**(1-2): p. 205-22.

33. Saini, G.S.S., et al., *Spectroscopic studies of rhodamine 6G dispersed in polymethylcyanoacrylate.* Spectrochimica Acta Part A: Molecular and Biomolecular Spectroscopy, 2005. **61**(4): p. 653-658.

34. Clague, D.S. and R.J. Phillips, *Hindered diffusion of spherical macromolecules through dilute fibrous media.* Physics of Fluids, 1996. **8**(7): p. 1720-1731.

35. Amsden, B., *Solute Diffusion within Hydrogels. Mechanisms and Models.* Macromolecules, 1998. **31**(23): p. 8382-8395.

3   Simulation of the hydrodynamic conditions of the eye to better reproduce the drug release from hydrogel contact lenses: experiments and modelling

Table of Contents

3.1 Introduction

For a controlled release system effectiveness evaluation, the amount of drug and time till total drug release are key factors, and are dependent on the pair drug-polymer physical-chemical interactions, which were the focus of the previous chapter. To obtain this information *in vitro* release studies are the most straightforward and used methods, but, although simple and useful to make comparative studies, they can fail to describe adequately the *in vivo* environment, especially the commonly used sink conditions. It is normally assumed that the release occurs in infinite sink conditions and the accumulation of drug in the solution surrounding the hydrogel is negligible, which can sometimes not be true. In fact, the low solubility of some drugs, the small volumes of release (e.g. 2-10 mL) and experiments performed without stirring often used in this type of experiments, may compromise the infinite sink conditions [1, 2]. It should be stressed that in the eye, sink conditions can be maintained if the drug clearance is high. However, the total clearance mechanism (including lacrimal turnover and absorption by conjunctiva) is complex and difficult to simulate in *in vitro* studies. Static conditions are generally used due to the simplicity of the experimental procedure and they are useful to compare different systems. However, they are far from simulating the real release conditions, since they do not match the ocular *in vivo* flow conditions. In a normal situation, the human eye contains a tear volume that ranges from 6.2 to 30.0 μL [3-5] and the tear flow rate assumes values between 0.9 and 2.1 μL.min^{-1} [6]. The use of contact lenses increases the tear turnover to values of the order 1.4-4.3 μL.min^{-1} [6]. In order to predict in a more reliable way the drug release kinetics in the eye, it is crucial to develop models that mimic, as close as possible, the hydrodynamic conditions of the eye.

Only a reduced number of articles have addressed this issue in the development of new therapeutic drug loaded SCLs. The group of M.E. Byrne used two microfluidic devices with different geometries [7, 8] to study the drug release behavior of SCLs materials under physiological flow rates. The results were compared with those obtained in static conditions. It was concluded that under flow conditions similar to those of the human eye, the release time of the drugs increased, and more sustained release profiles were obtained. More recently, Bajgrowicz et al. [9] achieved similar conclusions. They

compared the release of two drugs from commercial contact lenses, in static and dynamic conditions, and concluded that experimental parameters, such the volume of release and the flow rate, have a significant influence on the measured release profiles. Although the work of these groups has contributed to draw the attention to the importance of reproducing more closely the eye conditions in *in vitro* tests, in no case, a detailed characterization of the microfluidic devices operation was done. The use of numerical models yields information on the fluid flow inside the devices which is not accessible from experimental measurements. Furthermore, these models would allow predicting the impact of changing the inner chamber volume and/or the flow rate, on the drug release profiles.

In this chapter, a microfluidic cell is presented to mimic the tear flow rate and to approximate the *in vitro* drug release conditions to those found in the eye. Due to operational limitations, the volume of the inner chamber, where the hydrogel is placed, is higher than the tear film volume in the eye (while the minimum volume of the cell chamber that could be achieved was 45 µL, the maximum tear film volume in the eye is 30 µL). A conventional hydroxyethyl methacrylate-based hydrogel (HEMA/PVP) for SCLs loaded with an anti-inflammatory (diclofenac) was used as model system to obtain an experimental release profile using the microfluidic cell. This release profile was compared with the one obtained in static conditions.

The fluid dynamics in the microfluidic cell was fully characterized through numerical simulation using a computational model, in collaboration with Professors José M.C. Pereira and José C.F. Pereira from the Mechanical Engineering Department of the University of Lisbon. The fitting of the numeric model to the experimental drug release profile allowed the parametrical characterization of the system and the use of a release volume closer to the lower limit of the tear film volume. The *in vivo* drug release efficacy of the studied model system was predicted, taking into account the estimated drug concentration in the tear film volume.

3.3 Experimental Part

3.3.1 Materials

2-Hydroxyethyl methacrylate (HEMA), ethylene glycol dimethacrylate (EGDMA), 2,2'-azobis(2-methylpropionitrile) (AIBN), phosphate saline buffer (PBS, pH 7.4), phosphoric acid, monopotassium phosphate, diclofenac sodium (DCF), was all purchased from Sigma-Aldrich. Poly-(vinyl pyrrolidone) (PVP K30, Kollidon VR 30) was kindly provided by BASF. Acetonitrile and methanol were purchased from Fisher Scientific. A Millipore Milli-Q water purification system was used to get distilled and deionized (DD) water.

3.3.2 Hydrogels preparation

To prepare HEMA/PVP based hydrogels (98/2, w/w), an appropriate amount of the crosslinker EGDMA was dissolved in HEMA (hydrophilic monomer) to obtain a concentration of 80 mM. Then, the mixture was degassed by ultra-sounds (5 minutes) and bubbled with a gentle stream of nitrogen (15 minutes) before the addition of AIBN (initiator) to a final concentration of 10 mM, and PVP (hydrophilic additive) to a final concentration of 0.02 g.mL^{-1}. The solution was magnetically stirred for about 2 hours to obtain complete dissolution of PVP and injected into a mold consisting of two silanized glass plates (silanization procedure described in [10]) separated by a spacer of polyurethane. The polymerization reaction was performed at 50 °C for 14 hours, followed by 24 hours at 70 °C. The obtained hydrogel sheets were washed over 5 days, with DD water renewed three times a day, to remove unreacted monomers and to facilitate the cutting of the samples used in the study. The hydrated samples (thickness 0.30 mm) were cut with a leaker of diameter 1.4 cm and dried overnight in an oven at 35 °C.

3.3.3 Drug loading and drug release

The dry hydrogel samples were loaded with diclofenac by soaking in the drug solution (prepared with PBS) with a concentration of 1 mg.mL^{-1}, for 38 hours, at ambient temperature, in the dark. For the *in vitro* static drug release experiments, drug loaded samples were immersed in 4 mL of PBS solution in closed vessels, at 36 °C, under stirring

(180 rpm). At predetermined time intervals, 800 µl aliquots of the supernatant were collected and replaced by the same volume of fresh PBS solution.

In vitro dynamic drug release experiments were done in a microfluidic cell fabricated with in poly(methylmethacrylate) (PMMA). The microfluidic cell is constituted by one central feeding pipe and from eight radial exit pipes converging in a collector ring (see Figure 3.1). The cell was designed with a cylindrical inner chamber of 45 µL. This volume is slightly superior to the volume of the tear fluid present in the eye (6.2-30.0 µL) [3-5], but, due to operational constraints it could not be smaller.
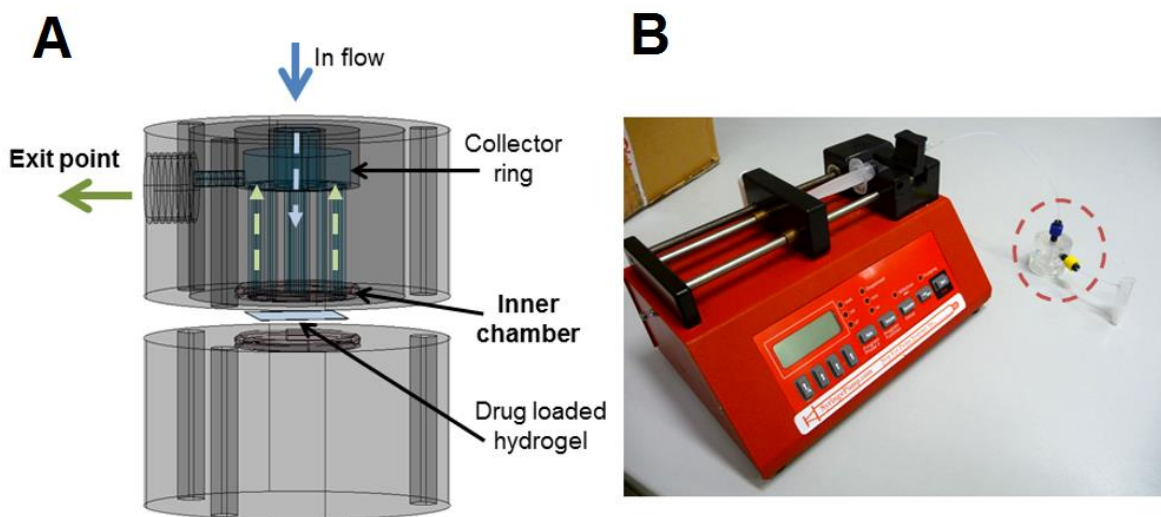
Figure 3.1 - A) Schematic representation of the microfluidic cell used to approximate *in vitro* to *in vivo*'s release conditions and B) experimental apparatus used in the dynamic release experiment

In order to approach the physiological conditions, the drug release experiments in the microfluidic cell were performed at 36°C and a continuous flow of PBS of 3 µL.min^{-1} was used. This flow rate is within the range of values found for contact lenses wearers (1.4-4.3 µL.min^{-1} [6]). At predetermined time intervals, the out flow solution was collected to be analyzed. All *in vitro* release experiments were carried out in triplicate.

The concentration of diclofenac in the collected samples was determined using a high performance liquid chromatograph (HPLC) with a Jasco UV–vis detector and a C-18 column Nova-Pak Watters, at the wavelength of 276. The mobile phase, consisting of phosphoric acid, acetonitrile and methanol (40/48/12 in volume), was introduced into the column at a flow rate of 1 mL.min^{-1} and a pressure of 14 MPa.

3.3.4 Numerical modeling of flow and transport

The flow inside the microfluidic cell was modeled through the numerical solution of the Navier-Stokes and continuity equations using the Star-CCM+ simulation package. The fluid was considered to be incompressible and with constant properties: density of 0.9937 g.cm^{-3} and dynamic viscosity of 0.0692 mPa.s at 36 ºC. The background fluid (tear fluid) was represented by the buffered saline (PBS). The drug flows in the tear fluid volume as a passive scalar. The passive scalar model is used since the drug properties do not affect the solution properties, due to the very low concentration of the drug. Diclofenac diffusivity in PBS, determined by Nuclear Magnetic Resonance (NMR), is 1.4x10^{-9} m^2.s^{-1}. Effective diffusivity in the hydrogels materials was determined by fitting the numerical model to the experimental release data obtained with the microfluidic cell (inner chamber 45 µL). The lens is modeled as a porous media with hydrodynamic permeability of 10^{-14} m^{2}s^{-1}Pa^{-1} [11, 12] and a polymer volume fraction in the swollen state of 0.62. The used mesh of trimmed topology comprises about one million control volumes, with higher cell density in the zone near the lens and tear film. The time step was 60 seconds. The effect of the mesh size and time stepping on the results was analyzed indicating independence on the used numerical parameters.

3.4 Results and Discussion

3.4.1 Comparison of static and dynamic release conditions

As previously referred, static conditions are used in drug release studies due to the simplicity of the experimental procedure. In Figure 3.2, the fractional cumulative DCF mass profile obtained in static conditions is compared with the one obtained using the microfluidic cell.
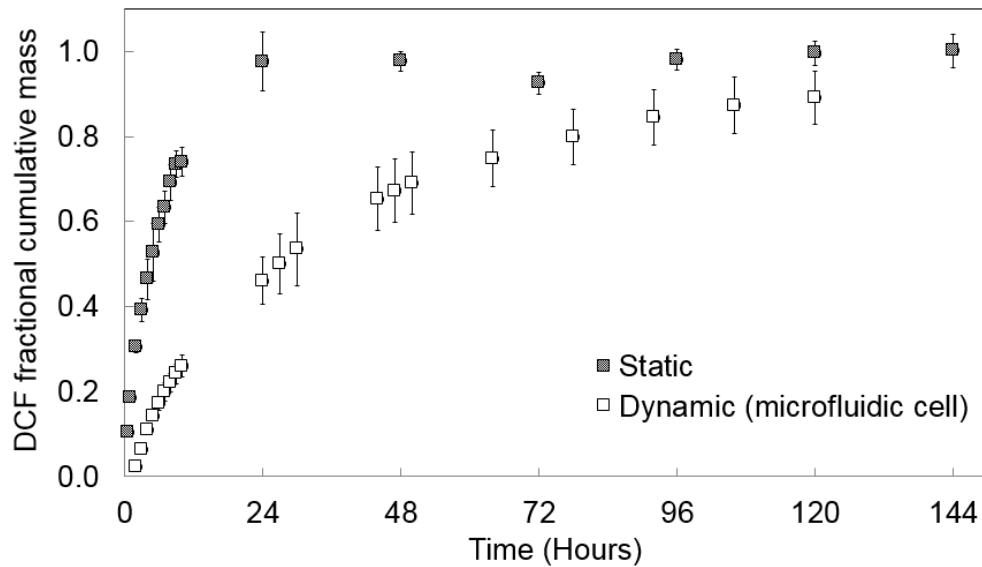
Figure 3.2 - DCF fractional cumulative mass release in static and dynamic conditions (microfluidic cell) from HEMA/PVP hydrogel

The release kinetics is greatly affected by the release conditions: in static conditions more than 90% of DCF is released upon the first 24 hours; in the inner chamber of the microfluidic cell the release progresses at a steady rate, reaching 90% of total release at approximately the 100th hour. Such differences in the drug release profiles can be understood through the analysis of the driving forces for drug release. The decrease of the release medium volume (from 4 mL, used in static experiments, to 45 µL in the microfluidic cell) leads to distinct concentration gradients between the drug loaded hydrogel and the release medium. In static experiments, the drug concentration in the release medium is well below the drug solubility limit, which is 6-9 mg.mL^{-1} for DCF in PBS [13]. In these conditions, the driving force produced by the gradient of concentrations between the hydrogel and the supernatant is maximum. Additionally, the mechanical stirring during the release experiment contributes to obtain a homogeneous medium and causes the disruption of any surface boundary effect. In turn, in microfluidic conditions, the more sustained release could be a consequence of the lower gradient of the drug concentration resultant from the small volume of release and flow conditions. Similar conclusions were achieved by other authors who compared the results in static conditions and under flow [7, 9]: the release time of the drugs increased under flow, being significantly affected by the volume of release and the flow rate.

Static conditions can be useful for an initial evaluation of a drug releasing system performance, as well as to make comparisons between different systems. Nevertheless, one should take in consideration that in static conditions the release environment is far from replicating the hydrodynamic conditions of the eye, as our results show.

A microfluidic system designed to approximate the *in vivo* conditions (volume and renovation rate) can provide more reliable information about the drug delivery system behavior, particularly in what concerns release rates and release amounts.

3.4.2 Evaluation of the microfluidic cell operation

In order to ensure that the designed cell behaves accordingly to the fluid mechanics principles, e.g. avoiding dead volumes, the cell operation was evaluated through the numerical flow modulation described above.

In terms of fluid dynamics, considering a flow rate of $3\mu L.min^{-1}$, the flow in the inner chamber of the microfluidic cell is found to stabilize due to the Stokes nature of the considered flow. Also, the unsteady diffusion of the drug into the inner chamber (further studied) appears to have a negligible effect in the fluid dynamic, again due to the very low concentration, both in mass and volume terms.

The fluid flows in the cell uniformly, as shown in the Figure 3.3 where some streamlines are drawn. The color is related to the local fluid velocity. Symmetric and very regular paths are followed by the fluid from the inlet pipe to the eight exiting pipes. In the leeward side of the returning pipes the velocity field also displays a regular pattern, therefore no dead zones are present in the flow. Vector field details are presented in Figure 3.3 B. From this figure one can verify the flow overall uniformity and alignment in the inner chamber.
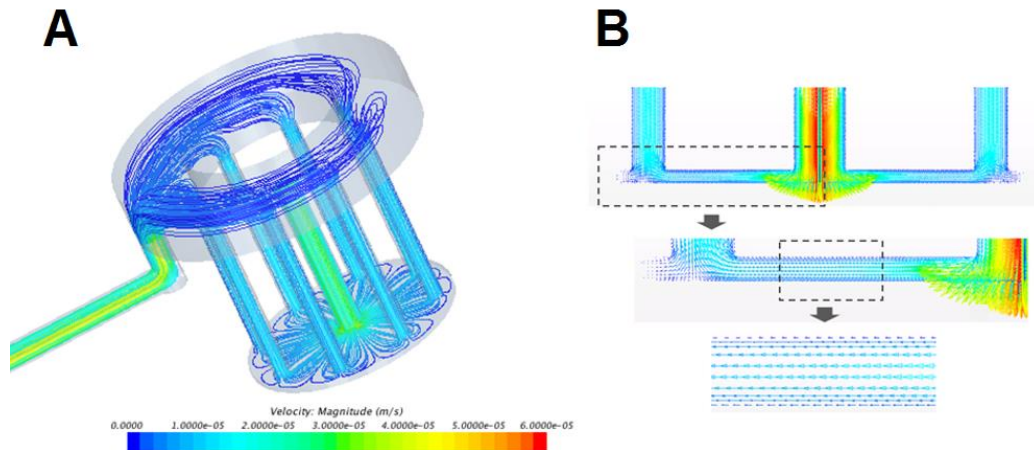
Figure 3.3 - A) Representation of the paths of fluid inside the microfluidic cell with a central entry point and eight radial exit points and B) vector field details in a cross section of the cell

3.4.3 Impact of the inner chamber volume on drug release profiles

Figure 3.4 presents the concentration profile of DCF released from HEMA/PVP hydrogel obtained with the microfluidic cell, whose inner chamber volume is 45 µL. The numerical model was fitted to the experimental data, setting the hydrogel properties (hydrodynamic permeability and porosity) and the external medium properties (density, viscosity and DCF diffusivity in PBS) - see values in Numeric flow modulation section.

Although a deviation between the data and the fitting is observed in the first 24 hours of release (r^2=0.734), the quality of the fitting greatly improved after that (r^2=0.964).

From the fitting, the effective diffusivity of DCF in the HEMA/PVP hydrogel was estimated to be 1.35 x10^{-13} m^2.s^{-1}.

Since it was not possible to design a microfluidic cell with an inner chamber volume inferior to 45 µL, the numerical tool was used to predict the drug release profile in a volume of 7 µL, which is close to the minimum value of the tear film, considering the value estimated for DCF diffusivity in HEMA/PVP. Both estimated profiles (for 45 µL and 7 µL) are also presented in Figure 3.4.
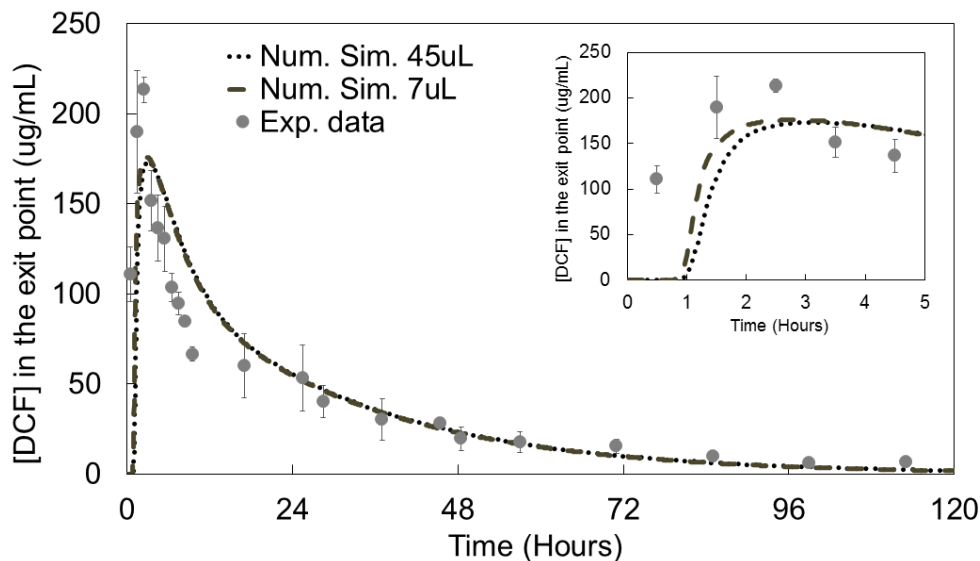
Figure 3.4 - Concentration profile of DCF released from HEMA/PVP at the exit point of the microfluidic cell and adjustment obtained using the numerical model for cells with inner chambers of 45 μL and 7 μL. Zoom for the first hours is included

It can be observed that the profiles estimated by numerical simulation are not significantly affected by the inner chamber volume. The initial lag observed in these curves does not find correspondence with the experimental data, because the experiment with the microfluidic cell started with the device filled with PBS to ensure that no air bubble was trapped inside. The first aliquot collected consists of PBS that was forced to pass through the inner chamber at a higher velocity, and thus, will drag some drug. This initial step could not be considered in the simulations. The obtained results allow us to conclude that our microfluidic cell is able to simulate the range of the human eye tear film volume (6.2 to 30.0 μL).

3.4.4 Efficacy of diclofenac loaded SCLs

It is important to stress that the results of simulation presented in Figure 3.4 are concentrations of DCF at the exit point of the system, since in the experimental assay this is the collection point of the aliquots for drug quantification. However, to approach the *in vivo* conditions, we should consider the concentration of DCF in the inner chamber (that represents the tear film volume), to estimate the efficacy of drug loaded SCLs. As far as

81

the authors know, all the reported studies using microfluidic devices to study drug release from SCLs rely on the measurement of drug concentrations at the exit point.

The drug concentration in the inner chamber can be estimated through the numerical simulation. In Figure 3.5, the predicted concentration profile of DCF for the 7 µL inner chamber of the microfluidic cell is shown. The concentration profile in the eye, resultant from application of commercial DCF eye drops, according to the recommend posology, is also represented. This profile was estimated considering the application of 1 drop of DCF commercial ophthalmic solution (e.g. Voltaren Ophthalmic®, 1 mg.mL^{-1}) each 4 hours during the day (the posology recommended for treatment of a post traumatic inflammation) and assuming that a volume of 7 µL of an eye drop remains in the eye and the tear renovation rate is 3 µL.min^{-1}.
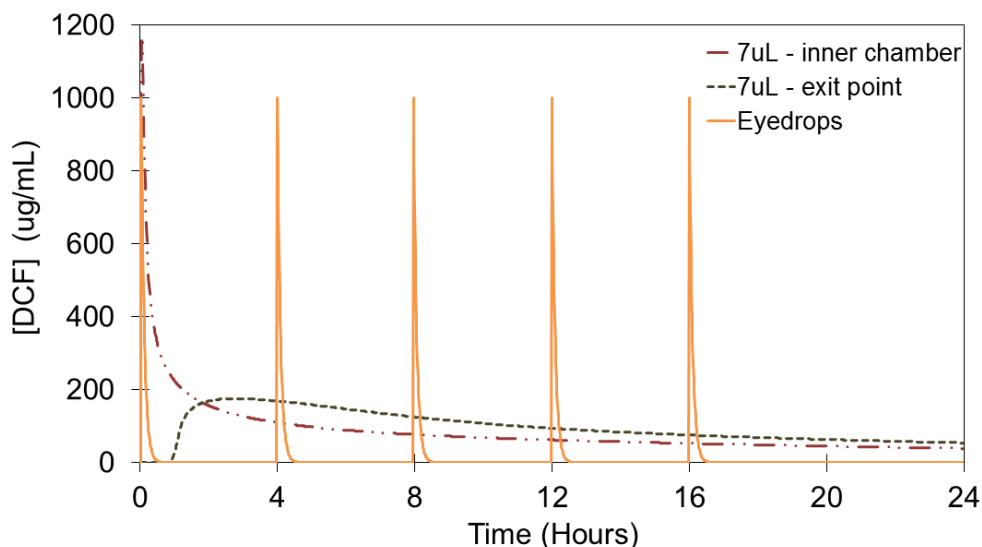
Figure 3.5 - Concentration profiles of DCF released from HEMA/PVP at the exit point and at the 7 µL inner chamber of the microfluidic cell, obtained using the numerical model. The concentration profile in the eye resultant from application of DCF eye drops is also shown

As expected, the periodic application of the eye drops leads to a saw shape drug concentration profile. In contrast, in the case of the drug loaded hydrogel, although the concentration profile at the inner chamber presents an initial burst, after the first few hours, a more sustained delivery is achieved. The maximum concentration achieved in the inner

chamber is slightly higher than that obtained by application of the eye drops. One should note that the chosen inner chamber volume is close to the lower limit of the tear film volume in the eye, whereby, higher tear film volumes should lead to lower burst values. The comparison of the concentration profiles correspondent to the inner chamber and the exit point shows a significant difference during the first 2 hours which faints afterwards.

To assess the efficacy of the drug release system herein studied, the therapeutic amount which has to be delivered to the eye was estimated. As mentioned above, when eye drops are applied, only 1-7% of the administered dose is absorbed. Considering an eye drop of 34 µl [14] and an effective absorption of 5%, the recommend posology delivers, in one day, 8.5 µg (5 x 1 drop). Taking this value into account, one can predict for how long the studied hydrogels release a therapeutic amount of drug. In Table 3.1 the DCF mass released per day from a SCL, obtained by numerical simulation for the inner chamber, is shown. An average dry weight of 30 mg was assumed for the SCL.

Table 3.1 - Amount of DCF released from HEMA/PVP SCLs, estimated by numerical simulation

Day	DCF mass (µg/lens)
1	420.0
2	127.7
3	54.0
4	22.8
5	9.7
6	3.6

The results analysis suggests that the HEMA/PVP SCLs loaded with DCF shall be effective during $\approx$ 5 days.

It should be underlined that the studied system (drug + hydrogel) is a model system. Thus, several aspects may require optimization to develop a commercial therapeutic device. For example, instead of using a HEMA-based, which has a low oxygen permeability, we could use the newer silicon hydrogels that, due to their higher oxygen permeability would be more suitable for a prolonged drug release [15]. Also, the loading procedure could be modified to adjust the amount of drug released. However, the focus

of this work is not the optimization of a specific drug delivery system, but rather finding a way to better simulate the behavior of the drug loaded lenses *in vivo*.

In conclusion, the use of the microfluidic cell to access the drug release profiles in hydrodynamic conditions which are closer to those found *in vivo* (in particular volume and renovation rate)*,* associated with the application of the numerical model that predicts the drug concentration in the tear film volume, shall be a valuable tool to design and optimize new therapeutic SCLs.

3.5 Conclusions

In the last years, an increasing number of studies has focused on the development of drug delivery systems for ophthalmic applications, based on SCLs. In almost all those studies, the *in vitro* drug release profiles are obtained in static conditions, very different from those found in the eye.

In this work, a microfluidic cell was designed to simulate the hydrodynamic conditions of the eye, namely the low volume of tear fluid and its continuous renovation. The release of a non-steroid anti-inflammatory commonly used in ocular therapy (diclofenac) from a conventional HEMA-based hydrogel for contact lenses was investigated. The drug release profiles in static conditions and obtained with the microfluidic cell were compared. As expected, the release time of the drugs increased under flow.

The flow inside the microfluidic cell was characterized using a computational fluid dynamics numerical model based on the Navier-Stokes and continuity equations. It was demonstrated that the fluid flows in the cell uniformly without dead zones, which testifies the adequate operation of the cell.

The numerical model was fitted to experimental data obtained with the cell, using as adjustment parameter the diffusivity of the drug in the hydrogel. The model was then used to evaluate the effect of changing the volume of liquid in contact with the hydrogel, on the drug release profiles. The reduction of the volume from 45 μL (the volume of the inner chamber of the cell used) to 7 μL (≈ the lower limit of the tear volume in the eye) led to minor differences in the concentration profiles of the solution collected from the cell,

demonstrating that the designed microfluidic cell may be used to simulate lower volumes, within the tear film volume range.

The numerical model was applied to estimate the drug concentration in the volume of liquid in direct contact with the hydrogel, which, in the first few hours, is significantly different from that measured experimentally (from solutions collected at the exit point of the microfluidic cell). This estimated concentration simulates the tear film concentration and allows a more reliable prediction of the *in vivo* efficacy of the drug loaded hydrogel than that based on common static drug release experiments.

3.6 References

1. Tieppo, A., et al., *Analysis of release kinetics of ocular therapeutics from drug releasing contact lenses: Best methods and practices to advance the field.* Cont Lens Anterior Eye, 2014. **37**(4): p. 305-13.
2. White, C.J., A. Tieppo, and M.E. Byrne, *Controlled drug release from contact lenses: a comprehensive review from 1965-present.* Journal of Drug Delivery Science and Technology, 2011. **21**(5): p. 369-384.
3. Mishima, S., et al., *Determination of Tear Volume and Tear Flow.* Investigative Ophthalmology & Visual Science, 1966. **5**(3): p. 264-276.
4. Stamper, R.L., M.F. Lieberman, and M.V. Drake, *CHAPTER 22 - Medical treatment of glaucoma: general principles*, in *Becker-Shaffer's Diagnosis and Therapy of the Glaucomas (8th Edition)*. 2009, Mosby: Edinburgh. p. 345-358.
5. Farris, R.L., *Tear analysis in contact lens wearers.* Transactions of the American Ophthalmological Society, 1985. **83**: p. 501-545.
6. Glasson, M.J., et al., *The effect of short term contact lens wear on the tear film and ocular surface characteristics of tolerant and intolerant wearers.* Cont Lens Anterior Eye, 2006. **29**(1): p. 41-7.
7. Ali, M., et al., *Zero-order therapeutic release from imprinted hydrogel contact lenses within in vitro physiological ocular tear flow.* J Control Release, 2007. **124**(3): p. 154-62.
8. Tieppo, A., K.M. Pate, and M.E. Byrne, *In vitro controlled release of an anti-inflammatory from daily disposable therapeutic contact lenses under physiological ocular tear flow.* European Journal of Pharmaceutics and Biopharmaceutics, 2012. **81**(1): p. 170-177.
9. Bajgrowicz, M., et al., *Release of Ciprofloxacin and Moxifloxacin From Daily Disposable Contact Lenses From an In Vitro Eye Model.* Invest Ophthalmol Vis Sci, 2015. **56**(4): p. 2234-42.
10. Vazquez, R., et al., *Stability of triglyceride liquid films on hydrophilic and hydrophobic glasses.* J Colloid Interface Sci, 2006. **299**(1): p. 274-82.
11. Pishko, G.L., et al., *Hydraulic permeability of a hydrogel-based contact lens membrane for low flow rates.* Journal of Applied Polymer Science, 2007. **104**(6): p. 3730-3735.
12. Refojo, M.F., *Permeation of water through some hydrogels.* Journal of Applied Polymer Science, 1965. **9**(10): p. 3417-3426.
13. *Diclofenac sodium salt, material safety DATA, product informations by Cayman Chemical Company.* 2014 [cited 2017 September]; Available from: https://www.caymanchem.com/msdss/70680m.pdf.
14. German, E.J., M.A. Hurst, and D. Wood, *Reliability of drop size from multi-dose eye drop bottles: is it cause for concern?* Eye, 1999. **13**(Pt 1): p. 93-100.
15. Nicolson, P.C. and J. Vogt, *Soft contact lens polymers: an evolution.* Biomaterials, 2001. **22**(24): p. 3273-3283.

4 Controlled release of moxifloxacin from intraocular lenses modified by Ar plasma-assisted grafting with AMPS or SBMA: an *in vitro* study

Table of Contents

4.1 Introduction

In this chapter, the potential of an antibiotic-eluting IOL, made from a hydrophilic polymethacrylate-based copolymer, to be used in postoperative prophylaxis of endophthalmitis will be investigated. The IOLs surface modification was done in the University of Coimbra, within the context of a collaborative research project funded through the M-ERA.NET consortium. The cytotoxic evaluation was performed in the research group headed by Professor Ilídio Correia at University of Beira Interior. Ellipsometry measurements were obtained through a collaboration with Professor Luís Santos, from Centro de Química Estrutural – University of Lisbon.

The chosen antibiotic was moxifloxacin (MFX) due to its activity against two of the most common postoperative pathogens, *Staphylococcus aureus* and *Staphylococcus epidermidis*, [1-3], combined with its stability and thermal resistance [4, 5]. Other ophthalmic antibiotics could not be used for this purpose due to their low stability in aqueous solution (e.g. cefuroxime suffers hydrolysis [6]). Thermal resistance is also a concern, since autoclaving at high temperatures is a common inexpensive method for terminal sterilization of IOLs. Surface modification of the polymeric material by argon plasma-assisted grafting was tested, aiming to create a physical/chemical barrier able to control the release of the antibiotic. Two electrically charged monomers were selected: (i) AMPS (2-acrylamido-2-methylpropane sulfonic acid), a monomer used in superabsorbent hydrogels [7], containing a sulfonic acid group with a very low pKa, which is completely ionized at physiological pH, and (ii) SBMA ([2-(methacryloyloxy)ethyl]dimethyl-(3-sulfopropyl)ammonium hydroxide), a zwitterionic monomer, also used in superabsorbent hydrogels, with antibiofouling and antimicrobial properties [8]. At physiological pH, most MFX molecules in solution are in the zwitterionic form and some, in the cationic form [9]. Thus, interactions of MFX with the negatively charged AMPS and with the zwitterionic SBMA are expected to affect the drug release kinetics. Plasma-assisted grafting copolymerization was selected as a surface modification method due to its advantages, in particular: (i) plasma penetrates organic matter just a few nanometers [10], which allows keeping the bulk of the sample unchanged; (ii) no polymerization initiators are required, avoiding the need to extract eventual residues; (iii) it is already used industrially for surface

modification of IOLs (e.g., to improve their hydrophilicity) [11]. After grafting, which was carried out in the presence or in the absence of MFX, samples were soaked in an MFX solution.

Drug release studies from the modified systems were performed under sink and dynamic conditions. A new microfluidic cell was used in the latter case, to approximate the conditions found in the eye, in particular, the volume and renovation rate of the aqueous humor. Several surface and bulk properties of the material were evaluated before and after surface modification: wettability, topography/morphology, transmittance, refractive index and coating thickness. Cytotoxicity towards relevant cells (rabbit corneal endothelial cells) was assessed. Based on the results of drug release studies and material characterization, the most promising modification was identified and applied to prototype IOLs made from the same material. The modified IOLs were then sterilized in the MFX loading solution, by autoclaving, and stored for 30 days. Drug release studies were repeated under dynamic conditions and the antibacterial activity of the drug released was tested against *S. aureus* and *S. epidermidis*.

4.2 Experimental Part

4.2.1 Materials

Prototype IOLs (+20 diopter) and discs (diameter 1.6 cm and thickness 1 mm), made from a poly[(2-hydroxyethyl methacrylate)-co-(methyl methacrylate)]-based copolymer (26% equilibrium water content) which contained a proprietary blue-light filtering yellow chromophore [12], were provided by PhysIOL S.A. (Belgium). Both lenses and discs were Soxhlet-extracted with distilled water before use (ca. 60 extraction cycles), to remove monomer and initiator residuals. Discs were cut into smaller samples with a cork borer (diameter of 5 mm). 2-Acrylamido-2-methylpropane sulfonic acid (AMPS) and [2-(methacryloyloxy)ethyl]dimethyl-(3-sulfopropyl)ammonium hydroxide (SBMA) were supplied by Sigma-Aldrich (Sintra, Portugal) and moxifloxacin hydrochloride was supplied by TSZCHEM/BioTang (USA). Hank's balanced salt solution (HBSS) was prepared by dissolving 8 gL^{-1} of NaCl, 0.4 gL^{-1} of KCl, 0.0356 gL^{-1} of Na_2HPO_4, 0.06 gL^{-1} of KH_2PO_4, 0.144 gL^{-1} of $CaCl_2$, 0.12 gL^{-1} of $MgSO_4$ and 0.35 gL^{-1} of $NaHCO_3$ in Milli-Q water, and

adjusting the pH value to 7.4. Culture medium for the antimicrobial activity evaluation (Muller Hinton agar) and the antimicrobial susceptibility testing discs were provided by Oxoid (UK). For the cytotoxicity evaluation, the determination of the number of viable cells was carried out with the MTS proliferation assay, employing the CellTiter 96® AQueous One Solution Reagent, which contains MTS [3-(4,5-dimethylthiazol-2-yl)-5-(3-carboxymethoxyphenyl)-2-(4-sulfophenyl)-2H-tetrazolium, inner salt] and PES (phenazine ethosulfate), from Promega (Madison, USA). Fetal bovine serum (FBS) was purchased from Biochrom AG (Berlin, Germany) and Eagle's Minimum Essential Medium (MEM), amphotericin B and trypsin were purchased from Sigma-Aldrich (St. Louis, USA). All chemicals and reagents were of analytical grade and were used as supplied.

4.2.2 Plasma grafting, drug loading and release experiments

Surface modification by plasma-assisted grafting with AMPS or SBMA was conducted in a prototype low-pressure plasma reactor (FEMTO, Diener Electronic GmbH, Germany), composed of a stainless steel chamber of 100 mm diameter and 270 mm length. Treatment of the discs surface was carried out by placing the samples 80 mm from the electrode and exposing each face for 3 min to argon plasma generated at a chamber pressure of 0.6 mbar and 100 W of power. Then, samples were immediately immersed in a 10% (v/v) solution of AMPS or SBMA in HBSS, in the absence or in the presence of MFX (5 mgmL^{-1}), and kept for 8 hours at 60 ºC. After a washing step, in which all grafted samples were thoroughly washed with distilled water to remove unreacted monomers, water in excess was blotted from the surface. Table 4.1 summarizes the different types of samples produced.

Table 4.1 - Modified samples studied.

Samples	Monomer used for grafting	Ar plasma-assisted grafting in the presence of MFX
AMPS_0	AMPS	No
AMPS_1		Yes
SBMA_0	SBMA	No
SBMA_1		Yes

All samples were then loaded with MFX by soaking in 250 μL of a 5 mgmL^{-1} solution in HBSS for 15 hours, at 37 ºC, under shaking at 100 rpm. Finally, after a quick dip in water, to remove surface-adsorbed MFX that would be released at the beginning of the drug release studies, all samples were vacuum dried at room temperature before use.

When prototype IOLs were employed, after the modification and drug loading steps, the lenses were sterilized in an autoclave (at 121 ºC, 1 bar, for 30 minutes) in the MFX loading solution and stored for 30 days at room temperature before use.

Drug release studies were carried out under sink and dynamic conditions. Release under sink conditions was performed by placing the MFX-loaded samples in closed vials containing 3 mL of HBSS, at 37 ºC, under shaking at 100 rpm. At predetermined time intervals, 0.5 mL aliquots of the release medium were collected and replaced with the same volume of fresh HBSS. The MFX concentration present in the collected samples was determined by UV-vis spectrophotometry at 290 nm, employing a Jasco V550 UV-vis spectrophotometer (Jasco Corp., Japan). To achieve dynamic conditions, a home-made microfluidic cell was employed (see Figure 4.1). It was fabricated in poly(methyl methacrylate) (PMMA) with a cylindrical inner chamber of 250 μL of capacity, similar to the average volume of the aqueous humour present in the eye [13]. The inner chamber of the cell admitted the HBSS solution through 8 radial entry points and released the drug eluting solution from a central exit point. In order to approximate the physiological conditions, the experiments were performed at 37 °C with a continuous HBSS flow of 2.5 μL min^{-1}, mimicking the aqueous humour renovation rate of ~1% min^{-1} [13]. At predetermined time intervals, the outflow solution was collected to be analysed. The drug concentration in the collected samples was quantified at 290 nm using a UV–VIS spectrophotometer (Multiscan GO from ThermoScientific®, USA).
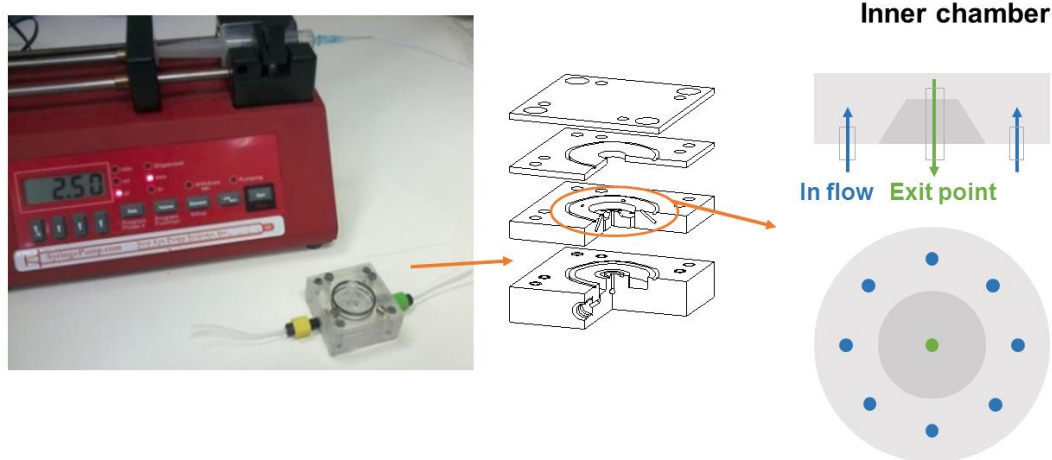
Figure 4.1 - Experimental apparatus used in the dynamic release experiment and schematic representation of the microfluidic cell inner chamber used to approximate *in vivo*'s release conditions.

Experiments were carried out in triplicate and each data point was the average of the obtained values. The results were expressed as mean ± standard deviation (SD).

4.2.3 Characterization

4.2.3.1 Swelling capacity and wettability

The swelling capacity was determined by placing pre-weighted dry discs in distilled water at room temperature. Their weight was monitored until equilibrium swelling was reached, by removing the sample, gently wiping the water remaining on the surface, and weighting. The swelling capacity was calculated according to Equation 4.1:

$$\textbf{Swelling capacity } (\%) = \frac{\boldsymbol{W_\infty - W_0}}{\boldsymbol{W_0}} \times \textbf{100} \qquad \textbf{Equation 4.1}$$

where w_∞ is the mass of the sample at equilibrium and w_0 is the mass of the dry sample. The experiment was carried out in triplicate and results were expressed as mean ± SD.

Wettability was assessed through the measurement of water contact angles on the hydrated discs, at room temperature, using the captive bubble method. The samples were placed horizontally in a measuring cell containing water. A micrometric syringe with a

curved-end needle was used to form air bubbles (3-4 µL) underneath the inferior surface of the samples. A set of images was acquired at pre-defined time intervals during 60 seconds using a video camera (JAI CV-A50) mounted on an optical microscope (Wild M3Z) and connected to a frame grabber (Data Translation DT3155). The acquisition and analysis of the images were performed using the ADSA-P software (Axisymmetric Drop Shape Analysis Profile). At least, ten bubbles were measured per sample.

4.2.3.2 Coating thickness, refractive index and transmittance

The thickness of the coating layer on the hydrated discs modified by Ar plasma grafting with AMPS or SBMA (AMPS_0 and SBMA_0) and the refractive index were determined with a spectral ellipsometer (UVISEL spectroscopic ellipsometer, from HORIBA, Japan) through the measurement of the relative changes in amplitude and phase of the polarized incident light before and after reflection on the surface of the samples. The measurements were done with an angle of incidence of 70°, in the wavelength range 300–850 nm. Modelling was done with the Deltapsi software associated to the equipment. The experimental data were modelled with a Cauchy transparent model, to extract the optical constants and the layer thicknesses. The transmittance of visible and near ultraviolet light through the hydrated discs was determined using a ThermoScientific® MultiscanGO UV–VIS spectrophotometer. Measurements were performed in the wavelength range 300−700 nm, with a 2 nm increment. Fully hydrated discs were cut properly and mounted on the inner frontal surface of a quartz cuvette.

The measurements were done in triplicate, after careful removal of the excess of water from the surface.

4.2.3.3 Topography/morphology

The surface of the samples was observed using a field emission gun scanning electron microscope (FEG-SEM) JEOL 7001F (voltage 5 kV). Samples were previously dried and coated with a thin layer of gold (thickness 30 nm).

Topographic images of the hydrated discs were obtained using an atomic force microscope (AFM) Nanosurf EasyScan 2. The analyses were done in contact mode, at room temperature, using silicon probes (force constant 0.01–1.87 Nm^{-1}), with an applied force of 18.8 nN and at a scan rate of 1.4 Hz. The average roughness (R_a) of the surfaces

94

was obtained considering the total area of the images (20×20 µm^2). The measurements were done in triplicate, after careful removal of the excess of water from the surface.

4.2.3.4 Cytotoxicity evaluation

Cytotoxicity evaluation was performed following the ISO 10993-5:2009 guidelines [14]. Rabbit corneal endothelial cells (CEC) were obtained as previously reported [15]. To assess cell adhesion and proliferation in the presence of the discs, samples with a diameter of 2 mm (quadruplicates) were placed in a 96-well plate and sterilized by UV radiation for, at least, 30 minutes. CECs were then seeded at a density of 2×10^4 cells/well in 200 µL of MEM, and incubated at 37 ºC in a humidified, 5% CO_2 atmosphere. The cell growth and morphology was monitored using an Olympus CX41 inverted light microscope (Olympus, Tokyo, Japan) equipped with an Olympus SP-500 UZ digital camera, at 1st, 2nd and 5th days.

To characterize cell viability in the presence of discs, CECs were seeded in 96-well plates containing the discs and MEM, and incubated as referred above. After the selected incubation periods (1, 2 and 5 days), cell viability was evaluated using the MTS assay by replacing the culture medium by 100 µL of fresh medium and 20 µL of MTS. After an incubation period of 4 hours at 37 °C in a humidified, 5% CO_2 atmosphere, the absorbance at 492 nm of each well was determined with a microplate reader (Bio-Rad xMark microplate spectrophotometer; Bio-Rad Laboratories, Inc, USA). Wells containing cells in the culture medium without discs were used as negative control (K-). The positive control (K+) was obtained by adding ethanol at 96% to wells containing cells without discs. Cell viability was expressed as a percentage of the negative control.

4.2.3.5 *In vitro* antibacterial activity

Microbiological tests were carried out only for the most promising system of the four systems described above, to assess the efficacy of the modified drug loaded material against *Staphylococcus aureus* and *Staphylococcus epidermidis*. Solutions collected in microfluidic assays were used for the antibacterial activity tests.

Prior to microbiological tests, *Staphylococcus aureus* ATCC 25923 and *Staphylococcus epidermidis* CECT 231 were incubated at 37 ºC for 24 hours. The growth was suspended in a 0.9% NaCl sterile solution to give an optical density of 1 McFarland.

Muller Hinton (MH) culture medium was prepared according to the producer recommendations and sterilized at 121 ºC, during 20 minutes. After MH medium temperature stabilization, 350 µL of the bacterial suspension were added to each 50 mL of medium and homogeneously distributed in square plates (120 mm × 120 mm). Antimicrobial susceptibility testing discs were placed in the plates and 15 µL of the drug solutions, collected at predetermined times (5th, 7th, 12th and 15th days), were carefully poured onto those discs (three duplicates were done for each condition). The plates were then kept at 37°C for 24 hours and, afterwards, the diameters of the inhibition halos were measured with an electronic calliper.

4.2.3.6 Statistical analysis

Results are presented as mean ± standard deviation. Comparisons between two means were carried out employing two-tailed unpaired Student's t test. For multiple comparisons, one-way ANOVA followed by Dunnett's post-test was employed. All statistical tests were carried out at a significance level of 0.05.

4.3 Results and Discussion

4.3.1 Characterization

The swelling behaviour of samples modified with AMPS and SBMA (designated by AMPS_0 and SBMA_0, according to Table 1) was evaluated. The swelling capacity increased slightly for the modified samples, with either AMPS or SBMA, but no statistical significance was found for the differences (see Table 4.2). Since both AMPS and SBMA monomers are employed in superabsorbent hydrogels [7], this result implies that the grafted polyAMPS or polySBMA layer have a low thickness and that the sample bulk was not affected by the surface modification. Ellipsometry studies confirmed the low thickness of the coatings (see Table 4.2).

Table 4.2 - Swelling capacity, water contact angle (WCA), refractive index (n) and average roughness (R_a) of the discs before and after modification by Ar plasma-grafting with AMPS (AMPS_0) or SBMA (SBMA_0). The thickness of the coatings determined by ellipsometry is also presented. Results are expressed as means ± standard deviation and the number of experiments carried out in each case is indicated.

	Swelling capacity (%)	WCA (°)	n	Coating thickness (nm)	R_a (nm)
	(n=3)	(n=10)	(n=3)	(n=3)	(n=3)
Unmodified disc	37 ± 1	44 ± 5	1.498 ± 0.001	[a]	12 ± 2
AMPS_0	38.3 ± 0.6[ns]	46 ± 3[ns]	1.52 ± 0.01[ns]	44 ± 12	15 ± 2 [ns]
SBMA_0	38.1 ± 0.8[ns]	47 ± 4[ns]	1.49 ± 0.01[ns]	34 ± 10	15 ± 1[*]

[*] Significant difference ($p < 0.05$) between modified and unmodified samples, employing a two-tailed, unpaired Student´s t test, at a confidence level of 95%.

[ns] Non significant difference ($p > 0.05$) between modified and unmodified samples, employing a two-tailed, unpaired Student´s t test, at a confidence level of 95%.

[a] Not applicable (uncoated sample).

No significant difference ($p > 0.05$) was observed between the water contact angles of modified and unmodified samples, indicating that surface hydrophilicity was not affected by the surface modifications. This result was unexpected, since surfaces of both polyAMPS and polySBMA are expected to show very low water contact angles [16, 17]. However, contact angle values of grafted polyAMPS close to the values found in this work have appeared in literature and were explained by hypothetical occurrence of molecular reorganization at the surface [18] and by low grafting density [17]. In the case of polySBMA, values close to those found in this work were also found in literature [19] and may also be explained by incomplete surface coverage.

Ellipsometry results confirmed the presence of a thin coating on the discs after modification of the surface. The obtained thicknesses for the coatings were 44 ± 12 nm and 34 ± 10 nm for the polyAMPS and polySBMA layers, respectively (Table 4.2). The large experimental errors associated to these measurements could be due to some dehydration of the samples which may occur during the experimental procedure. The refractive indexes of both modified samples were not significantly different ($p > 0.05$) from

those of the unmodified samples (see Table 2**Error! Reference source not found.**) and lie within the optimal interval for IOLs (1.42 - 1.55) [20].

The average transmittance values in the wavelength range 500-700 nm varied from 93 ± 2%, for the unmodified discs, to 94± 2%, after Ar plasma-assisted grafting with AMPS or SBMA. These values are in accordance with those reported in the literature for other IOL materials (higher than 90% above 500 nm) [21, 22].

Scanning electron microscopy images of discs unmodified and modified with Ar plasma-assisted grafting with AMPS or SBMA are presented in Figure 4.2. Some deposits/heterogeneities can be observed in all samples. Formation of blisters was observed during the SEM analysis of the modified samples (Figure 4.2 E, F) when magnification of the image was increased, but this phenomenon did not occur with the unmodified samples at the same magnification (Figure 4.2 D). Although there are no obvious differences on the surfaces of the unmodified and modified samples, the different behaviour of the two surfaces during SEM examination can be seen as an indirect evidence of the presence of a surface coating on the modified discs.
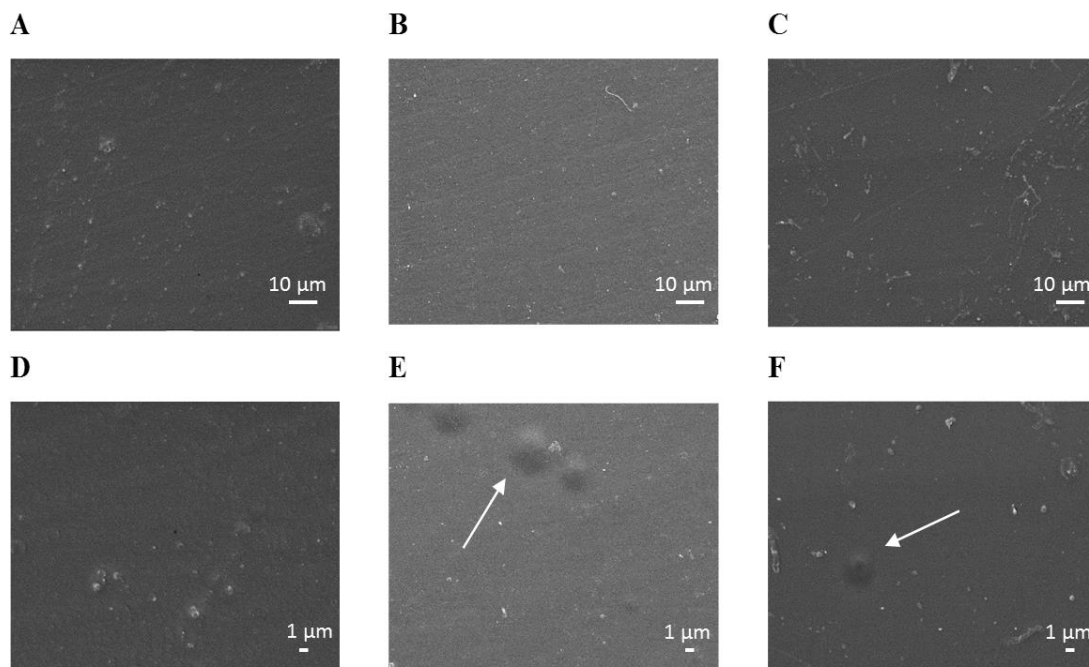
Figure 4.2 - SEM images of unmodified discs (A, D) and of discs modified by Ar plasma-assisted grafting with AMPS (AMPS_0; B, E) or SBMA (SBMA_0; C, F). A, B, C: Magnification ×1000 and D, E, F: Magnification ×3000.

Based on 20 × 20 µm AFM topographic images (see Figure 4.3) the average roughness of the surfaces was determined. The obtained values are presented in Table 4.2. The difference between unmodified and AMPS-modified samples is not statistically significant ($p > 0.05$), whereas, a statistically significant difference was found ($p = 0.04$) between unmodified and SBMA-modified samples. In both cases, the average roughness values tend to increase slightly after the coating process. The images do not allow to conclude about the surface coverage degree.
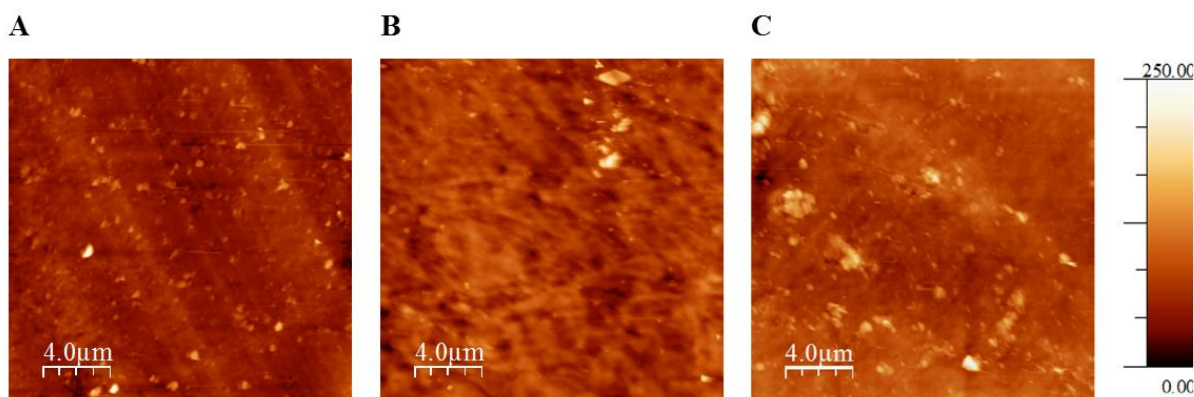
Figure 4.3 - AFM images of unmodified discs (A) and of discs modified by Ar plasma-assisted grafting with AMPS (AMPS_0; B) and SBMA (SBMA_0; C).

4.3.2 Drug release

Unmodified and modified samples referred in Table 4.1 were loaded with MFX (soaking in 5 mg/mL solution 15 hours, 37 ºC, 100 rpm) and submitted to release tests under sink conditions. The obtained cumulative mass release curves are presented in Figure 4.4.

Concerning the total mass released, the discs modified in the absence of MFX (AMPS_0 and SBMA_0) released less drug than the unmodified discs. Considering that MFX loading was done after surface modification, one possible explanation is that the coating acts as a barrier to the penetration of MFX. Attempts to quantify the amount of MFX loaded into the samples, by MFX depletion from the soaking solution, failed, since no differences in the absorbance of the MFX solution before and after the loading could be detected. When grafting was done in the presence of MFX (AMPS_1 and SBMA_1), an increase on the total MFX mass released was observed (approximately 4 and 2.5 fold,

respectively) in comparison with grafting in the absence of MFX (AMPS_0 and SBMA_0). This may be attributed to the entrapment of drug in the coating during the Ar plasma-assisted grafting. Furthermore, the release curves of the AMPS-modified samples were clearly above those of the SBMA-modified samples. Larger amounts of drug may be entrapped in the case of samples modified with AMPS, due to the low final pH value (close to 1) of the solution used for the grafting (AMPS and MFX dissolved in HBSS),. At this pH, MFX has a predominant positive electrical charge and may interact with negatively ionized AMPS. As such, MFX would be entrapped in the polyAMPS layer during its formation and would be removed during the subsequent extensive washing with water. This would result in the presence of MFX-shaped cavities in the formed polyAMPS layer, which would confer high affinity for MFX molecules during the following drug loading step (molecular imprinting [23]). In the case of SBMA, the interaction with MFX should be weaker because the grafting solution had a pH value of 7.4, at which both MFX and SBMA will be predominantly in their zwitterionic form. Additionally, the thickness of the polyAMPS and polySBMA grafted layers was of the same order of magnitude (see Table 4.2) but the size of the SBMA side-chain is larger than that of AMPS, implying that the polySBMA layer must be more compact, providing higher steric hindrance to drug entry/release. In the case of SBMA, the unmodified sample showed a released amount similar to the SBMA_1 sample, suggesting that two opposite effects have similar weights: the increase in drug loading during the polymerization step is compensated by the barrier effect in the second loading step. Comparison of the release profiles clearly shows that there is an extended release in the presence of SBMA film, although the quantities of drug incorporated/released are approximately the same. Discs modified by Ar plasma-grafting with AMPS released the largest amount of MFX (~8 µg MFX/mg of discs) and showed a release duration of approximately 21 days.
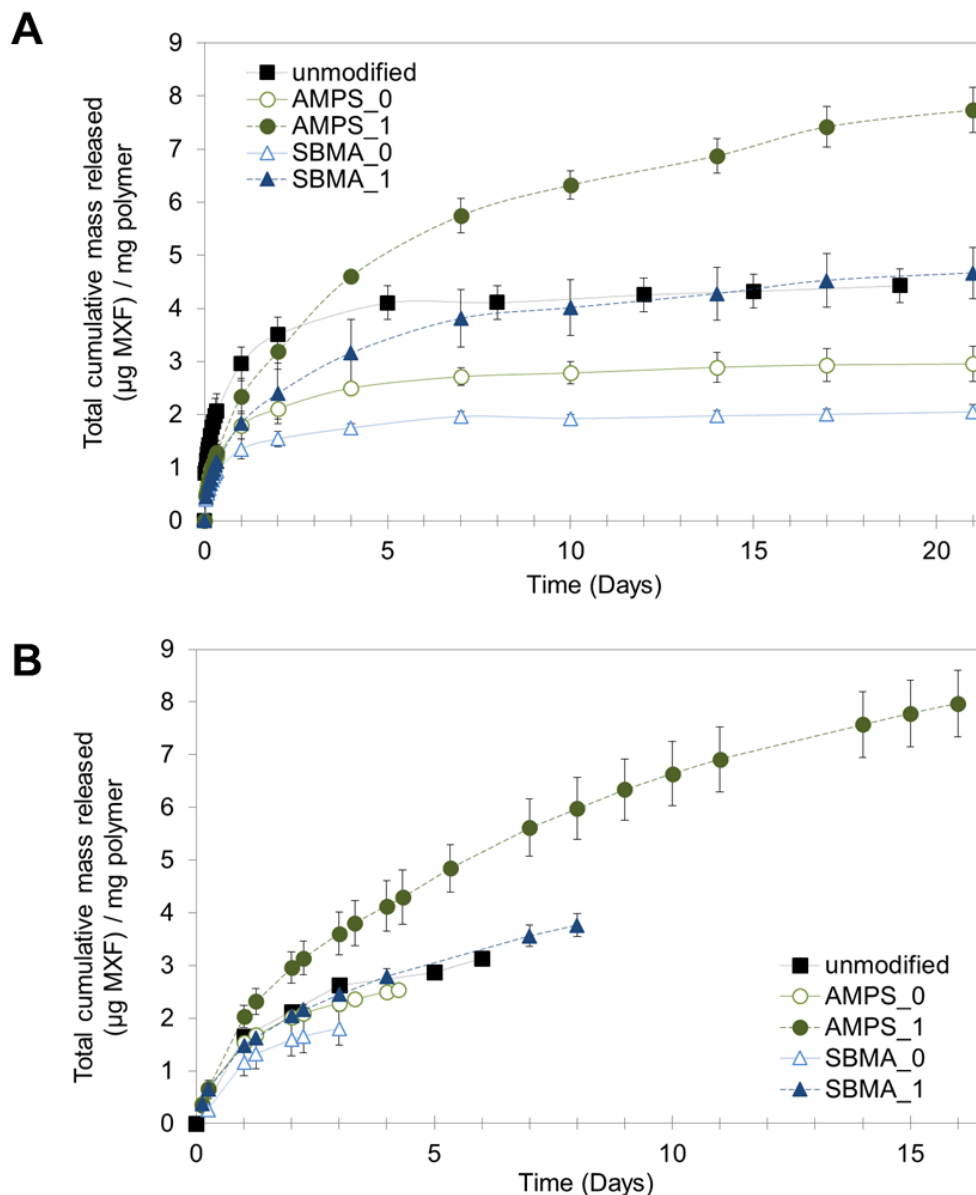
Figure 4.4 - Cumulative drug release profiles of MFX obtained under A) sink and B) dynamic conditions, for the different types of drug loaded discs (unmodified, AMPS_0, AMPS_1, SBMA_0, SBMA_1). The lines shown are guides to the eye. The dynamic release experiments were stopped at different times, corresponding to the situations where the lower detection limit of the spectrophotometer was attained. Results are presented as mean ± standard deviation (n=3). The lines shown are guides to the eye.

Dynamic release conditions allow an approximation to the hydrodynamic conditions of the aqueous humour in the eye, where the drug delivery from the IOL is expected to occur.

In this work, a microfluidic cell was used to simulate the volume of the aqueous humour and its renovation rate. Quantification of MFX in the solution collected from the cell shows that the concentrations of the drug are quite bellow its solubility limit, matching the definition of "sink conditions" usually reported in the literature for dissolution/release studies. These concentrations allow to obtain the drug release profiles under dynamic conditions and to estimate the concentration of antibiotic released into the eye [24], providing information that can be useful when comparing the efficiency of different drug release systems. In Figure 4.4 B, drug release results obtained under dynamic conditions are presented as MFX cumulative mass release curves. The results obtained under dynamic conditions were in agreement with the results under sink conditions since for both conditions:

(i) discs modified in the presence of MFX released more antibiotic than when they were modified in its absence;

(ii) discs modified by Ar plasma-grafting with AMPS in the presence of MFX (AMPS_1) released the highest amount of MFX, during, at least, 16 days;

(iii) the total amount of MFX released was similar for all studied modifications. It must be stressed that in the case of dynamic conditions assays, in which the concentration of released MFX decreases with time, a plateau in the cumulative mass release curves was not observed, since the collection of samples did not proceed after MFX concentration reached the lower detection limit for quantification.

4.3.3 Cytotoxicity evaluation

The sample AMPS_1 which led to the best MFX release profile, was further evaluated concerning its cytotoxicity through a direct contact assay with cells which are relevant for the intended application: rabbit corneal endothelial cells (CEC). Cell adhesion and proliferation of unmodified discs, AMPS_0 and AMPS_1 were evaluated by optical microscopy, after a contact time of 1, 2 and 5 days. As can be observed in Figure 4.5 A, cells in contact with all discs were able to proliferate for, at least 5 days, in a manner similar to those which did not contact any disc (negative control, K-). As such, there was

no indication of detrimental effects on cell morphology and proliferation resulting from contact with either unmodified discs, modified discs or modified discs loaded with MFX.
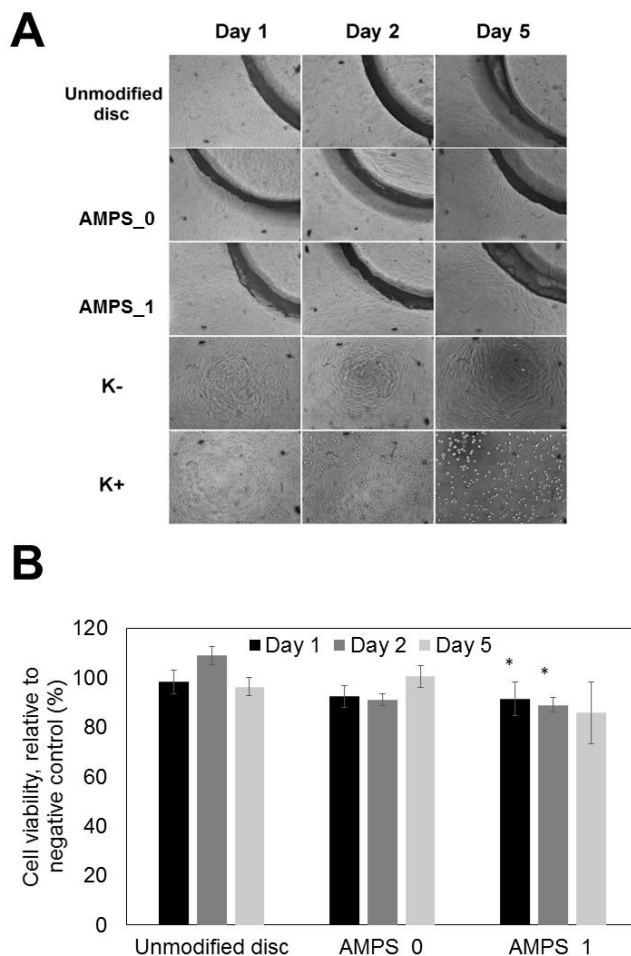
Figure 4.5 - Characterization of the cytotoxic profile of the best MFX release system (AMPS_1) and of the unmodified discs: A) representative micrographs of CECs grown in the presence or absence of modified or unmodified discs, after 1, 2 and 5 days; B) CECs viability after 1, 2 and 5 days in the presence or absence of modified or unmodified discs, measured by the MTS assay. Results are expressed as percentages in relation to the negative control, K- (mean ± standard deviation, $n = 4$).

$* - p < 0.05$ for comparisons of each sample with the negative control of the same day (one-way ANOVA followed by Dunnett's multicomparison test, at a confidence level of 95%).

Cell viability in the presence of the discs was also assessed (Figure 4.5 B), employing the MTS assay, which allows quantification of metabolically active cells based in the reduction of a soluble tetrazolium salt (MTS) to a soluble, colored formazan product, in the presence of an electron coupling agent (PES). For 5 days, there were no signs of an overt decrease in cell viability after contact with both AMPS_0 and AMPS_1 samples. In addition, the decrease in cell viability after exposure to any of the discs was always well below the threshold for a cytotoxic effect (30%, according to the ISO 10993-5:2009 standard [14].Thus, AMPS_1 seems a promising system to be used as an MFX-releasing device for prophylaxis of postoperative endophthalmitis.

4.3.4 Studies with prototype IOLs

The promising results obtained with the disks prepared from a material used in the manufacture of IOLs and with dimensions similar to these lenses, led us to test prototype IOLs made of the same material and modified/loaded according to the best conditions found in this study. Prototype IOLs were submitted to Ar plasma-grafting with AMPS in the presence of MFX, and further MFX loaded by soaking (AMPS_1). To better simulate the processing conditions of real IOLs, the modified/loaded IOLs were sterilized by autoclaving (30 min at 21ºC and at 1 bar, conditions which are used industrially to sterilize these IOLs) in the presence of the MFX loading solution, and stored for 30 days, at room temperature. The drug release profiles were then obtained, under dynamic conditions. The results obtained (see Figure 4.6) showed that modified, prototype IOLs had a MFX release behaviour even better than the equivalent discs, releasing more MFX (~11 µg MFX / mg polymer) for at least 16 days. This increase in the total amount of MFX released when compared to the discs may be attributed to further loading of MFX as a consequence of the sterilization and storage in the MFX solution. The wettability, transmittance and topography/morphology of these coated IOLs were assessed and no significant changes were observed when compared with the AMPS_1 samples.
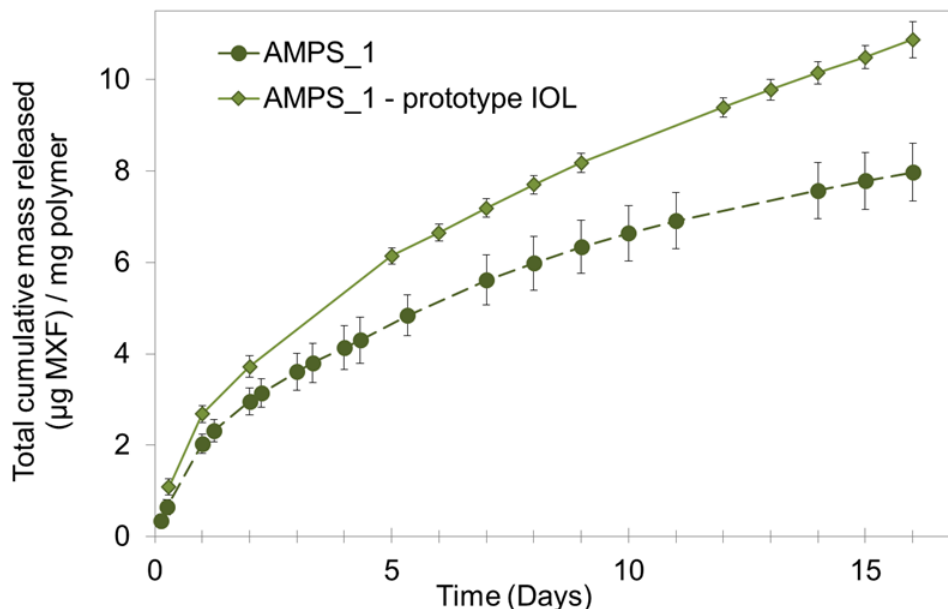
Figure 4.6 - Cumulative drug release profiles of MFX obtained under dynamic conditions, for discs modified (AMPS_1) and IOLs modified and sterilized in the MFX loading solution (AMPS_1 prototype IOLs). Results are presented as mean ± standard deviation (*n*=3). The lines shown are guides to the eye.

To check if the drug released from modified IOLs was effective against common postoperative endophthalmitis pathogens, antibacterial activity tests were carried out. Solutions collected during the drug release experiment under dynamic conditions, at days 5, 7, 12 and 15 were tested against *Staphylococcus aureus* and *Staphylococcus epidermidis*. Bacteria growth inhibition halos where observed for all solutions collected till day 12 of release (see Figure 4.7).
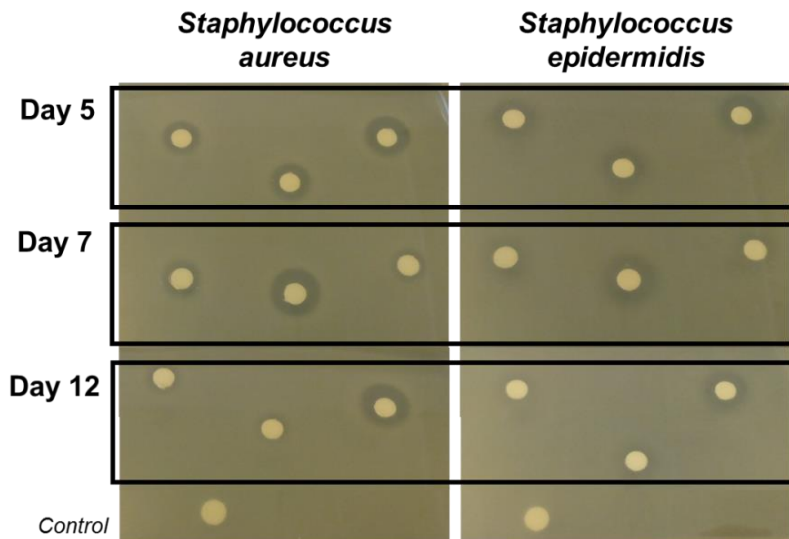
Figure 4.7 - Inhibition halos for *Staphylococcus aureus* and *Staphylococcus epidermidis* obtained with drug released from prototype IOLs with modification AMPS_1 at days 5, 7 and 12

4.4 Conclusions

In the work in this chapter, intraocular lenses were explored as a vehicle to deliver an antibiotic (MFX) to the eye, in a continuous mode, during the recommended postoperative prophylaxis period for cataract surgery. Ar plasma-grafting with AMPS and SBMA was used to produce coatings with the aim of controlling the drug release from the material. Characterization of the modified samples showed that the coatings did not affect significantly the relevant properties of the lenses. Concerning drug release profiles, the most promising results were obtained with AMPS grafting in the presence of MFX. The utilization of a microfluidic cell allowed the study of the antibiotic eluting behaviour from prototype IOLs under hydrodynamic conditions similar to those in the eye, namely volume and renovation rate of the aqueous humour. These systems showed no cytotoxicity and are effective against both *Staphylococcus aureus* and *Staphylococcus epidermidis* until the 12th day of release. Since the recommended duration of antibiotic therapy is about two weeks, the modified IOLs present potential to be used in cataract surgery, with a prophylactic effect against postoperative endophthalmitis.

4.5 References

1. Kim, D.H., et al., *Aqueous penetration and biological activity of moxifloxacin 0.5% ophthalmic solution and gatifloxacin 0.3% solution in cataract surgery patients.* Ophthalmology, 2005. **112**(11): p. 1992-6.

2. Dajcs, J.J., et al., *Effectiveness of ciprofloxacin, levofloxacin, or moxifloxacin for treatment of experimental Staphylococcus aureus keratitis.* Antimicrob Agents Chemother, 2004. **48**(6): p. 1948-52.

3. O'Brien, T.P., S.A. Arshinoff, and F.S. Mah, *Perspectives on antibiotics for postoperative endophthalmitis prophylaxis: potential role of moxifloxacin.* J Cataract Refract Surg, 2007. **33**(10): p. 1790-800.

4. Hubicka, U., et al., *Kinetic and thermodynamic studies of moxifloxacin hydrolysis in the presence and absence of metal ions in acidic solutions.* Acta Pol Pharm, 2012. **69**(5): p. 821-31.

5. Lalitha Devi, M. and K.B. Chandrasekhar, *A Validated, Specific Stability-Indicating RP-LC Method for Moxifloxacin and Its Related Substances.* Chromatographia, 2009. **69**(9): p. 993-999.

6. Wang, D. and R.E. Notari, *Cefuroxime hydrolysis kinetics and stability predictions in aqueous solution.* J Pharm Sci, 1994. **83**(4): p. 577-81.

7. Okay, O. and S. B. Sariisik, *Swelling behavior of poly(acrylamide-co-sodium acrylate) hydrogels in aqueous salt solutions: theory versus experiments*. Vol. 36. 2000. 393-399.

8. Lalani, R. and L. Liu, *Electrospun Zwitterionic Poly(Sulfobetaine Methacrylate) for Nonadherent, Superabsorbent, and Antimicrobial Wound Dressing Applications.* Biomacromolecules, 2012. **13**(6): p. 1853-1863.

9. Neves, P., et al., *Influence of structural factors on the enhanced activity of moxifloxacin: a fluorescence and EPR spectroscopic study.* Anal Bioanal Chem, 2007. **387**(4): p. 1543-52.

10. Gerenser, L.J., *XPS studies of in situ plasma-modified polymer surfaces.* Journal of Adhesion Science and Technology, 1993. **7**(10): p. 1019-1040.

11. Huang, Q., et al., *Surface Modification of Intraocular Lenses.* Chinese Medical Journal, 2016. **129**(2): p. 206-214.

12. M. E. van S. C. Pagnoulle, M.A.R., *Yellow chromophore agent composition for intraocular lenses and the thus obtainable lense*. 2006: Belgium.

13. Goel, M., et al., *Aqueous Humor Dynamics: A Review*: Open Ophthalmol J. 2010;4:52-9. doi:10.2174/1874364101004010052.

14. Standardization, I.O.f., *ISO 10993-5: Biological evaluation of medical devices — Part 5: Tests for in vitro cytotoxicity*. 2009.

15. Natu, M.V., et al., *Controlled release gelatin hydrogels and lyophilisates with potential application as ocular inserts.* Biomed Mater, 2007. **2**(4): p. 241-9.

16. Zhou, T., et al., *Surface functionalization of biomaterials by radical polymerization.* Progress in Materials Science, 2016. **83**: p. 191-235.

17. Song, L., et al., *Biocompatibility of polypropylene non-woven fabric membrane via UV-induced graft polymerization of 2-acrylamido-2-methylpropane sulfonic acid.* Applied Surface Science, 2011. **258**(1): p. 425-430.

18.   Dutschke, A., C. Diegelmann, and P. Lobmann, *Preparation of TiO2 thin films on polystyrene by liquid phase deposition.* Journal of Materials Chemistry, 2003. **13**(5): p. 1058-1063.

19.   Kuo, W.-H., et al., *Surface Modification with Poly(sulfobetaine methacrylate-co-acrylic acid) To Reduce Fibrinogen Adsorption, Platelet Adhesion, and Plasma Coagulation.* Biomacromolecules, 2011. **12**(12): p. 4348-4356.

20.   Bellucci, R., *An introduction to Intraocular Lenses: Material, Optics, Haptics, Design and Aberration*, in *Cataract*, G. J.L., Editor. 2013, S. Karger AG: Basel. p. 38-55

21.   Artigas, J.M., et al., *Spectral transmittance of intraocular lenses under natural and artificial illumination: criteria analysis for choosing a suitable filter.* Ophthalmology, 2011. **118**(1): p. 3-8.

22.   Tanito, M., et al., *Measurements of transmission spectrums and estimation of retinal blue-light irradiance values of currently available clear and yellow-tinted intraocular lenses.* Japanese Journal of Ophthalmology, 2012. **56**(1): p. 82-90.

23.   Alvarez-Lorenzo, C., et al., *Imprinted soft contact lenses as norfloxacin delivery systems.* Journal of Controlled Release, 2006. **113**(3): p. 236-244.

24.   Pimenta, A.F., et al., *Simulation of the hydrodynamic conditions of the eye to better reproduce the drug release from hydrogel contact lenses: experiments and modeling.* Drug Deliv Transl Res, 2016. **6**(6): p. 755-762.

5 Diffusion-based design of multi-layered ophthalmic lenses for controlled drug release

Table of Contents

5.1 Introduction

In the present chapter, description and characterization through a diffusion-based mathematical model of multi-layered drug-loaded lenses will be investigated. A triple layer system was considered, where drug is only loaded, through soaking, at the middle/inner layer, maintaining the outer layers non-loaded, aiming a controlled initial drug burst, and a near zero-order release kinetics. We chose to investigate a conventional PHEMA based hydrogel, and chlorhexidine (antibacterial agent and topical disinfectant [1]) and levofloxacin (antibiotic [2]) as model material and drugs.

The mathematical modeling of the different mechanisms responsible for controlled release from hydrogels such as diffusion, swelling or degradable controlled systems is well described in literature [3, 4]. Mathematical description and characterization of the release behavior allows the prediction and selection of the system parameters in order to tailor the drug release profile. Siepmann and Siepmann provided an overview on the current state of the art of modeling drug release from delivery systems, which are predominantly controlled by diffusional mass transport [5]. An analytic solution presented in their work was considered for comparison to the herein numeric solution described. Briefly, our multi-layer lenses can be described as a reservoir type system with non-constant activity source, where the drug molecules, present in an inner hydrogel layer, diffuse out of the lens through the non-loaded coating hydrogel layer. Also assumed, is the non-replacement of drug molecules, thus drug concentration decreases at the inner layer over time.

In section 5.3.1, the parameters for the characterization of the multi-layer lens were obtained through fitting of the mathematical model to experimental data (for PHEMA hydrogel and the two studied drugs), and used in section 5.3.2.1 for prediction of the experimental mass release profiles of different *sandwich like* lenses. This first part of the Results and Discussion section aimed to validate and present the potential of a mathematical model as tool on the design of drug elution ophthalmic lenses. Then, we used the model in the following section 5.3.2.2, to predict the drug release behavior of different systems, with non-specified materials or drugs, with the goal of analyzing the

contributions of the multi-layered lens parameters on the initial drug burst and release kinetics, namely the roles of the drug diffusion coefficient, the layers thicknesses, and interfacial transport resistance between the layers. We show that the initial burst may be minimized, and near zero-order release conditions may be achieved by properly selecting the relative dimensions and characteristics of the loaded/non-loaded layers of the lenses.

5.2 Experimental Part

5.2.1 Materials

2-hydroxyethyl methacrylate (HEMA), ethylene glycol dimethacrylate (EGDMA), 2,2-azobis(2-methylpropionitrile) (AIBN) and levofloxacin (LVF) were all purchased from Sigma-Aldrich. Poly(vinylpyrrolidone) (PVP, KollidonVR 30) was kindly provided by BASF. Sodium chloride was obtained from Merck, and chlorhexidine diacetate monohydrate (CHX) was obtained from AppliChem. A Millipore Milli-Q water purification system was used to prepare distilled and deionized (DD) water.

5.2.2 Hydrogel preparation, drug loading and release experiments

PHEMA-based hydrogel (HEMA/PVP) was prepared by dissolving appropriate amounts of the EGDMA crosslinker and the AIBN initiator in HEMA to obtain final concentrations of 80 mM and 10 mM, respectively. PVP was added to the mixture at a ratio of 98/2 HEMA/PVP (w/w). The mixture was poured into a mold that consisted of two parallel silanized glass plates, and the mixture was thermopolymerized at 50 ⁰C for 14 hours followed by 24 hours at 70 ⁰C. The obtained hydrogel sheet was soaked in DD water for 5 days to remove unreacted monomers, cut into discs (2 cm^2, average thickness of 0.3 mm), which were then dried in an oven at 40 ⁰C overnight and stored. Additional details on the protocol followed for the preparation of the hydrogel can be found in Paradiso *et al.* [6].

Levofloxacin was dissolved in saline solution at concentrations of 5 mg.mL^{-1} and 10 mg.mL^{-1}. Chlorhexidine was dissolved in DD water at concentrations of 1 mg.mL^{-1} and 2.5 mg.mL^{-1} due to its reduced solubility in saline solution. The hydrogels were drug loaded

by soaking each disc in 5 mL of the drugs solutions for 5 days at 4⁰C. *In vitro* drug release tests were performed at 37 ºC while stirring (180 rpm) 5 mL saline solution until the release of the drug was complete. At chosen time intervals, aliquots of 0.5 mL of the supernatant were collected and replaced by the same volume of fresh saline solution. The drug concentration values in the release medium were quantified using a spectrophotometer UV–VIS MultiscanGO from Thermo Scientific® at wavelengths of 255 nm for CHX and 290 nm for LVF. All the experiments were carried out in triplicate.

To experimentally simulate the multi-layered lens system, a support ring made of *Perspex®* acrylic was designed. A drug-loaded PHEMA disc was placed between two non-loaded PHEMA discs inside the support, and the disks were pressed against one another in the peripheral zone. A schematic representation of the experimental multi-layered system is presented in Figure 5.1. *In vitro* drug release was characterized in a volume of saline solution proportional to the volume used in the single-lens drug release assays, i.e., maintain the ratio of the cross-sectional area/volume of the supernatant.
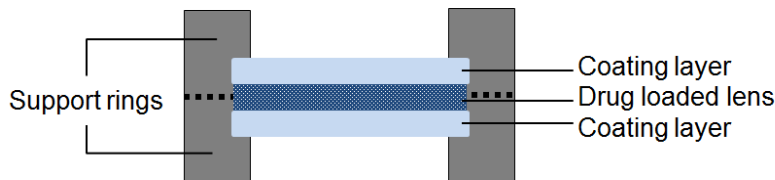
Figure 5.1 - Schematic representation of the experimental multi-layered drug-releasing system.

5.2.3 Mathematical model for simulation of in vitro release – monolayered

The simplest case that can be used to describe the drug release from the drug-loaded homogeneous lens immersed in a liquid, considers a plate of infinite surface area and finite thickness, with h as the lens half-thickness, and Fick's second law of diffusion can be applied to solve it. Assuming an effective diffusivity, D_e, independent of time and space, taking the space coordinate y, $y = 0$ on the center of the lens, and t is time. The mass

113

transfer problem considering a material with a certain concentration of drug ($C(y, t)$) can be described using the following equation:

$$\frac{dC}{dt} = D_e \frac{\partial^2 C}{\partial y^2}$$

Equation 5.1

The boundary conditions for the drugs release experiments are the following:

$$\frac{\partial C}{\partial y}(y = 0, t) = 0$$

Equation 5.2

$$C(y = h, t) = 0$$

Equation 5.3

The first boundary condition accounts for the symmetry at the center of the lens and the second boundary condition is based on the sink assumption.

The known initial condition is the concentration of drug in the lens, C_i:

$$C(y, t = 0) = C_i$$

Equation 5.4

Continuity of flux at the lens boundary and a well-mixed assumption for the fluid yields the following equation for the mass balance on the release phase, with $A_{surface}$ as the lateral lens area and C_r and V_r as the concentration and volume of the release medium, respectively:

$$-2D_e A_{surface} \frac{\partial C}{\partial y}(y = h, t) = V_r \frac{dC_r}{dt}$$

Equation 5.5

The diffusion based problem can be solved analytically and, when fitted to the experimental data, D_e can be determined (Equation 5.1) [7].

5.2.4 Mathematical model for simulation of in vitro release – multi-layered lenses

In this section, we assume the ophthalmic lens as a *sandwich* in which each layer is characterized by a certain thickness and a certain diffusivity of the drug loaded within it. In this case, the drug diffusivity in the coating layer and in the inner-loaded layer may be equal or different. The thicknesses of the lateral coatings (l) are equal. This system can

be described by C_{in} and D_{e_in} as the drug concentration and diffusivity, respectively, of the interior layer and by C_{out} and D_{e_out} as the drug concentration and diffusivity, respectively, of the outer layers (see Figure 5.2).
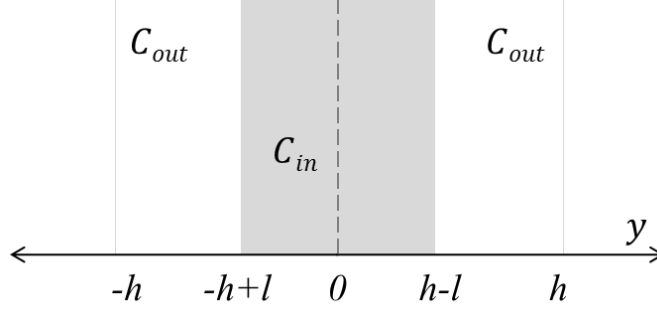
Figure 5.2 – Schematic representation of the multi-layered lens.

At $t = 0$ only the inner layer has a certain concentration of drug, C_i, with the exterior layers having null drug concentrations. As in the system described in the previous section, a symmetry condition is imposed at the center of the lens (inner + outer layers). The initial and boundary conditions for the drugs release experiments are the following:

$$C_{in}(y, t = 0) = C_i$$

Equation 5.6

$$C_{out}(y, t = 0) = 0$$

Equation 5.7

$$\frac{\partial C}{\partial y}(y = 0, t) = 0$$

Equation 5.8

$$C_{out}(y = h, t) = 0$$

Equation 5.9

$$C_{in}(h - l, t) = \alpha\, C_{out}(h - l, t) \text{ and } C_{in}(-h + l, t) = \alpha\, C_{out}(-h + l, t)$$

Equations 5.10

Continuity of flux at the lens inner interfaces is considered, with resistance to the mass transport through the accounted by with an experimentally adjustable parameter α (Equations 5.10). Continuity of flux at the lens boundaries and a well-mixed assumption for the fluid yields the equation for the mass balance on the release phase:

$$-2D_{e_{out}}\, A_{surface}\, \frac{\partial C}{\partial y}(y = h, t) = V_r \frac{dC_r}{dt}$$

Equation 5.11

5.3 Results and Discussion

5.3.1 Adjustment to experimental results: determination of system parameters

The initial condition for the loaded lens, either for the single-layer model (Equation 5.4) or the multi-layer model (Equation 5.6) requires that at the beginning of the experiment, the concentration of drug through the entire lens must be equal. Therefore, soaking in the drug solution should be sustained for a sufficient amount of time to ensure drug homogeneity in the lens. Different loading times were tested, and it was concluded that 5 days was enough time to achieve this condition. To ensure that the concentration of drug in the surface of the lens is zero at $t \geq 0$, the release was performed while stirring and within a sufficiently large volume of medium, which could be considered as infinitely diluted (sink condition).

To compare the experimental profiles with the calculated profiles, the released mass was normalized, i.e., the mass released up to time t, $M(t)$, was divided by the total mass $M(\infty)$, and a constant volume of the lens was assumed. Then, the calculated normalized profiles can be directly compared with the normalized experimental profiles, and the adjustable parameters D_e and α (α for multi-layered systems) can be extracted.

The first step was to adjust our model to the experimental results derived from the non-coated lenses to obtain the diffusivity values of the studied drugs in the studied material. Figure 5.3 shows two examples of theoretical curves fitted to experimental points for two different lens/drug systems: PHEMA-LVF system (Figure 5.3 A) and a PHEMA-CHX system (Figure 5.3 B). For each drug, two different concentrations of soaking solution were used. The lenses that were soaked in more concentrated solutions released higher amounts of drug by $t = \infty$. However, the normalized experimental curves for the two soaking conditions did not present significantly different release kinetics for the studied drugs, as was expected because the diffusivity of the drug is independent of its concentration. This finding is also illustrated in Figure 5.3, where the experimental data points refer to the normalized mass release of levofloxacin and chlorhexidine loaded from solutions of different concentrations. As a result, it can be concluded that the diffusivity

values are independent of the concentration of the soaking solution. The diffusivity values obtain for levofloxacin and chlorhexidine were 7.5 x10^{-13} and 5.0 x10^{-13} m^{2}s^{-1}, respectively.
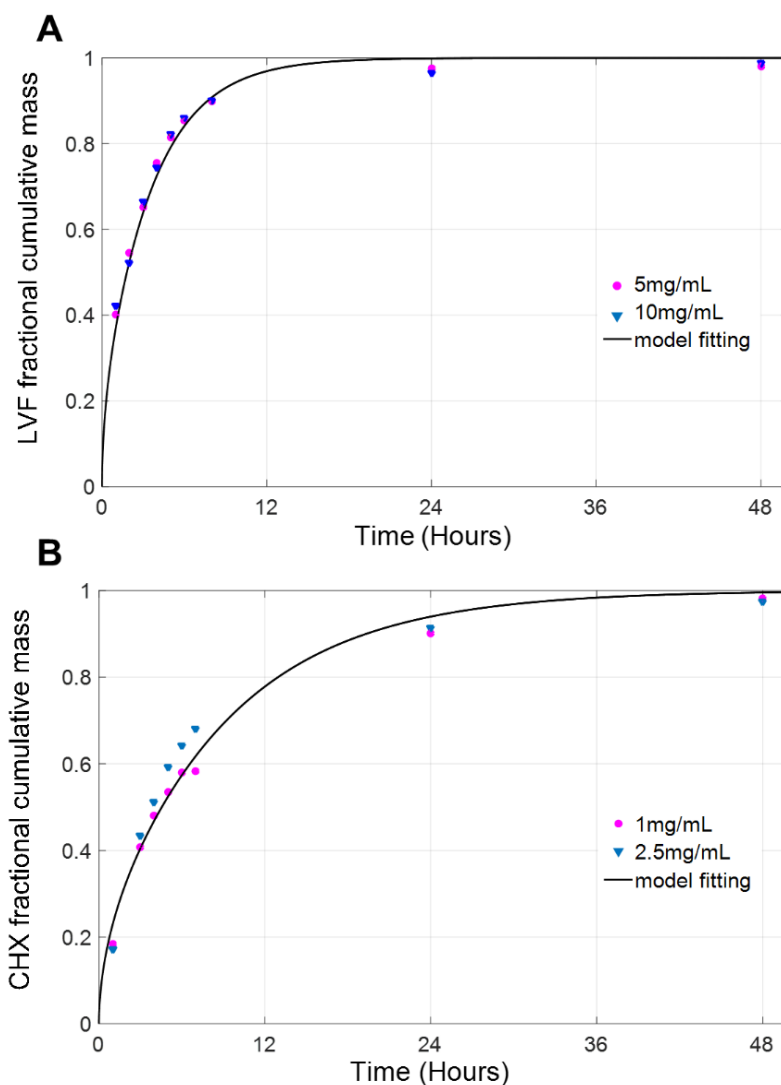
Figure 5.3 - Adjustment of the numerically fit models to experimental points obtained from the release assays for infinite sink conditions. (A) Levofloxacin and (B) chlorhexidine from PHEMA hydrogels. The concentrations are given in the inserts.

The second step, in adjusting the mathematical model to experimental results, was to obtain an estimate for α, the parameter related to the mass transfer within the interface between the loaded and non-loaded lens in the multi-layered system. Experimental data were obtained for a levofloxacin-loaded PHEMA lens compressed between two non-loaded PHEMA lenses with the same thickness as the loaded lens (0.4 mm/layer). The

diffusivity of 7.5x10^{-13} m^{2}s^{-1} corresponded to the value previously obtained for this drug in the PHEMA system. The adjustment to the experimental release data, as shown in Figure 5.4, revealed that an $\alpha = 0.07$ resulted in a good adjustment between the experimental points and the model trend line. Fitting of the experimental data to a general analytic solution of Fick's law described by Siepmann and Siepmann (Equation (3) in [5]) is also presented in Figure 5.4 (dashed blue line). The same diffusivity was used and the fitting was optimized by adjusting the partition coefficient, $K = 1.8$.
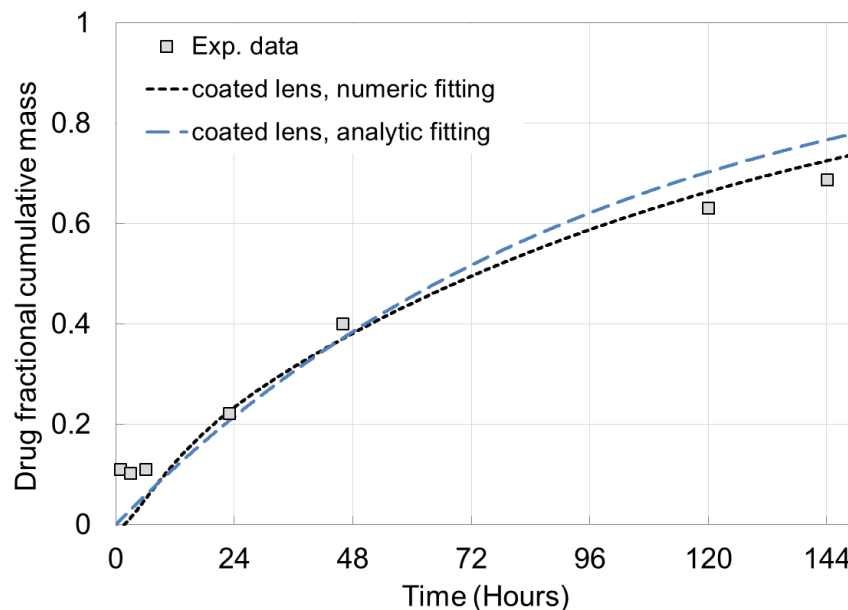
Figure 5.4 - Predicted fractional release mass profiles given by numerical simulation: Comparison of experimental results of levofloxacin release from a PHEMA multi-layered system (squares) fitting through a numeric solution (full black line) and a analytic solution (Equation (3) in Reference [5], dashed blue line).

Though both fits are acceptably good it should be noted that:

1-   the analytic solution, for the sake of simplicity, only accounts for the diffusivity through the external layer;

2-   conversely, the numerical solution accounts for both the external and inner layer diffusivities which can be dissimilar and determined a priori for the design of optimized systems (treated in the final section of the present paper);

3-   finally, the analytic model does not predict the delay time of the drug crossing the outer layers, which, in a more realistic manner, is predicted by the numerical model.

5.3.2 Application of the design of the multi-layered drug-loaded lens

In this section, we use the previously presented approach in two example applications. In the first example, we establish as target objective multi-layered PHEMA lenses that could release levofloxacin and chlorhexidine over the course of one week at a nearly zero-order release rate. To simulate these model lenses, we used the diffusional and interfacial parameters determined in the previous section. Then, we manufacture the *sandwich* lenses (as described in section 5.2.2) and compared the predicted release results with the experimental release results. In the second example application of the model, we used the approach in a general manner to analyze the influence of the drug/lens parameters of the obtained release profiles.

5.3.2.1 Slow-release multi-layered PHEMA lens loaded with levofloxacin and chlorhexidine: simulation and experimental results of the model systems

As shown in the previous section, by using the calibrated drug diffusivity parameters and after gauging the α interface parameter, it is possible to numerically simulate different systems to obtain optimal multi-layered lenses for desired applications. Preliminary calculations showed that, for the PHEMA system and for a typical lens thickness of 1.2-1.6 mm, if the loaded core is approximately the same thickness as the un-coated layers, a slow drug release over the course of a week with a nearly constant release rate and minimal drug bursts can be achieved. Fabrication of contact lens with such large thickness does not seem viable [8]. Whereas, intraocular lenses can have a higher center thicknesses, depending on the desired refractive power, e.g. 1.83 mm for a +24 diopter intraocular lens [9, 10].

The first system (#1) that we modeled and tested consisted of a lens formed by a drug-loaded core of 0.4 mm and coated un-loaded layers of the same size (0.4 mm), such that the total thickness of the model lens was 1.2 mm. A factor α of 0.07 was obtained

previously from fitting system #1 experimental data to the numerical model and was used for the following simulation. The second system (#2) consisted of a drug-loaded core of 0.4 mm and coated un-loaded layers of 0.6 mm, such that the total thickness of the model lens was 1.6 mm. For both model systems, we used levofloxacin (diffusivity of 7.5×10^{-13} $m^2 s^{-1}$) and chlorhexidine (diffusivity of 5×10^{-13} $m^2 s^{-1}$) as the release drugs in the experimental validation.

In Figure 5.5, a numerical simulation of the drug release from these systems (the first and second systems are designated as #1 and #2, respectively, in the figure) is shown and compared with the experimental points measured after 6, 24, 48, 72, 120 and 144 h of release. For system #2, numerical predictions for both levofloxacin and chlorhexidine slightly overestimate the release profiles when compared to the experimentally obtained curves. We observed that the increase in the coating thickness by a factor of 1.5 significantly affected the absolute value of the drug release with time but not the release kinetics. In fact, for both of these model lenses and for both drugs tested, we observed that, theoretically and experimentally, after the first day, essentially a zero-order release rate was obtained up to at least 150 h of release. Predictions for coatings with half of the thickness of system #1 are also presented and are designated as system #3.

The results presented in this section support the hypothesis that the experimental release profile of a coated lens can be tailored by the parameters of the overall system. In the next section, we assume this premise to provide a general overview of the influence of the control parameters (diffusion coefficient, interfacial transfer coefficient and thickness of the lens) on the drug release profiles.
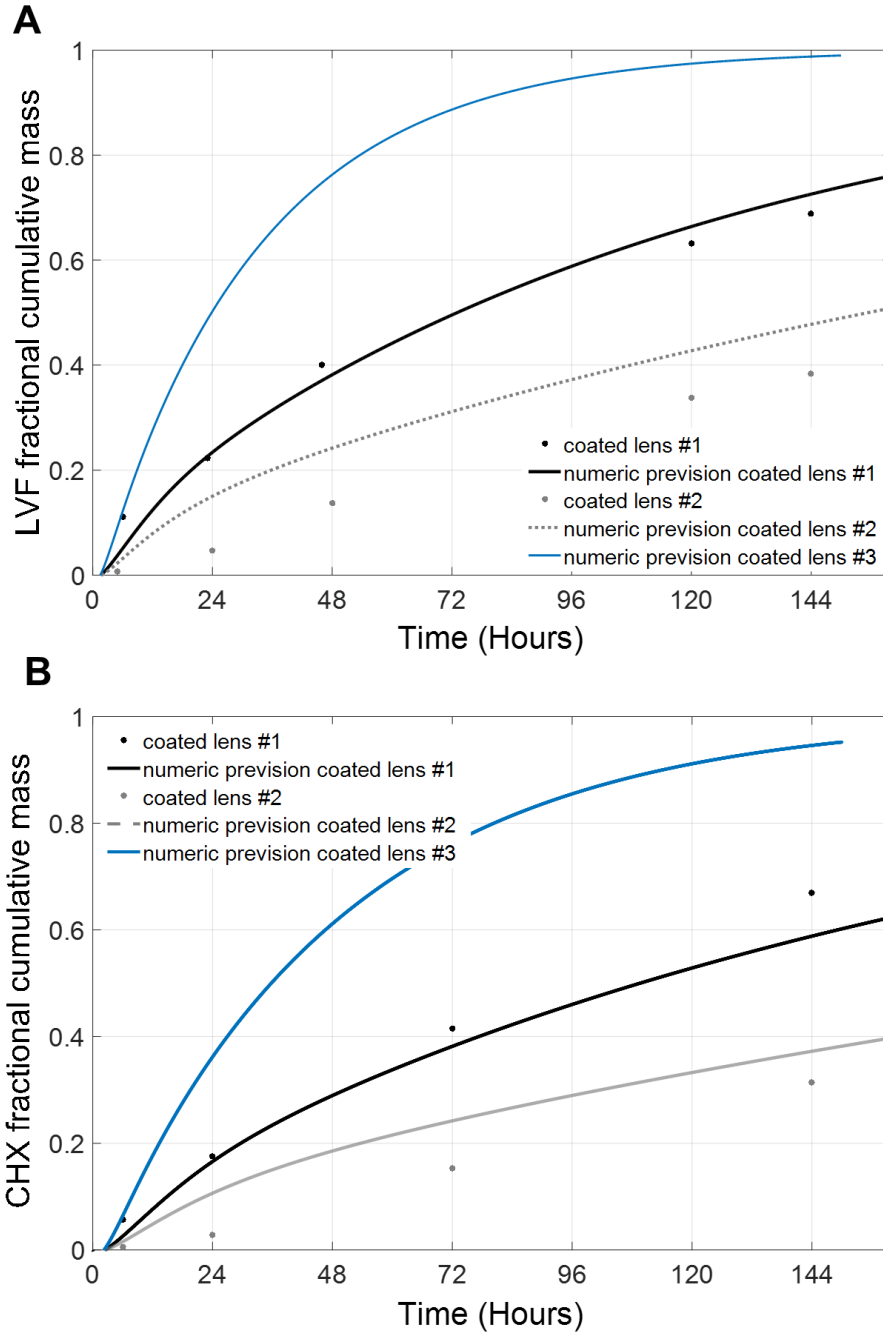
Figure 5.5 - Predicted fractional release mass profiles given by the numerical simulation for coated PHEMA lens systems. Inner and outer lens thicknesses of 0.4 mm/layer (coated lens #1), inner lens thickness of 0.4 mm and an outer lens thickness of 0.6 mm/lens (coated lens #2), and inner lens thickness of 0.4 mm and an outer lens thickness of 0.2 mm/lens (coated lens #3). Experimental release experiments data (black and gray dots) for (A) levofloxacin and (B) chlorhexidine.

5.3.2.2 Design of multi-layered drug-loaded lens: a generalist approach

In this section, we present illustrative cases for which the thickness of the coating, the diffusivity of the drug in the coating, and the interface mass transport resistance parameter are varied. In addition to the predicted fractional mass release profiles, the predicted normalized drug concentration profiles if the systems were placed, as intraocular lenses, in the eye aqueous humor (volume of 0.250 mL) and assuming a physiological renovation rate of 1% per minute were also considered [11]. The predicted drug concentrations were estimated from the theoretical fractional mass release profiles, based on the semi-empirical Korsmeyer-Peppas model as described in Paradiso *el al.* [6]. With this, we aimed to achieve only a comparative study of the concentration profiles, namely initial drug burst and lag time assessment, and not a quantitative or efficacy drug concentration study. Here, the thickness of the inner loaded lens was maintained at 0.5 mm, and the drug diffusivity in that material was maintained at 7.5×10^{-13} $m^2 s^{-1}$.

Figure 5.6 shows the influence of the coating thickness on the release profile of the lens, keeping the drug diffusivity ($D_{e\_in} = D_{e\_out} = 7.5 \times 10^{-13}$ $m^2 s^{-1}$) and the inner interface mass transfer related parameter ($\alpha = 0.07$) constant. It can be observed that by increasing the thickness of the coating, the total time to release the drug increases because the drug must traverse a greater distance. More interesting is the decrease in the initial burst of drug (Figure 5.6 B) with increased coating thicknesses.
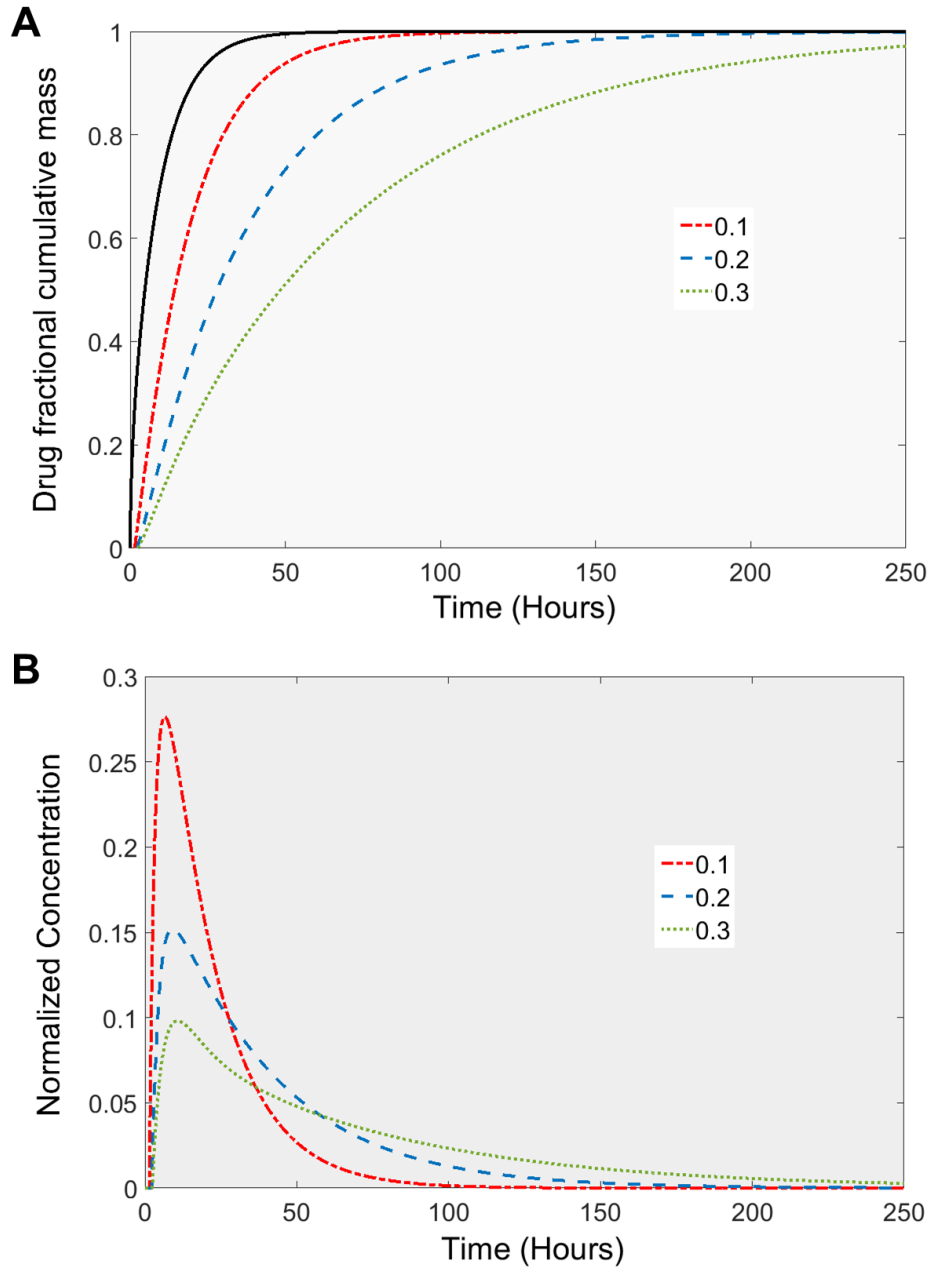
Figure 5.6 - Influence of the coating thickness in the drug release.(A) predicted fractional release mass profiles given by numerical simulation; (B) estimated normalized concentration of drug in the aqueous humor volume taking into account its renovation rate for coated lenses. Coating thickness values (in mm/coating layer) are shown in the figure (full black line: single lens; dashed lines: coated lenses).

Next, the effect of resistance to the mass transfer at the coating interface was estimated by altering the parameter α. Drug diffusivity in the coating was maintained equal to the diffusivity in the inner lens ($D_{e\_in} = D_{e\_out} = 7.5 \times 10^{-13}$ m^{2}s^{-1}). The coating thickness was set at a fixed value of 0.2 mm on each side. Being a mass transport resistance, α will vary with the chosen materials and/or drug, for instance the materials at the inner and outer layers are different, or the drug molecules present very distinct intrinsic characteristics when compare to those herein utilized, which are only used as reference values. Figure 5.7 shows the dependence of the resulting mass release profile and concentration burst on this adjustable parameter.

By decreasing the parameter α by one order of magnitude, a significant change occurs in the release kinetics. With $\alpha = 0.01$, an almost zero-order release is achieved. In addition, the time lag for drug release increases (abscissa axis; Figure 5.7 A) due to the resistance to drug transport in the interface. This lag time must be accounted for very carefully in drug delivery ophthalmic lenses because, during this time period, no drug would be available in the eye. The initial drug burst can be significantly decreased if the mass transfer in the interface is precisely calibrated.
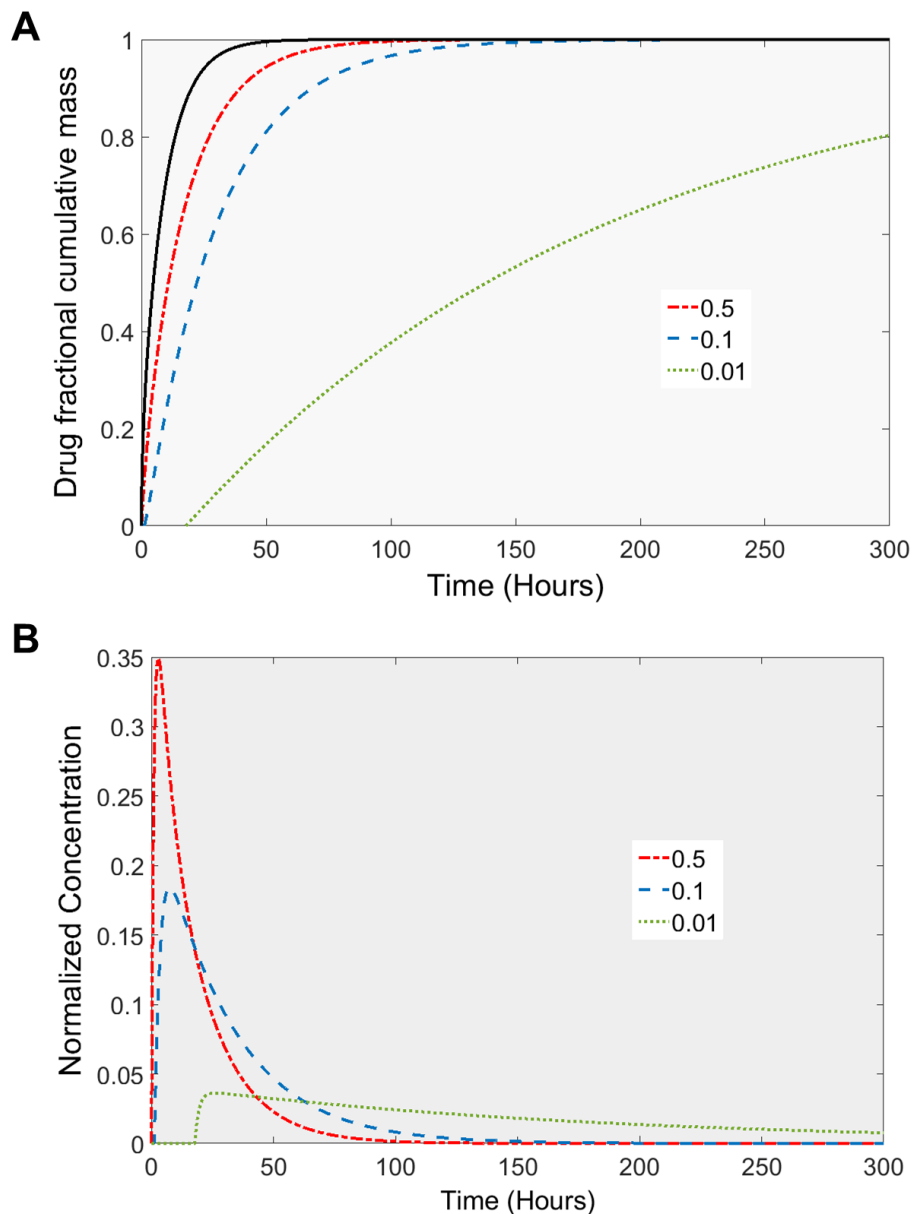
Figure 5.7 - Influence of the resistance to the mass transport through the interfaces in the drug release. (A) predicted fractional release mass profiles given by numerical simulation;(B) estimated normalized concentration of drug in the aqueous humor volume taking into account its renovation rate in coated lenses. The values of α are shown in the figure (full black line: single lens; dashed lines: coated lenses).

The role of the drug diffusivity in the coating was also assessed by maintaining its thickness at a fixed value of 0.2 mm on each side and considering $\alpha = 0.01$. As shown in Figure 5.8, by decreasing the drug diffusivity in the coating to one-third of the diffusivity in the drug-loaded lens, the kinetics of the mass release are greatly altered, and the mass is released at lower rate. Note that the burst and the time lag are also markedly affected by this variation. In contrast, if the drug diffusivity of the coating is superior to that of the lens, the total mass release occurs more quickly.

Considering the above results and the requirements for efficient drug release, a theoretical optimized multi-layered intraocular lens can be designed based on the input values given in Table 5.1.

Table 5.1 - Input values for numeric simulation.

Lens thickness (mm)	0.5
Coating thickness (mm)	0.2
α	0.01
Drug diffusivity in the lens (m^2s^{-1})	7.5×10^{-13}
Drug diffusivity in the coating (m^2s^{-1})	7.5×10^{-13}

The fractional mass release profile and expected normalized drug concentration in the aqueous humor for use of this theoretically designed lens are depicted in Figure 5.8. A theoretical optimal ophthalmic lens depends on multiple factors (physiological, pharmacokinetics, etc.) and on the desired application (treatment requirements). Here, we aimed to achieve an effective intraocular lens that could be used during the critical period after cataract removal surgery to prevent the development of postoperative endophthalmitis.

The initial time lag of this multi-layered system was estimated to be approximately 24 hours, corresponding to the time period during which antibiotic intracameral injections that are commonly applied following this type of surgery are estimated to be effective [12]. After this time lag, the release of drug from the multi-layered system is sustained for a

period of at least 12 days and is likely sufficient to prevent acute endophthalmitis, which most likely develops within 1-2 weeks after surgery [13].

It must be taken into account that the concentration values presented in Figure 5.6, Figure 5.7, and Figure 5.8 are estimated from a fractional release mass curve and are, therefore, normalized. As mentioned above, the total mass released and, consequently, the *in vivo* drug concentration are dependent on the drug-soaking solution concentration, which determines the total mass of drug uptake. A lens loaded with a solution of a higher drug concentration will release greater amounts of mass while not affecting the kinetics of release, as demonstrated in Figure 5.3.
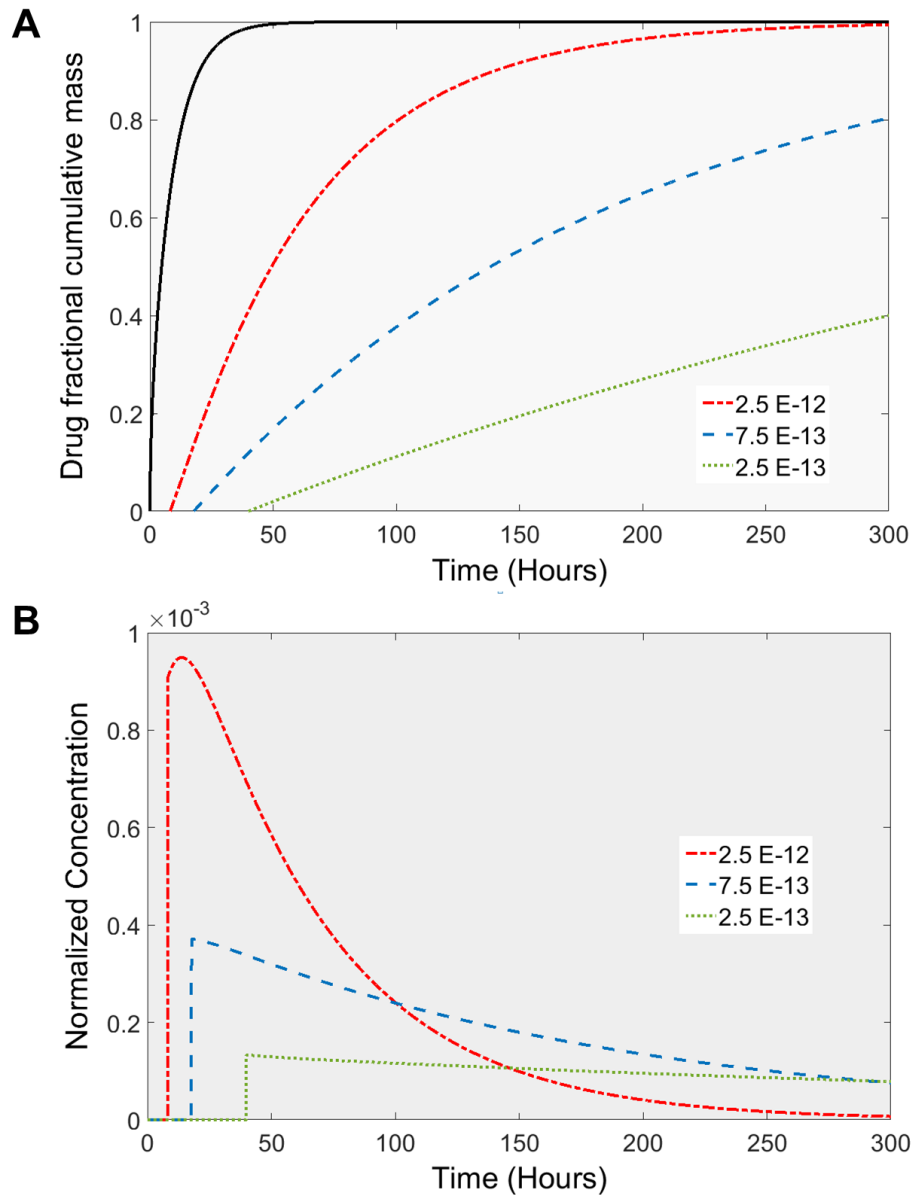
Figure 5.8 - Influence of the coating drug diffusivity in the drug release. (A) Predicted fractional release mass profiles given by numerical simulation; (B) estimated normalized concentration of drug in the aqueous humor volume taking into account the renovation rate of coated lenses. Coating diffusivity values are shown in the figure (full black line: single lens; dashed lines: coated lenses).

5.4 Conclusions

As previously described, the primary aim of ocular drug release studies is to minimize the initial burst of drug release and to achieve a constant target release rate over an adequate time interval. Coating the drug-loaded lenses is a common strategy adopted to achieve these aims. Here, a mathematical model based on a numerical solution of Fick's second law of diffusion is proposed to predict how a certain coating layer influences the drug release profile from a given material. The model predictions were compared with experimentally obtained results to validate the model and were then used to predict the behavior of the drug-loaded multi-layered lens. Results presented in this chapter show that by properly controlling the materials of a multi-layered lens and the interfacial mass flux properties, controlled drug delivery can be achieved. Additionally, by manipulation of the system characteristics (e.g., thickness of the layers, diffusivity of the drugs), a tailored drug release profile can be designed to achieve the desired therapy.

5.5 References

1.   Mathers, W., *Use of higher medication concentrations in the treatment of acanthamoeba keratitis*: Arch Ophthalmol. 2006 Jun;124(6):923.

2.   Dajcs, J.J., et al., *Effectiveness of ciprofloxacin, levofloxacin, or moxifloxacin for treatment of experimental Staphylococcus aureus keratitis.* Antimicrob Agents Chemother, 2004. **48**(6): p. 1948-52.

3.   Lin, C.C. and A.T. Metters, *Hydrogels in controlled release formulations: network design and mathematical modeling.* Adv Drug Deliv Rev, 2006. **58**(12-13): p. 1379-408.

4.   Peppas, N.A. and A.R. Khare, *Preparation, structure and diffusional behavior of hydrogels in controlled release.* Advanced Drug Delivery Reviews, 1993. **11**(1): p. 1-35.

5.   Siepmann, J. and F. Siepmann, *Modeling of diffusion controlled drug delivery.* J Control Release, 2012. **161**(2): p. 351-62.

6.   Paradiso, P., et al., *Comparison of two hydrogel formulations for drug release in ophthalmic lenses.* J Biomed Mater Res B Appl Biomater, 2014. **102**(6): p. 1170-80.

7.   Paradiso, P., et al., *Controlled Release of Antibiotics From Vitamin E-Loaded Silicone-Hydrogel Contact Lenses.* J Pharm Sci, 2016. **105**(3): p. 1164-72.

8.   Lira, M., et al., *Importance of contact lens power and thickness in oxygen transmissibility.* Cont Lens Anterior Eye, 2015. **38**(2): p. 120-6.

9.   Song, H., X. Yuan, and X. Tang, *Effects of intraocular lenses with different diopters on chromatic aberrations in human eye models.* BMC Ophthalmology, 2016. **16**: p. 9.

10.   Kugelberg, U., et al., *Intraocular lens thickness and ocular growth in newborn rabbits.* Acta Ophthalmol Scand, 1997. **75**(3): p. 272-4.

11.   Goel, M., et al., *Aqueous Humor Dynamics: A Review.* The Open Ophthalmology Journal, 2010. **4**: p. 52-59.

12.   Kowalski, R.P., et al., *Gatifloxacin and moxifloxacin: an in vitro susceptibility comparison to levofloxacin, ciprofloxacin, and ofloxacin using bacterial keratitis isolates.* Am J Ophthalmol, 2003. **136**(3): p. 500-5.

13.   Packer, M., et al., *Prevention, diagnosis, and management of acute postoperative bacterial endophthalmitis.* J Cataract Refract Surg, 2011. **37**(9): p. 1699-714.

6 Drug delivery to the anterior chamber by intraocular lenses: an *in vivo* concentration estimation model

Table of Contents

6.1 Introduction

In this chapter attention will be given to the *in vivo* environment where a therapeutic intraocular lens is expected to perform, with the development of a mathematical tool for estimation of drug concentration in the aqueous humor. Most part of the experiments here reported were performed at the University of Florida in Gainesville, USA, under the supervision of Professor Anuj Chauhan.

As exposed in Section 1.2.1 of this thesis, post-operative endophthalmitis (POE) is an inflammation of the intraocular tissues that can occur in an acute phase after surgery, but also in a later stage [1, 2]. Acute POE is usually induced, due to the nature of the ocular surgery, open-globe injury and intravitreal injections [3]. To avoid the evolution of POE, prevention of infection becomes a priority during pre and post-operative cataract removal surgery. Usually, prevention of POE involves topical application of antibiotic drugs, through eye drops delivered into the tear film and afterwards absorbed by the cornea and conjunctiva to deeper tissues of the eye. Intraocular lenses could potentially be used as alternative to topical administration of ophthalmic drugs, since IOLs are implanted in situ where POE may occur. Nonsteroidal anti-inflammatory drugs (NSAIDs) are also prescribed postoperatively for inflammatory response control, and prevention of cystoid macular edema [4].

In the work herein presented we aimed 1) to develop a mathematical tool to estimate the *in vivo* efficacy of drug eluting IOLs, and 2) to predict the performance of commercially available materials used in intraocular lenses manufacturing in what concerns the delivery of antibiotic and anti-inflammatory drugs. The development of a mathematical model arises since *in vivo* conditions, where the IOLs are implanted, are different from those used in our laboratories to study drug release kinetics. The application of animal models is not always an alternative, due to economical and/or ethical reasons [5]. This mathematical tool is, therefore, a first step for selection of the most promising drug delivery systems that can, then, be further tested and optimized.

Two different materials were selected for the case study, a hydrophilic acrylic based material and a silicone hydrogel. For the case here presented, we chose to study two

antibiotics (moxifloxacin and levofloxacin) and two nonsteroidal anti-inflammatories (diclofenac and ketorolac). *In vitro* drug release studies under static/sink conditions were performed to characterize the partition and diffusivity of drugs in the studied materials. To validate our simulation results obtained from the mathematical model, moxifloxacin concentration measured *in vivo* after implantation of a drug loaded IOL by Kleinmann and co-workers [6] were compared to those obtained in this work. *In vivo* results obtained by our group were also used for model validation.

6.2 Experimental Part

6.2.1 Materials

Discs (thickness 1 mm), made from 1) poly[(2-hydroxyethyl methacrylate)-co-(methyl methacrylate)]-based copolymer with 26% equilibrium water content (from this point on mentioned as 26Y) and 2) Definite50-Contamac® with 50% equilibrium water content (from this point on mentioned as DEF50) were provided by PhysIOL S.A. (Belgium). Discs were cut into smaller samples with a cork borer (diameter of 5 mm). Moxifloxacin hydrochloride (MFX), levofloxacin (LVF), diclofenac sodium salt (DCF) and ketorolac tromethamine (KETO) were purchased from Carbosynth Limited (UK). Phosphate saline buffer (PBS, pH 7.4) was purchased from Sigma-Aldrich (USA).

6.2.2 Drug loading procedure

Drug loaded samples were prepared by soaking discs into 1 mL of drug solution (5 mg.mL^{-1}). All drug solutions were prepared with PBS. The loading period was chosen to be 15 days, since, from previous studies, this time period is expected to be enough to ensure drug equilibrium inside the samples with the loading solution, at room temperature. After the loading period, samples were gently immersed in deionized water and blotted in lab paper, to remove drug in the samples surface.

6.2.3 *In vitro* drug release experiments and determination of K and D$_e$

Drug release was performed in 10 mL of PBS at room temperature and under mild shaking. At predetermined times drug concentration was measured in a Thermo Scientific™ GENESYS™ 10S UV-Vis spectrophotometer (USA), in the range 190 – 320

nm or in an UV–VIS MultiscanGO from ThermoScientific® spectrophotometer in the range 200 – 400 nm.

Partition coefficient K can be calculated through the following equation based on the release data:

$$K = \frac{V_r C_{f,r}}{V_{gel} C_{f,l}}$$
Equation 6.1

where $C_{f,r}$ is the final concentration of the release medium, V_r is the volume of the release medium, V_{gel} the volume of the fully hydrated gel sample and $C_{f,l}$ the concentration in the loading solution.

As in section 5.2.3, the effective diffusivity, D_e, can be determined with an analytically model based on the one-dimensional diffusion equation when fitted to experimental release data. Briefly, the drug transport can be described through a uniform thickness film through the Fick's second law:

$$\frac{\partial C}{\partial t} = D_e \frac{\partial^2 C}{dy^2}$$
Equation 6.2

where $C(y,t)$ is the concentration of the drug in the lens, y is the spatial coordinate, $y = 0$ is the center of the lens, and t is time. The boundary conditions for the drugs release experiments are the following, with h as the lens half-thickness:

$$\frac{\partial C}{\partial y}(y = 0, t) = 0$$
Equation 6.3

$$C(y = h, t) = 0$$
Equation 6.4

The first boundary condition accounts for the symmetry at the center of the lens and the second boundary condition is based on the sink assumption. The known initial condition is the concentration of drug in the lens C_i

$$C(y, t = 0) = C_i$$
Equation 6.5

A mass balance on the aqueous release phase yields:

$$-2D_e A_{surface} \frac{\partial C}{\partial y}\Big|_{y=h} = V_r \frac{dC_r}{dt}$$
Equation 6.6

Where $A_{surface}$ is the lateral area of the lens, C_r is the release phase drug concentration and V_r the release phase volume. The diffusion based problem can be solved and, when fitted to the experimental data, D_e can be determined.

6.2.4 *In vivo* drug release model

We develop a model to predict the drug concentration in the aqueous humor released from a soaked intraocular lenses placed in the eye as substitute of a cataract. In Figure 6.1, a representation of an IOL placement in the eye is shown, the model geometry herein used is also shown in Figure 6.1.
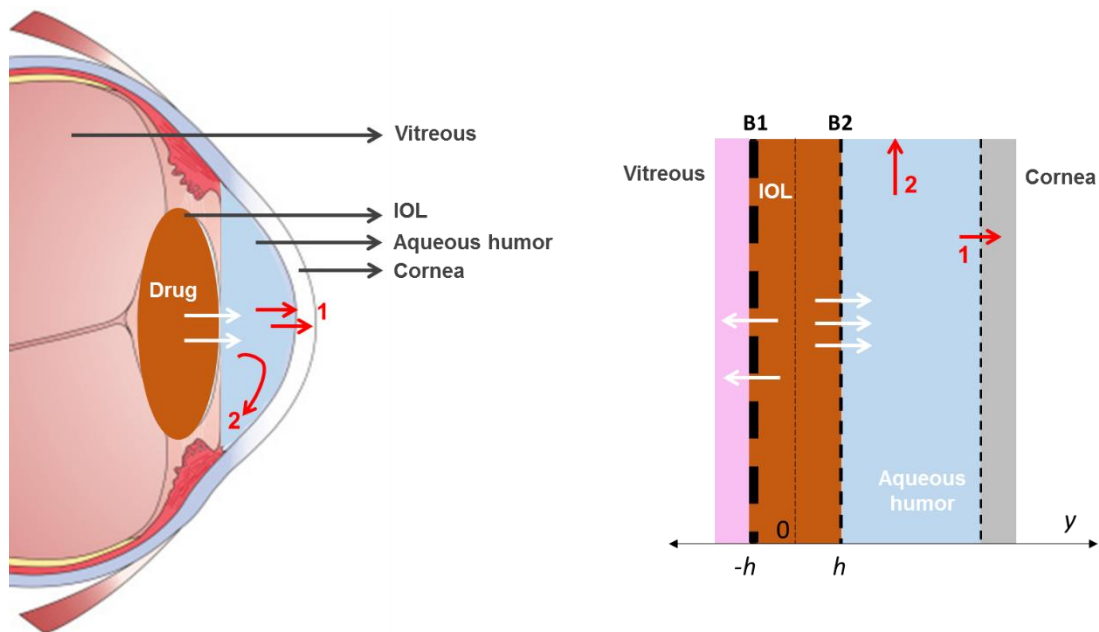
Figure 6.1 – Schematic representation of the IOL placement in the eye (left) and the mathematical model design (right) with (1) drug permeation to the cornea and (2) drug loss due to aqueous humor turnover.

The aqueous humor is represented as a flat, two-dimensional film bounded by a non-deformable cornea and a non-deformable IOL. The IOL is treated as a two-dimensional object with a half-thickness of h. The assumption of a two-dimensional geometry has been made to simplify the problem. Considering that the diffusion of the drug through the IOL gel matrix is a purely diffusive process it can be described with Equation 6.2. To solve the diffusion problem it is necessary to represent mathematically the boundary conditions

between both the vitreous-IOL (B1 on Figure 6.1) and the aqueous humor-IOL (B2 on Figure 6.1).

Regarding the first boundary, with the common use of the extracapsular cataract extraction technique, the elastic capsular bag that covers the lens is left in the eye partially intact after surgery. This capsule remains between the implanted IOL and the vitreous. Published reports suggest that this thin envelop (thickness ranging from 3.5 to 16 μm [7]) is permeable to small molecules, but that capsule permeability can be also dependent on other factors, besides size, such as the molecule charge [8, 9]. As for the vitreous, it is a mostly avascular and transparent thick, gel-like fluid that occupies the space between the lens and the retina. Vitreous volume in rabbits was reported to be 1.15 mL and in humans 4 mL [10]. This fluid is composed of 99.9% water and 0.01% collagen fibrils, hyaluronic acid and ions [11]. The diffusion of solutes in the vitreous has been previously described as unrestricted due to the low concentration of collagen [12]. Davis and co-workers developed an empirical relationship to determine if the concentration of collagen and hyaluronic acid would affect drug diffusivity in the vitreous [13]. For a molecular weight of 100.000 Da the ratio between diffusivity in the vitreous and in a polymer-free aqueous solution was 0.992, which taking into account the small molecular weight of ophthalmic drugs suggests that for these drugs, if no biding interaction exist, diffusivity in the vitreous is equivalent to that in free aqueous solution.

Considering that all drugs used in this work are soluble in water and assuming that when in the vitreous drug molecules will rapidly be diffused from the lens surface, since no data is available for our drugs on that, a sink condition for the boundary vitreous-IOL was considered. It must be stressed that this is clearly the scenario that will maximize the fraction of drug delivered to the vitreous, hence minimizing the drug delivery to the aqueous. The other extreme scenario would be to consider a completely impermeable vitreous-IOL boundary. Since we do not possess information about the capsule permeability to our drugs we cannot define an intermediate case that would probably more accurately describe the real condition. In section 6.3.2.1, the drug concentration profiles in the aqueous humor are presented for the two extreme cases above described, for the sake of comparison.

As for aqueous humor-IOL boundary, the drug molecules diffusing towards the anterior chamber will either (1) permeate through the cornea, or (2) will be washed out due to the aqueous humor turnover (see Figure 6.1). Aqueous turnover in humans is approximately 1% of the aqueous total volume (2.5 µL.min^{-1}) [11], which is nearly the same observed in rabbits [14, 15]. Permeability through the cornea will be dependent on the nature of the drug and consequently interactions with corneal layers. Prausnitz and Noonan [16] published an extensive review on the permeability of different drugs in ocular tissues and stablish relations between different drug characteristics, such as molecular radius, and corneal permeability. The values of permeability considered in this work, obtained from different literature sources, are presented in Table 6.1.

Table 6.1 – Corneal permeability of drugs studied in this chapter.

	Corneal permeability (cm.s^{-1})	Ref.
Moxifloxacin	1.58 x10^{-6}	[17]
Levofloxacin	3.94 x10^{-6}	[18]
Diclofenac	2.65 x10^{-7}	[19]
Ketorolac	5.31 x10^{-6}	[20]

Taking into account the facts mentioned above and the assumptions done, the following equations may be set:

$$\frac{\partial C}{\partial y}(y = 0, t) = 0 \qquad \textbf{Equation 6.7}$$

$$C(y = -h, t) = 0 \qquad \textbf{Equation 6.8}$$

$$C(y = h, t) = KC_{aq} \qquad \textbf{Equation 6.9}$$

As for the *in vitro* drug release experiments, the first condition (Equation 6.7) accounts for the symmetry at the center of the lens. The second boundary condition (Equation 6.8) is based on the sink assumption at the vitreous-IOL boundary, and the third (Equation 6.9) assumes equilibrium between the drug concentration in the lens and that in the aqueous humor (C_{aq}), considering the partition coefficient (*K*).

The initial conditions for the concentration of drug in the lens and in the aqueous humor are given by

$$C(y, t = 0) = C_i(y)$$ **Equation 6.10**

$$C_{aq}(t = 0) = 0$$ **Equation 6.11**

For the initial condition inside the lens, either a uniform concentration C_i was chosen or a spatial dependent concentration, for a loading time inferior to the required to achieve equilibrium.

Taking the assumptions above described, drug concentration in the aqueous humor $C_{aq}(t)$ can be estimated considering the accumulation of drug from the IOL into the aqueous humor and the loss of drug due to the renovation of the aqueous (q) and drug permeation into the cornea ($k_{cornea}A_{cornea}$) yielding the following equation:

$$V_{aq}\frac{dC_{aq}}{dt} = A_{surface}D_e\frac{\partial C}{\partial y}\Big|_{y=h} - (k_{cornea}A_{cornea} + q)C_{aq}$$ **Equation 6.12**

The above set of equations was solved numerically to obtain $C_{aq}(t)$.

6.3 Results and Discussion

6.3.1 Validation of the *in vivo* drug release model

As mentioned above, to validate the *in vivo* drug release model herein described effective diffusivity and partition coefficients of MFX were determined, through *in vitro* release experiments, and mathematical prediction of MFX concentration in the aqueous humor was investigated, and compared to that obtained in the *in vivo* studies involving implantation of moxifloxacin loaded IOLs.

Data publish by Kleinmann and co-workers [6] were selected. They implanted acrylic IOLs (C-flex®, Rayner Intraocular Lenses, Ltd.), composed by hydrophilic HEMA and hydrophobic MMA, the soaked in moxifloxacin solution (Vigamox®, 5 mg.mL^{-1}) for 24 hours, in the capsular bag of fifteen rabbits. Aqueous humor from the anterior chamber was collected 4, 8 and 12 hours after IOL implantation and MFX concentration was measured.

Since C-flex® IOLs composition is similar to those provided to our group by PhysIOL S.A. the latter were used for moxifloxacin's effective diffusivity and partition coefficient determination. The fractional cumulative release profile resulting from experiments and correspondent fitted data are plotted in Figure 6.2. The good fit between the experimental data and the model results suggested that diffusion shall be the main mechanism of the drug release. The effective diffusivity of MFX in the acrylic IOLs was determined through this fitting (Equation 6.2) and the partition value obtained was obtained through Equation 6.1 (Table 6.2).
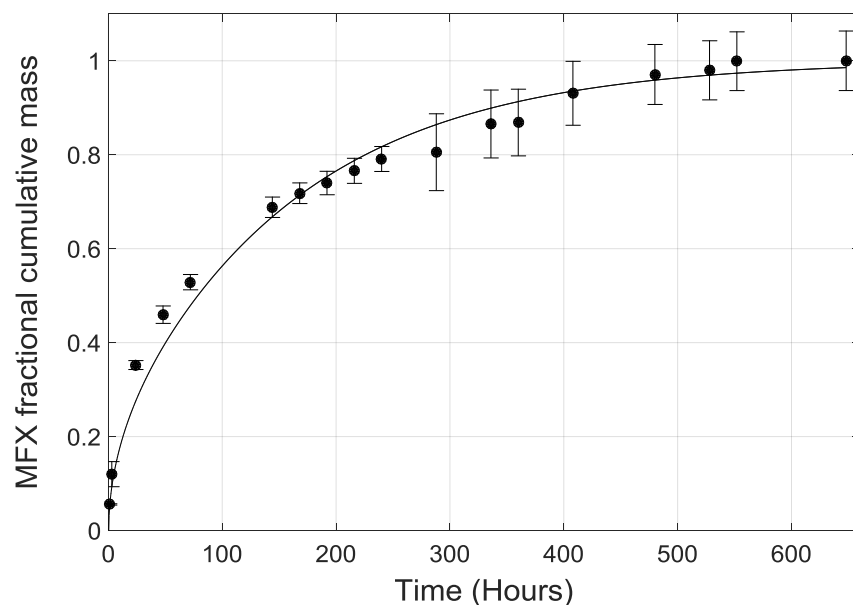
Figure 6.2 – MFX (●) average fractional release profiles (results are presented as mean ± standard deviation, *n*=3) and fitted data (solid line).

Table 6.2 - Partition coefficient, effective diffusivity and MFX mass released.

K	1.88 ± 0.12
D_e (m^2s^{-1})	$1.59 \times 10^{-13} \pm 9.3 \times 10^{-15}$
Mass released (µg/mg dry gel)	6.27 ± 0.38

Kleinmann and co-workers chose to load IOLs for only 24 hours, which we suspected to be an insufficient period to achieve equilibrium between IOLs and loading solution. In Figure 6.3, MFX concentration profile inside the lens after 24 hours and 15 days of

loading is plotted - these profiles are also obtained through the mathematical solution of Equation 6.2, with modified initial conditions (null initial drug concentration in the lens and constant drug concentration - 5 mg.mL^{-1} - in the aqueous phase). As is possible to observe the lens is not at equilibrium when implanted *in vivo*, resulting in the underestimation of the full potential (in release time and drug mass) of these lenses, since a lens at equilibrium would be loaded with more drug.
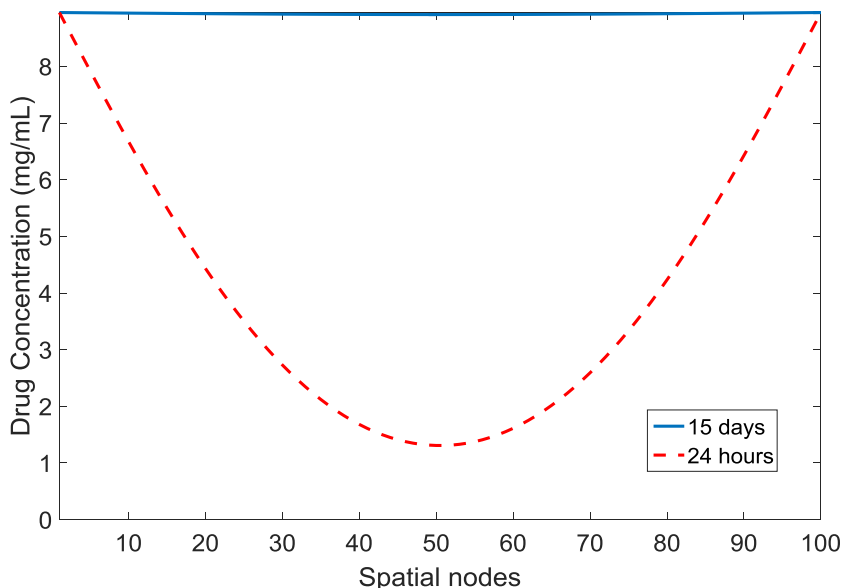
Figure 6.3 – Moxifloxacin concentration profile in the lens after 24 hours and 15 days of loading

Once the diffusivity and partition values were determined, simulations of the release *in vivo* for an IOL (with an approximate IOL geometry: 0.6 mm of thickness and 6 mm of diameter) loaded in the same conditions as described by Kleinmann *et al.* were done, taking into account the experimental standard deviations for K and D$_e$. An aqueous volume of 0.250 mL, aqueous turnover of 2.5 μL.min^{-1}, and moxifloxacin corneal permeability of 1.58 x10^{-6} cm.s^{-1} were considered for all the simulations presented in this section (see Section 6.2.4).

The shaded region in Figure 6.4 represents the expected aqueous humor concentrations from our simulation results considering as extremes the maximum value of K and the minimum of D$_e$, and the maximum value of D$_e$ and the minimum of K.

141
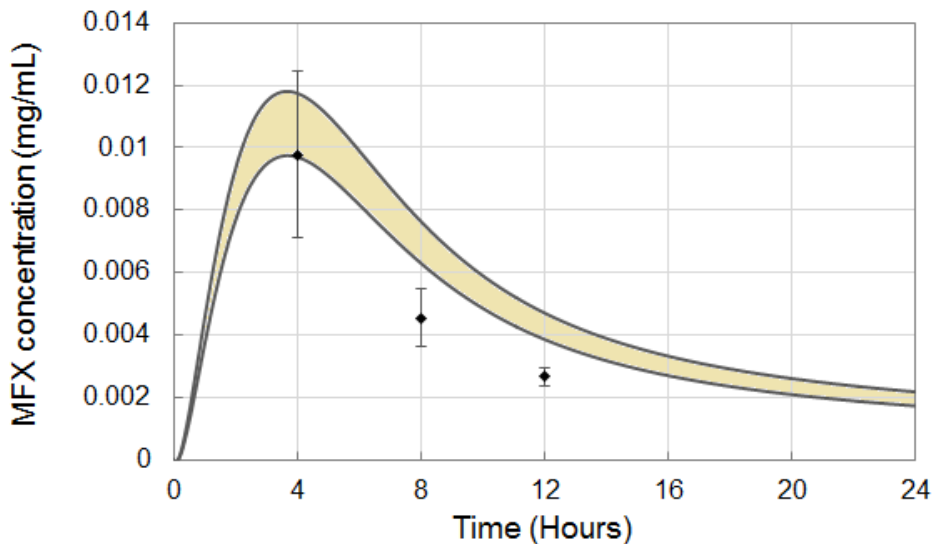
Figure 6.4 – Aqueous humor concentrations of MFX (♦) obtained by Kleimann and co-workers (±STDV) [6] and mathematical prediction of MFX concentration shaded region for 24 hours of loading.

Although visually is possible to observe that the model prediction follows the data tendency, the simulation tends to overestimate the concentration. This discrepancy can be, for instance, result of experimental deviations, biological or other factors that are not account for in this simplified model, but, in general, a good approximation was obtained.

In our research group, in the context of a European funded M-ERA.NET project ("Surflenses"), different MFX loading strategies of the 26Y material have been attempted (e.g., see Chapter 4). One of the studied IOL-MFX systems consisted, briefly, of a 26Y IOLs sterilized and loaded until equilibrium in a 5 mg.mL^{-1} MFX solution. Afterwards, IOLs were implanted in six 8-week-old New-Zealand rabbits, and an aqueous humor sample was collected after one week. The determined concentration was ~523 ± 51 ng/mL (*n*=6). This value was plotted in Figure 6.5 together with the expected concentration region for IOLs loaded until equilibrium. As is possible to observe, our model predicts with great accuracy the *in vivo* obtained result.
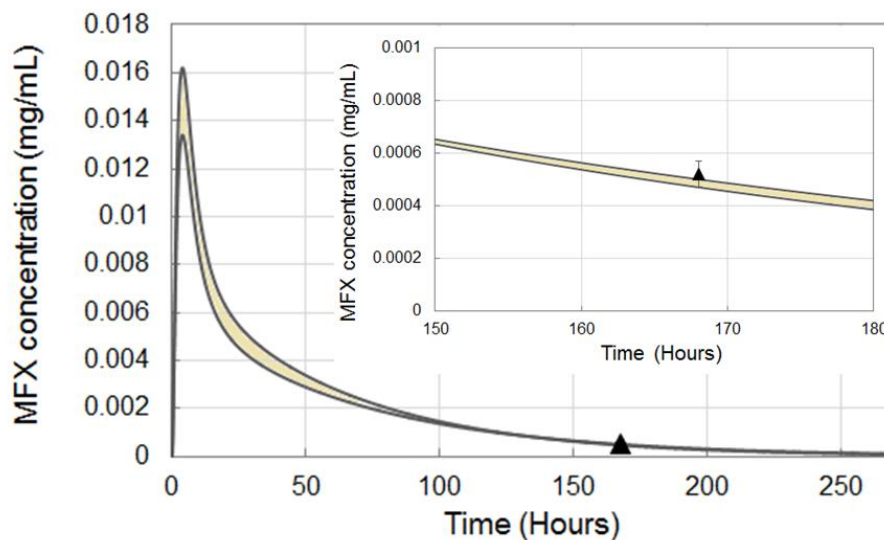
Figure 6.5 - Aqueous humor concentrations of MFX (▲) obtained by our group and mathematical prediction of MFX concentration shaded region for the loading conditions used.

The results presented in this section, allow us to say that the mathematical tool herein developed can provide useful information about the *in vivo* performance of a drug eluting IOL, with only partition and diffusivity values, easily obtained through in-lab loading and release experiments. Therefore, in section 6.3.2.2, other materials and drugs are screened, with the aim of achieving the best potential therapeutic IOL for post-cataract removal surgery prophylaxis.

6.3.2 Simulations with the *in vivo* model

6.3.2.1 Impact of vitreous permeability, aqueous turnover and corneal permeability

Before the *in vivo* efficacy investigation of the studied drugs loaded in commercially available materials, in this section a brief analysis of the different inputs considered in the model is presented. The partition and effective diffusivity of moxifloxacin in the hydrophilic acrylic (Table 6.2) were considered as reference in this section, and, if not otherwise mentioned, simulation parameters were made with aqueous volume equal to 0.250 mL, aqueous turnover rate 2.5 $\mu L.min^{-1}$, and corneal permeability of moxifloxacin 1.58 x10^{-6} cm.s^{-1}.

As explain in section 6.2.4, a sink condition was considered since a non-restricted diffusion to and in the vitreous was assumed. In Figure 6.6, a comparison between the aqueous humor concentration for a sink condition or a no-flux condition on the boundary vitreous-IOL is plotted. The initial burst of drug does not change when a no-flux condition is imposed, since it is mainly consequence of short-term release from diffusing drug molecules close to the aqueous-IOL boundary (see Figure 6.1). The no-flux condition becomes relevant after approximately 48 hours, when is possible to observe higher values for drug concentration when compared to those obtained for the sink boundary condition.

The best adjustment of our model to the *in vivo* implantation data used for validation (see section 6.3.1) was obtained for the experimental aqueous humor collected at day 7, which could suggest that our model assumptions regarding the vitreous-IOL boundary are reasonable. Nonetheless, more *in vivo* experimental data should be compared to our model predictions for further conclusion. Unfortunately, not many studies are available for comparison and most of available studies focus on the early days of implantation for aqueous humor sample collection.
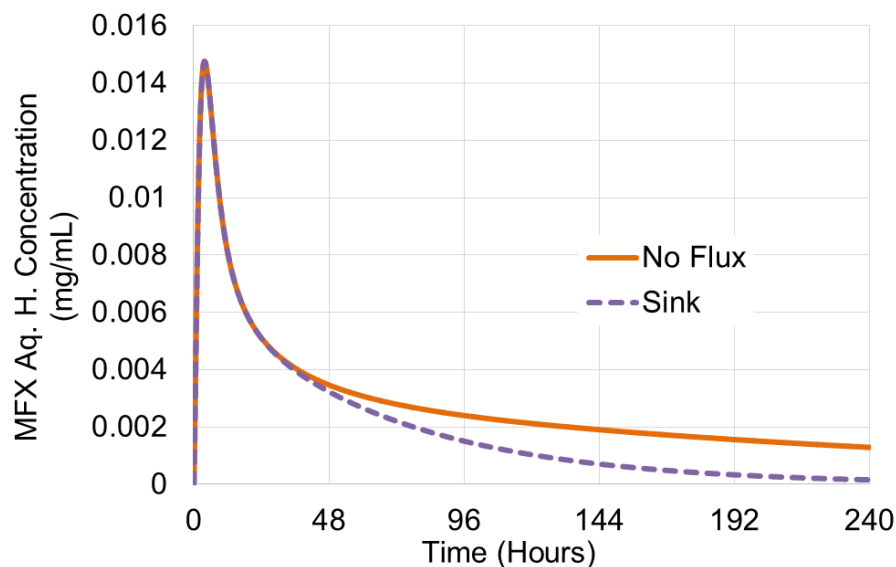
Figure 6.6 - Prediction of MFX concentration in the aqueous humor considering a sink or a no-flux lens/vitreous boundary condition.

The second aspect to be consider was the aqueous turnover, in our previously shown simulations we assumed it to be 1% of the aqueous total volume (2.5 µL.min^{-1}) [11]. This

is an average value, since the rate of aqueous humor flow varies, for instance, according to a circadian rhythm with different rates of flow during day time and night [21, 22]. In Figure 6.7, prediction of MFX concentration in the aqueous for different turnover rates are shown. Changes in the turnover rate impact the concentration of drug present in the aqueous, with an inverse relation. If aqueous turnover oscillations with time are known, they could be introduced in the model for better prediction of the *in vivo* concentration.
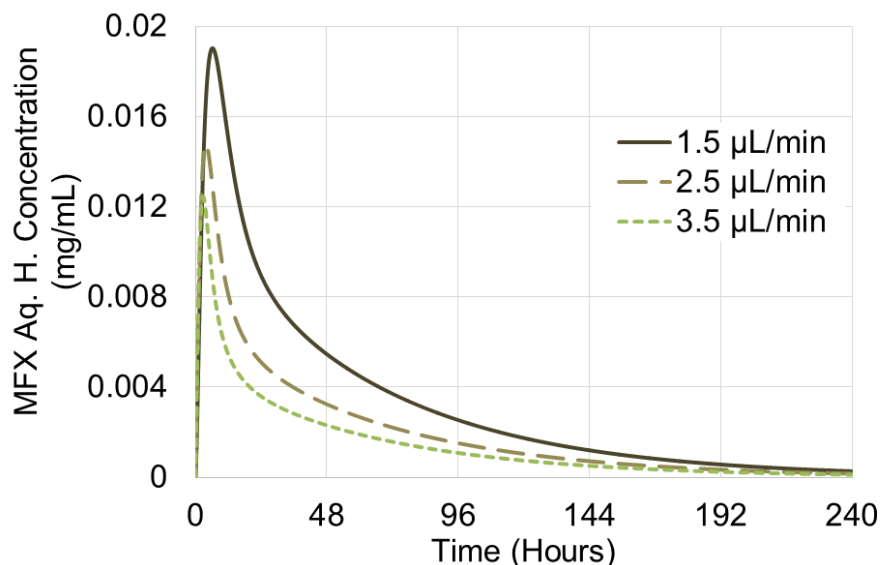
Figure 6.7 - Prediction of MFX concentration in the aqueous humor considering different turnover rates.

Finally, the last theoretical simulation of this section takes into account corneal permeability variations. Each drug possesses intrinsic properties that will influence its partition or diffusivity in a certain material, and the permeability in the different corneal layers. Accurate values will result in more accurate model predictions, but since it is not always possible to obtain experimentally or from the literature exact values of corneal permeability, as it is to experimentally attained D_e or K values, it becomes relevant to understand the impact on model results of the considered corneal permeability. Corneal permeability of moxifloxacin was considered 1.58 x10^{-6} cm.s^{-1} [17], and simulation with permeability values an order of magnitude above or below are presented in Figure 6.8. No significant difference is observe for permeability values of 1.58 x10^{-6} cm.s^{-1} or 1.58 x10^{-7} cm.s^{-1}, suggesting the existence of an inferior limit value for permeability, from which

the concentration in the aqueous will only depend on the drug flux from the lens, and the turnover rate.
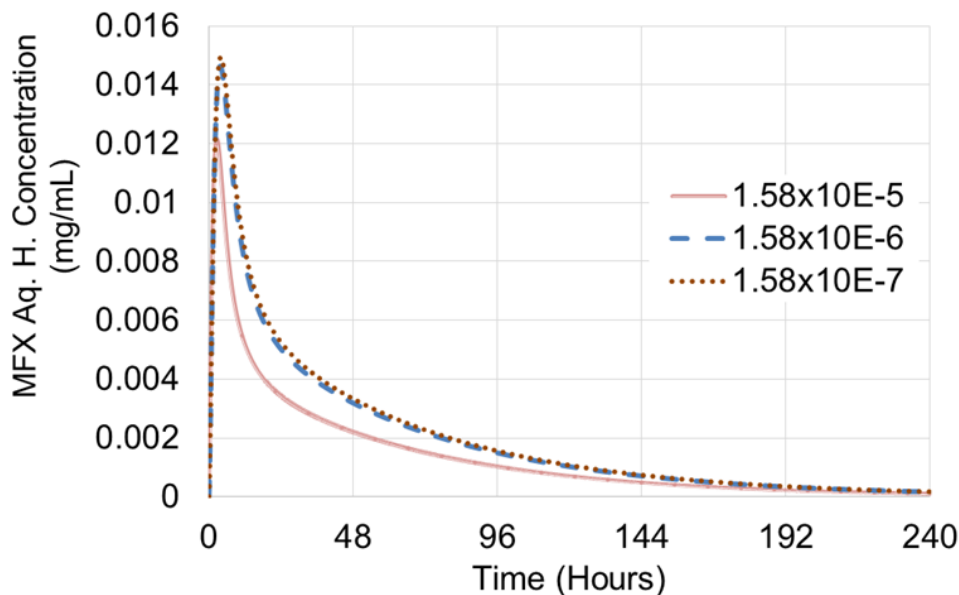
Figure 6.8 - Prediction of MFX concentration in the aqueous humor considering different corneal permeability values.

6.3.2.2 Efficacy estimation of different material/drug IOL systems

In the present section, the *in vivo* efficacy of four drugs (two antibiotics and two NSAIs) released from two commercially available materials for IOLs will be investigated. The aim was to obtain information about these drug/material systems that could provide indication of their potential suitability as devices for post-cataract removal prophylaxis.

The first step was to determine the partition and effective diffusivity coefficients of drugs, as detailed in section 6.2.3. Results for the silicone hydrogel and hydrophilic acrylic are presented in Table 6.3. A hydrophobic acrylic was also tested but, due to the low water content of this material (4%), it was not possible to achieve a successful drug loading through the soaking method. Since many consider hydrophobic acrylic to be one of the most popular types of IOLs, other loading strategies for this material could be attempted as future work. From the results presented in Table 6.3, one can conclude that, for all drugs, partition into the silicone hydrogel is higher than that to the acrylic material, which could be explained, for instance, by the lower equilibrium water content of the latter. Other

146

interactions, as those studied in Chapter 2 of this thesis, could also be responsible for this fact.

Table 6.3 - Partition and effective diffusivity coefficients.

DEF50 - Silicone hydrogel		
	K	**D_e (m^2s^{-1})**
Moxifloxacin	3.42 ± 0.02	$2.98 \times 10^{-12} \pm 3.47 \times 10^{-13}$
Levofloxacin	0.72 ± 0.01	$5.50 \times 10^{-12} \pm 2.0 \times 10^{-13}$
Diclofenac	33.07 ± 6.50	$7.59 \times 10^{-13} \pm 2.10 \times 10^{-13}$
Ketorolac	3.14 ± 0.21	$3.43 \times 10^{-12} \pm 1.85 \times 10^{-13}$
26Y - Hydrophilic acrylic		
	K	**D_e (m^2s^{-1})**
Moxifloxacin	1.88 ± 0.12	$1.59 \times 10^{-13} \pm 9.3 \times 10^{-15}$
Levofloxacin	0.60 ± 0.05	$5.93 \times 10^{-13} \pm 1.28 \times 10^{-13}$
Diclofenac	16.21 ± 1.12	$2.14 \times 10^{-13} \pm 5.56 \times 10^{-15}$
Ketorolac	2.89 ± 0.17	$4.54 \times 10^{-13} \pm 6.99 \times 10^{-14}$

For estimation of the aqueous humor concentration, simulations with an aqueous volume of 0.250 mL, and aqueous turnover rate of 2.5 µL.min^{-1} were considered. Drug corneal permeability for the four drugs values are presented in Table 6.1. Time of IOL loading was stablished as 15 days with concentrations as those used in experimental assays (5 mg.mL^{-1}), and an approximate IOL geometry with 0.6 mm of thickness and 6 mm of diameter.

To exemplify how this *in vivo* model can be used on the evaluation of drug eluting IOLs efficacy, criteria regarding the drug effective concentration must be drawn.

For antibiotics, a minimum inhibitory concentration (MIC), defined as the lowest concentration of an antimicrobial that will inhibit the visible growth of a microorganism, can be considered as reference value. The major pathogens associated to post-operative endophthalmitis are coagulase-negative staphylococci, responsible for about 70% of the POE cases in the USA [23], *Staphylococcus aureus*, streptococci, other Gram-positive cocci, including enterococci and mixed bacteria, and Gram-negative bacilli [24]. Most of

the coagulase-negative staphylococci associated with clinical disease belong to the normal skin flora, being *Staphylococcus epidermidis* the most predominant species [25]. We selected *Staphylococcus aureus* and *Staphylococcus epidermidis* as target bacteria, and considering the MIC values found in literature for these bacteria. MIC values can vary significantly within the same species, dependent on the chosen strain. In this work, we did not aim to extensively study or discuss the clinical aspect from a bacterial endophthalmitis epidemiology perspective, as such, only representative values of MIC for two susceptible *Staphylococcus aureus* and *Staphylococcus epidermidis* strains were chosen (see Table 6.4).

The anti-inflammatory action of NSAIDs is produced by the inhibition of cyclooxygenase isoenzymes, COX-1 and COX-2, which catalyze the formation of prostaglandins, mediators of pathogenic mechanisms, including the inflammatory response [26, 27]. For these drugs, half maximal inhibitory concentration (IC_{50}), a measure of the effectiveness of a substance in inhibiting a specific biological or biochemical function, was used as reference concentration value. In literature, IC_{50} concentration ranges were found to diclofenac and ketorolac, and used as reference values (see Table 6.4).

Table 6.4 - Minimum inhibitory concentration for antibiotics and half maximal inhibitory concentration for NSAIs [28-30].

	MIC (μgmL^{-1})	
	Moxifloxacin	**Levofloxacin**
S. aureus	0.06	0.5
S. epidermidis	0.03	0.25
	IC_{50} (μgmL^{-1})	
	Diclofenac	**Ketorolac**
COX-1	0.038 to 0.302	0.005 to 0.008
COX-2	0.010 to 0.029	0.034 to 0.045

From Figure 6.9 to Figure 6.12 results obtained for aqueous humor concentration estimative are presented as concentration profiles, for each drug in both materials. The

148

initial drug burst concentrations of the antibiotics and the NSAIDs are plotted in Figure 6.9 and Figure 6.10, respectively. For all drugs, higher peak concentrations are estimated for DEF50 during the initial drug burst, explained by the higher effective diffusivity values when compared to those in 26Y. A relevant initial burst concentration could potentially be relevant in the case of the antibiotics to significantly reduce the bacteria initially present in the anterior chamber. Nowadays, this initial reduction is achieved through the use of intracameral antibiotic injections during the surgical procedure [31]. DEF50 released a significant initial concentration of MFX (see Figure 6.9 B), but it is not able to release concentrations of MFX for prolonged time periods, whereas 26Y, with smaller initial burst concentrations seems to be able to release the soaked drug over longer periods.
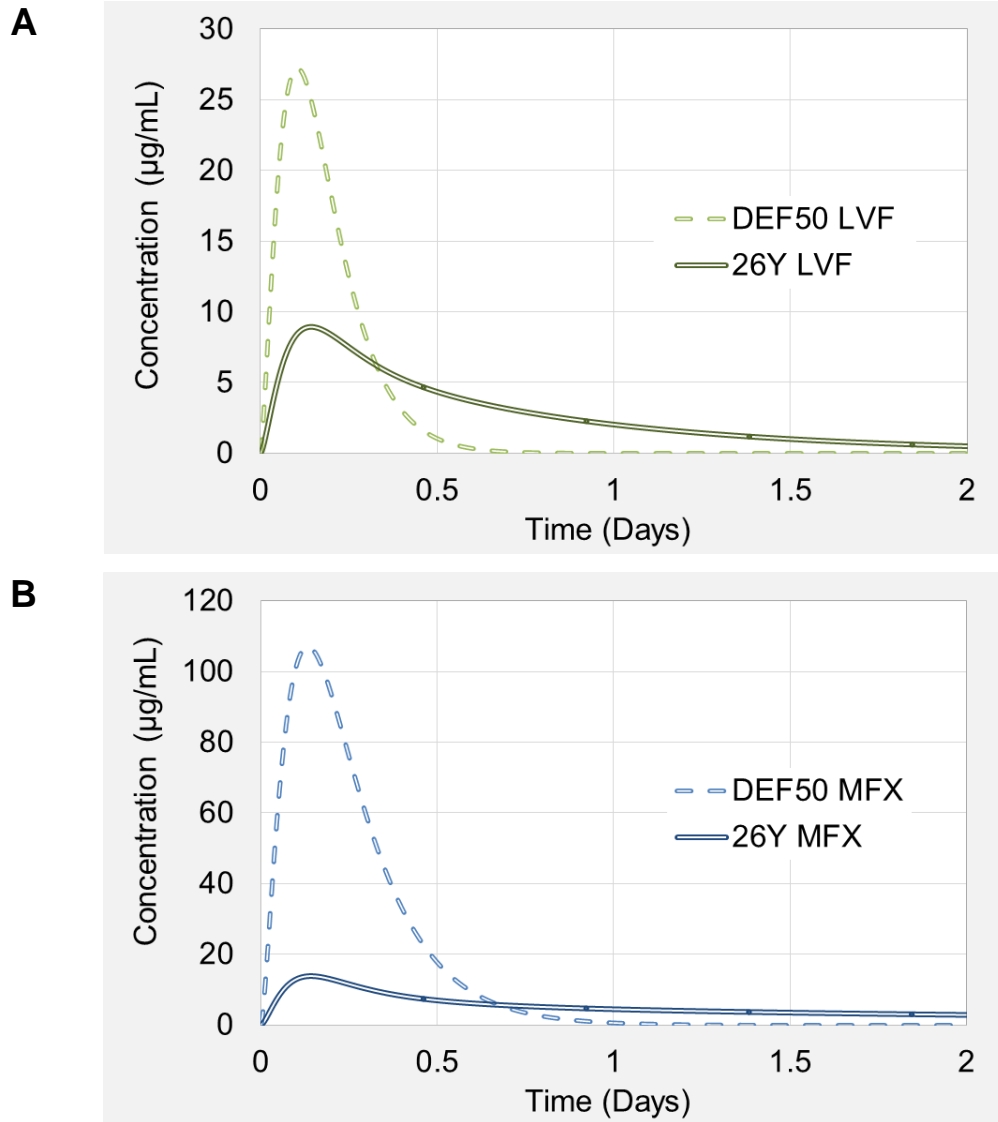
Figure 6.9 - Prediction of A) levofloxacin and B) moxifloxacin initial burst concentration in the aqueous humor for DEF50 or 26Y IOLs.

Analogously to the results obtained with the antibiotics, the 26Y material presents higher potential to be used as platform for extended release of NSAIDs (see Figure 6.10), with smaller initial burst concentrations.
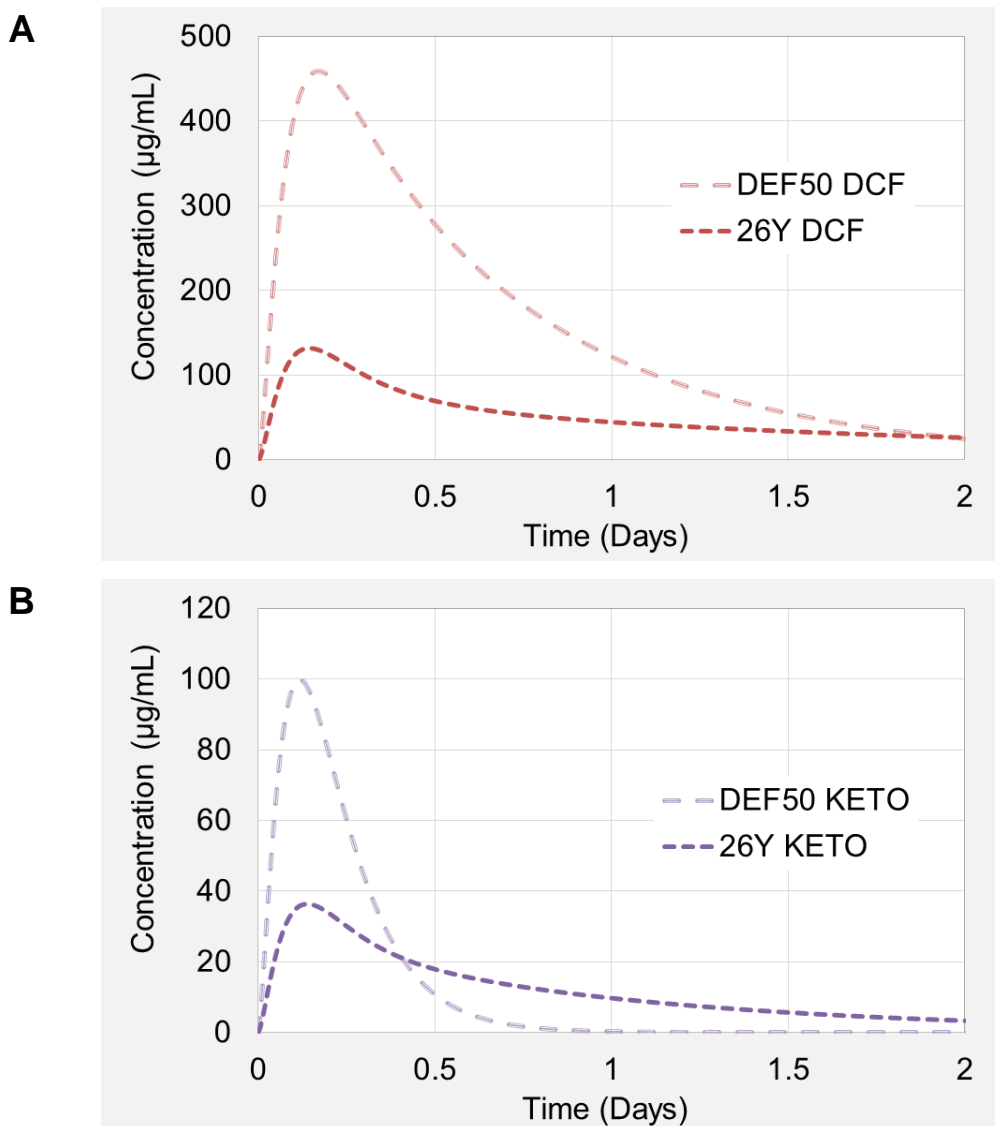
Figure 6.10 - Prediction of A) diclofenac and B) ketorolac initial burst concentration in the aqueous humor released for DEF50 or 26Y IOLs.

Prediction of effective time periods for the antibiotics was done through comparison to the reference MIC values (Table 6.4). 26Y-LVF and DEF50-LVF IOLs present an expected effective life-span approximately of two and one days, respectively (see Figure 6.11 A). Low partition of LVF for both materials justifies the small *in vivo* concentrations,

151

and poorer potential of this drug to be used in a device such as the one envisioned in this work.

In opposition to LVF, MFX *in vivo* concentrations estimations for the hydrophilic acrylic material 26Y indicate that the MFX eluting IOL could be effective, against susceptible *S. aureus and S. epidermidis*, up to twelve days (see Figure 6.11 B). These IOLs could be used as prophylaxis for acute post-cataract endophthalmitis as substitutes of the topical administration of eye drops, and complementary to the intracameral injections provided during surgery. As expected DEF50 material shows poor extended release performance, with total drug release expected after two days of implantation.
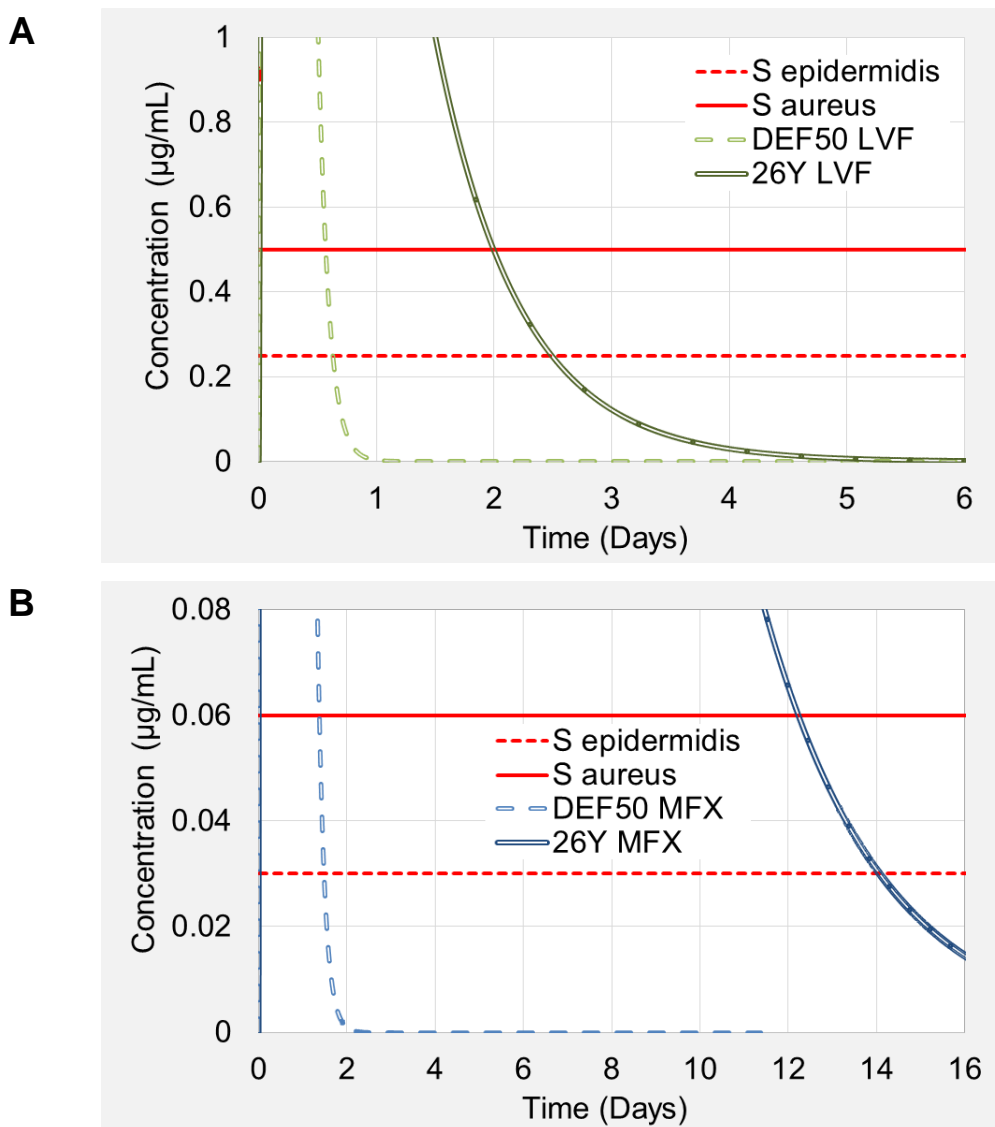
Figure 6.11 - *In vivo* efficacy time period prediction for A) levofloxacin and B) moxifloxacin released from DEF50 or 26Y IOLs.

For the studied NSAIDs, we consider as the reference value the highest reported half-maximal response value (IC_{50}) for each drug (see Table 6.4). We estimate that a DEF50-DCF IOL could release an amount of drug enough for inflammatory response inhibition for five days, whereas a 26Y-DCF IOL could achieve this goal for a period of eleven days, presenting, therefore, the higher potential to be used as delivery platform for prevention of inflammatory response (see Figure 6.12 A).

KETO eluting DEF50 or 26Y IOLs present an inferior effective life-span, when compare to DCF eluting IOLs, with an expected effective performance *in vivo* for DEF50 IOLs of approximately one day, and six days for 26Y IOLs (see Figure 6.12 B).

Since we considered the highest reported IC_{50} values for DCF and KETO, these effective time periods are probably underestimating the real potential of the materials as NSAIDs controlled release platforms.
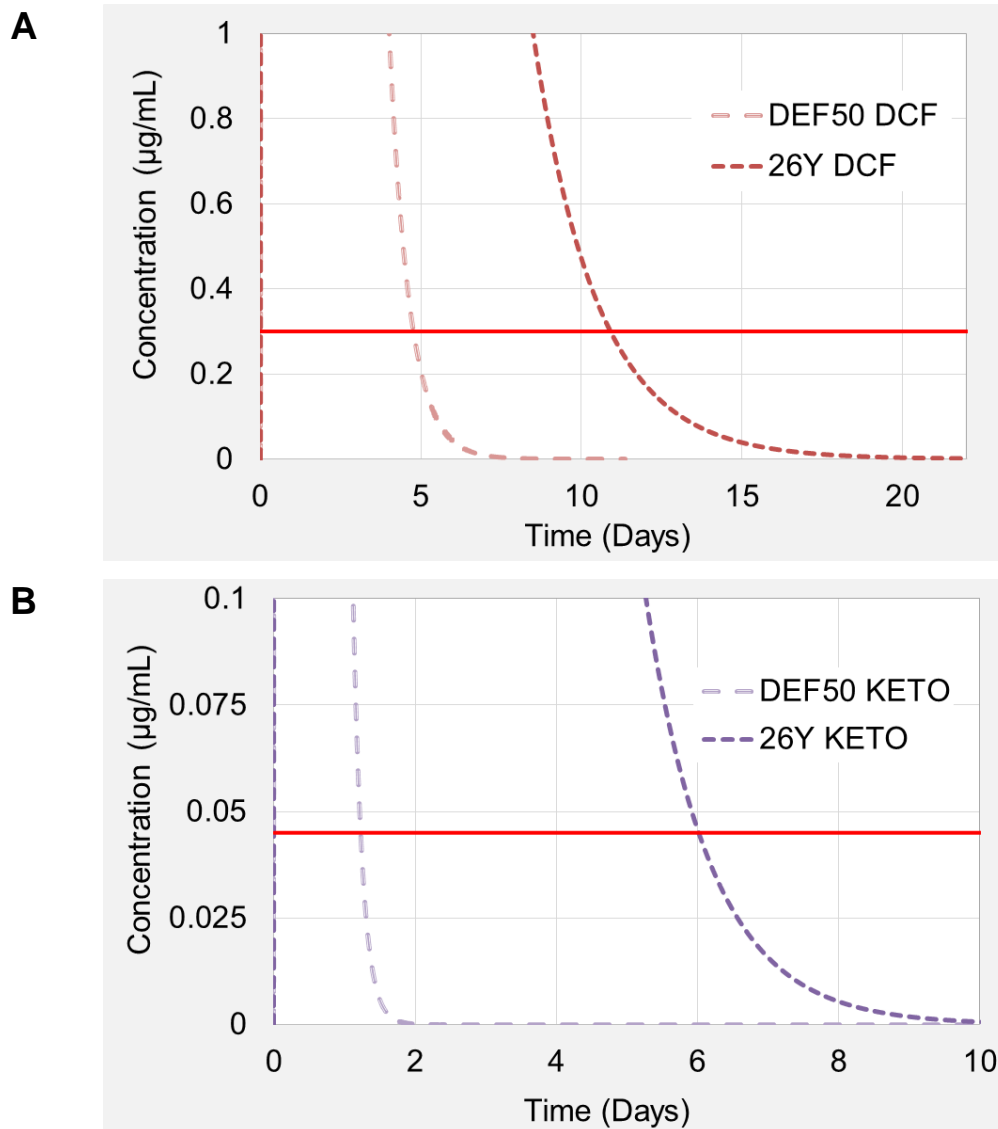
Figure 6.12 - *In vivo* **efficacy time period prediction of A) diclofenac and B) ketorolac released from DEF50 or 26Y IOLs.**

Simulations presented in Figure 6.9 to Figure 6.12 were made considering a loading concentration of 5 mg.mL^{-1}. If other concentration were used, concentration profiles *in vivo* are expected to change accordingly. As example, in Figure 6.13 concentration predictions for 26Y-MFX IOLs loaded in solutions with concentrations ranging from 1 to 10 mg.mL^{-1} are plotted. Inferior loading concentrations result in less drug inside the IOL when equilibrium concentration between loading solution and lens is attained. This fact has as consequences: 1) lower drug burst concentrations on the first hours of release, and 2) MICs are reached quicker.

For a given lens-drug system, it is possible to predict the effective concentration time period, and to tailor the loading protocol to the desired application. For instance, for prevention of acute post-cataract endophthalmitis, which can occur up to two weeks after surgery, prescription of antibiotic during that time period is widely accepted [31]. For a 26Y-MFX IOL a minimum loading concentration of 10 mg.mL^{-1} is necessary for an estimated effective concentration of 14 days against both *Staphylococcus epidermidis* and *Staphylococcus aureus*.
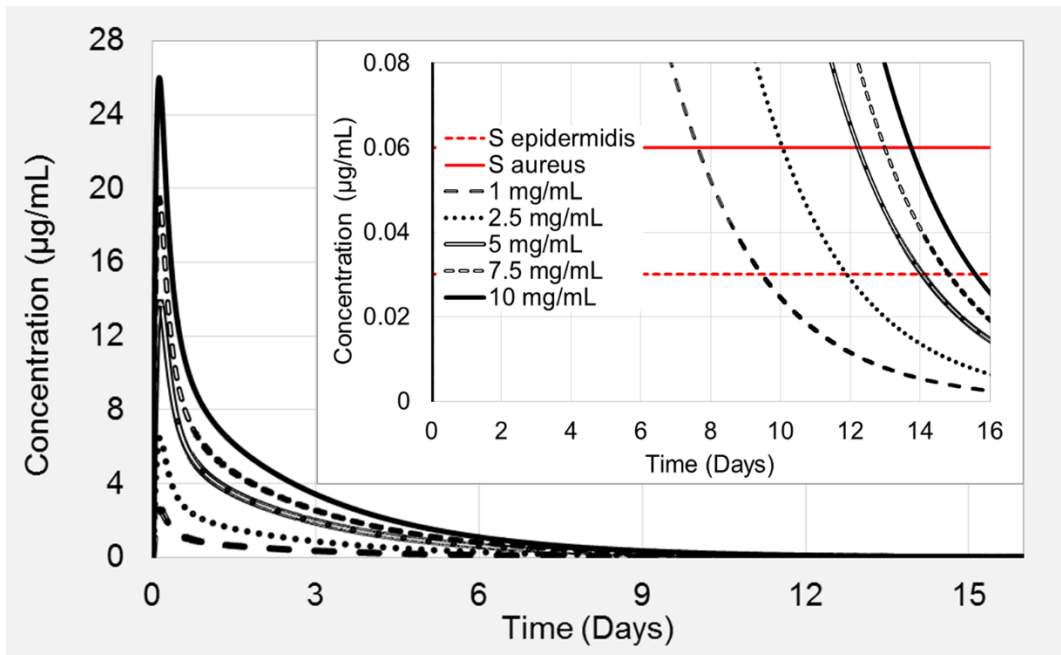
Figure 6.13 - Prediction of moxifloxacin concentration in the aqueous humor released from 26Y IOLs loaded with different concentration solutions, and representative bacteria MICs.

6.4 Conclusions

In the present chapter, a mathematical model for estimation of drug concentration in the aqueous humor was developed. This model can work either as a complementary tool to experimental drug release evaluation studies or to design and prepare drug eluting lenses for a given prophylaxis. With partition and effective diffusivity data collected from sink release experiments it was possible to predict *in vivo* concentration profiles in agreement to results obtained with moxifloxacin eluting IOLs implanted in rabbits. After validation of the model, it was possible to demonstrate how the different inputs considered on the model impact the concentration profile in the aqueous humor.

The work herein presented shows the potential of this model, by comparing the expected *in vivo* performance of two different commercially available materials as antibiotic and anti-inflammatory delivery platforms.

The drug release from the silicone hydrogel occurs very quickly, with consequent short effective concentration duration. Whereas, the hydrophilic acrylic presents promising results, especially with moxifloxacin and diclofenac, with *in vivo* simulations pointing to the possibility of this material be used as platform of effective release during at least two weeks.

6.5 References

1. Kinnear, F.B. and C.M. Kirkness, *Advances in rapid laboratory diagnosis of infectious endophthalmitis.* J Hosp Infect, 1995. **30**: p. 253-61.
2. Schwartz, S.G. and H.W. Flynn, Jr., *Update on the prevention and treatment of endophthalmitis.* Expert Rev Ophthalmol, 2014. **9**(5): p. 425-430.
3. Tranos, P., et al., *Current Perspectives of Prophylaxis and Management of Acute Infective Endophthalmitis.* Adv Ther, 2016. **33**(5): p. 727-46.
4. Kessel, L., et al., *Post-cataract Prevention of Inflammation and Macular Edema by Steroid and Nonsteroidal Anti-inflammatory Eye Drops: A Systematic Review.* Ophthalmology, 2014. **121**(10): p. 1915-1924.
5. Arora, T., et al., *Substitute of Animals in Drug Research: An Approach Towards Fulfillment of 4R's.* Indian Journal of Pharmaceutical Sciences, 2011. **73**(1): p. 1-6.
6. Kleinmann, G., et al., *Hydrophilic acrylic intraocular lens as a drug-delivery system for fourth-generation fluoroquinolones.* J Cataract Refract Surg, 2006. **32**(10): p. 1717-21.
7. Barraquer, R.I., et al., *Human Lens Capsule Thickness as a Function of Age and Location along the Sagittal Lens Perimeter.* Investigative Ophthalmology & Visual Science, 2006. **47**(5): p. 2053-2060.
8. Danysh, B.P. and M.K. Duncan, *The Lens Capsule.* Experimental Eye Research, 2009. **88**(2): p. 151-164.
9. Kastner, C., et al., *Permeability of the Anterior Lens Capsule for Large Molecules and Small Drugs.* Current Eye Research, 2013. **38**(10): p. 1057-1063.
10. del Amo, E.M. and A. Urtti, *Rabbit as an animal model for intravitreal pharmacokinetics: Clinical predictability and quality of the published data.* Experimental Eye Research, 2015. **137**: p. 111-124.
11. Cholkar, K., et al., *1 - Eye: anatomy, physiology and barriers to drug delivery*, in *Ocular Transporters and Receptors*. 2013, Woodhead Publishing. p. 1-36.
12. Cunha-Vaz, J.G. and D.M. Maurice, *The active transport of fluorescein by the retinal vessels and the retina.* J Physiol, 1967. **191**(3): p. 467-86.
13. Davis, B.K., *Diffusion of polymer gel implants.* Proc Natl Acad Sci U S A, 1974. **71**(8): p. 3120-3.
14. Alvarez, L.J., A.C. Zamudio, and O.A. Candia, *Sildenafil stimulates aqueous humor turnover in rabbits.* Exp Eye Res, 2013. **111**: p. 67-70.
15. Toris, C.B., G.L. Zhan, and M.A. McLaughlin, *Effects of brinzolamide on aqueous humor dynamics in monkeys and rabbits.* J Ocul Pharmacol Ther, 2003. **19**(5): p. 397-404.
16. Prausnitz, M.R. and J.S. Noonan, *Permeability of cornea, sclera, and conjunctiva: a literature analysis for drug delivery to the eye.* J Pharm Sci, 1998. **87**(12): p. 1479-88.
17. Robertson, S.M., et al., *Ocular Pharmacokinetics of Moxifloxacin After Topical Treatment of Animals and Humans.* Survey of Ophthalmology, 2005. **50**(6): p. S32-S45.
18. Liu, Z., et al., *Effects of Transcutol P on the corneal permeability of drugs and evaluation of its ocular irritation of rabbit eyes.* J Pharm Pharmacol, 2006. **58**(1): p. 45-50.

19. Valls, R., et al., *Transcorneal Permeation in a Corneal Device of Non-Steroidal Anti-Inflammatory Drugs in Drug Delivery Systems.* The Open Medicinal Chemistry Journal, 2008. **2**: p. 66-71.

20. Fathalla, Z.M., et al., *Formulation and corneal permeation of ketorolac tromethamine-loaded chitosan nanoparticles.* Drug Dev Ind Pharm, 2016. **42**(4): p. 514-24.

21. Koskela, T. and R.F. Brubaker, *The nocturnal suppression of aqueous humor flow in humans is not blocked by bright light.* Invest Ophthalmol Vis Sci, 1991. **32**(9): p. 2504-6.

22. Reiss, G.R., et al., *Aqueous humor flow during sleep.* Invest Ophthalmol Vis Sci, 1984. **25**(6): p. 776-8.

23. Callegan, M.C., et al., *Bacterial endophthalmitis: epidemiology, therapeutics, and bacterium-host interactions.* Clin Microbiol Rev, 2002. **15**(1): p. 111-24.

24. Durand, M.L., *Endophthalmitis.* Clin Microbiol Infect, 2013. **19**(3): p. 227-34.

25. Thore, M., et al., *Drug-resistant coagulase-negative skin staphylococci. Evaluation of four marker systems and epidemiology in an orthopaedic ward.* Epidemiology and Infection, 1990. **105**(1): p. 95-105.

26. Fitzpatrick, F.A., *Cyclooxygenase enzymes: regulation and function.* Curr Pharm Des, 2004. **10**(6): p. 577-88.

27. Ricciotti, E. and G.A. FitzGerald, *Prostaglandins and Inflammation.* Arteriosclerosis, thrombosis, and vascular biology, 2011. **31**(5): p. 986-1000.

28. Odenholt, I. and O. Cars, *Pharmacodynamics of moxifloxacin and levofloxacin against Streptococcus pneumoniae, Staphylococcus aureus, Klebsiella pneumoniae and Escherichia coli: simulation of human plasma concentrations after intravenous dosage in an in vitro kinetic model.* J Antimicrob Chemother, 2006. **58**(5): p. 960-5.

29. Lister, P.D., *Pharmacodynamics of moxifloxacin and levofloxacin against Staphylococcus aureus and Staphylococcus epidermidis in an in vitro pharmacodynamic model.* Clin Infect Dis, 2001. **15**(32): p. S33-8.

30. Reddy, R. and S.J. Kim, *Critical appraisal of ophthalmic ketorolac in treatment of pain and inflammation following cataract surgery.* Clinical Ophthalmology (Auckland, N.Z.), 2011. **5**: p. 751-758.

31. Barry, P., et al., *ESCRS study of prophylaxis of postoperative endophthalmitis after cataract surgery: Preliminary report of principal results from a European multicenter study.* J Cataract Refract Surg, 2006. **32**(3): p. 407-10.

7 Antibiotic and nonsteroidal anti-inflammatory simultaneous release for post-cataract endophthalmitis and cystoid macular edema prevention

Table of Contents

7.1 Introduction

In the previous chapter, different commercial materials were tested as antibiotic and anti-inflammatory drug delivery vehicles to the anterior chamber of the eye. Individual loading of the drugs was tested, but, since usually a combination of antibiotic and nonsteroidal anti-inflammatory drugs (NSAIDs) is prescribed after cataract removal surgery [1, 2], we decided to investigate the simultaneous release of both as an approach for endophthalmitis and macular edema prevention. Most part of the experiments here reported were performed at the University of Florida in Gainesville, USA, under the supervision of Professor Anuj Chauhan.

Drug dual/simultaneous release from hydrogels has been address in the last years for the most different applications. In a report published by Cheng and co-workers, doxorubicin and cisplatin, two chemotherapy drugs, were loaded into a dual delivery system, designed to be an *in situ* forming hydrogel for intratumoral treatment [3]. Murata and co-workers designed hydrogels that covalently contained polymeric micelles that possessed different drug release properties, and successfully exhibit independent release behaviors of two compounds, rhodamine B and auramine O [4]. In the field of ocular drug delivery through contact or intraocular lens, Hsu and co-workers loaded commercially available contact lenses containing vitamin E with two drugs for glaucoma treatment, timolol and dorzolamide, and successfully increased the release duration [5]. A similar approach was followed by Rad and Mohajeri that studied the simultaneous loading and release of ciprofloxacin and betamethasone from vitamin E loaded silicone-based soft contact lenses [6]. White and co-workers engineered via molecular imprinting strategies silicone hydrogel contact lenses to simultaneously release up to four template molecules including hydropropyl methylcellulose, trehalose, ibuprofen, and prednisolone [7]. To the best of our knowledge, intraocular lenses, either commercially available or lab-made, were not explored as platforms for multiple drug release.

Postoperative endophthalmitis (POE) may manifests itself through patient complaints of decreased vision, pain, redness, and eyelid edema after cataract removal surgery [8, 9]. Studies report that in an acute phase, endophthalmitis could occur up to 13 days after surgery [10, 11]. Increasing evidence supports the use of antibiotics to reduce the bacterial

load, and risk of endophthalmitis. Survey data from 2014 of the American Society for Cataract and Refractive Surgery members found that 85% of the respondents used topical antibiotic prophylaxis preoperatively, and 97% of the respondents postoperatively [12]. Moreover, 83% of the respondents of the survey said that they would use intracameral antibiotics if an approved product were available.

Although a controversial topic, published studies suggest benefits to early visual recovery of topical application of NSAIDs, and also in the decrease of likelihood of postoperative cystoid macular edema (CME). In a randomized clinical trial, 42 patients were given diclofenac eye drops after cataract extraction and 46, placebo. Eye drops were administered from 3 days before surgery until 3 months after, in a four drops per day regime. Results showed that patients that applied diclofenac eye drops presented reduced ocular inflammation and the occurrence of angiographic CME after cataract surgery [13]. Kessel and co-workers performed a systematic literature search in four databases to identify randomized trials published from 1996 till 2014 comparing topical steroids with topical NSAIDs in controlling inflammation and preventing CME in patients undergoing cataract extraction. They found low to moderate evidence that topical NSAIDs are more effective in controlling postoperative inflammation after cataract surgery [14].

The purpose of this work is to investigate the dual release of an antibiotic and a NSAID from IOL materials, to prevent POE and CME. We chose moxifloxacin and diclofenac, as they presented the most promising results in Chapter 6, and also because they are well studied for prevention of POE and CME. Aiming the optimization of the drug release behavior, we investigate different home-made hydrogels and select the most promising, from individual drug release experiments, to be used as platform for simultaneous release. The *in vivo* efficacy of the released drugs was predicted using the model presented in Chapter 6.

7.2 Experimental Part

7.2.1 Materials

2-Hydroxyethyl methacrylate (HEMA), ethylene glycol dimethacrylate (EGDMA), 2,2'-azobis(2-methylpropionitrile) (AIBN), methyl methacrylate (MMA), phosphate saline buffer

(PBS, pH 7.4) were purchase from Sigma-Aldrich (USA). Moxifloxacin hydrochloride (MFX) and diclofenac sodium salt (DCF) were purchase from Carbosynth Limited (UK).

7.2.2 Hydrogels preparation

HEMA_MMA hydrogels were prepared with two different HEMA:MMA ratios (80:20 and 90:10 %v/v). A HEMA hydrogel was also prepared with 20 wt% DI water. Three different contents of cross-linker were used for all the hydrogels (0.5, 2.5 and 5 wt% EGDMA). Hydrogels are from this point referred by their corresponding monomer volume in the precursor polymer solution (HEMA80_MMA20, HEMA90_MMA10, and HEMA100). To prepare the hydrogels HEMA and MMA or HEMA and water were mixed with the cross-linker and bubbled with a gentle stream of nitrogen (30 minutes) before addition of AIBN (initiator) to a final concentration of 25 mM. After complete dissolution of the initiator the solution was injected into a mold consisting of two glass plates separated by a 0.254 mm Teflon spacer. The polymerization reaction was performed at 60ºC for 24 hours. The obtained hydrogel sheets were washed over 5 days with DD water to remove unreacted monomers. The hydrated samples (thickness 0.254 mm) were cut with a leaker of diameter 1.5 cm and finally dried (dried masses ranged from 35 to 50 mg).

For the dual drug loading/release, HEMA90_MMA10 2.5 wt% CL hydrogel was produced following the description in section, with a thickness approximated to that of the IOLs (0.5 mm). Samples were cut with 1 cm of diameter, and had weight values within the range 40-42 mg.

7.2.3 Water and PBS content and swelling capacity

Determination of the swelling capacity and water and PBS content after equilibrium is achieved was performed by placing dried samples of each composition (in triplicates) in 10 mL of water or PBS at room temperature. Several weight measurements were done until equilibrium was obtained. Swelling capacity, SC, was estimated as the relative weight gain during the hydration:

$$SC = \frac{W_\infty - W_o}{W_o}$$
                                                                    Equation 7.1

Where W_o is the weight of the dry sample and W_∞ is the sample weight at equilibrium. Total absorption capacity (TAC) of water or PBS was determined as:

$$TAC = \frac{W_\infty - W_o}{W_\infty}$$

Equation 7.2

7.2.4 Drug loading procedure

Individual drug loading of the hydrogels was achieved through soaking in drug solutions in PBS for 7 days at room temperature with concentrations of 5 mg.mL^{-1} for MFX and 1 mg.mL^{-1} for DCF. Dual loading was done sequentially, in a first step DCF (5 mg.mL^{-1}) was loaded through soaking for 6 days, and in a second step MFX (5 mg.mL^{-1}) loading was performed either for 3, 7 or 10 days. After the loading period, the hydrogel samples gently immersed in deionized water and blotted, to remove residual drug solution from the samples surface.

7.2.5 *In vitro* drug release experiments

Drug release (*n*=3) was performed in 15 mL of PBS at room temperature and under mild shaking. At predetermined times drug concentration was measured in a Thermo Scientific™ GENESYS™ 10S UV-Vis spectrophotometer (USA), in the range 190 – 320 nm or in an UV–VIS MultiscanGO from ThermoScientific® spectrophotometer in the range 200 – 400 nm. The partition (*K*) and effective diffusivity (*D*$_e$) coefficients were attained as described in section 6.2.6.

7.3 Results and Discussion

7.3.1 Water and PBS content and swelling capacity

In Figure 7.1, results for total absorption capacity and swelling capacity for water, and PBS, for the three monomer compositions, and three contents of crosslinking (CL) herein studied are shown. Dependence on mixing ratio of the hydrophilic (HEMA) and hydrophobic (MMA) monomer, and amount of added cross-linker was observed. Decrease of both TAC and SC as consequence of increased MMA content or increased amount of cross-linker was obtained. For HEMA100 hydrogels linear dependence of

cross-linker wt% was observed within the studied range (0.5 to 5 wt%). For HEMA_MMA hydrogels a non-linear dependence was found. Results suggest that when more MMA is present in the hydrogel, TAC and SC become independent of the cross-linker amount, from a certain wt% up. In fact, HEMA80_MMA20 hydrogels with 2.5 and 5 wt% of cross-linker show similar TAC and SC. Further combination of monomer mixing ratio, and amount of added cross-linker should be explored to confirm this tendency. In general, higher values of TAC and SC are observed when in presence of water when compare to those values in PBS.
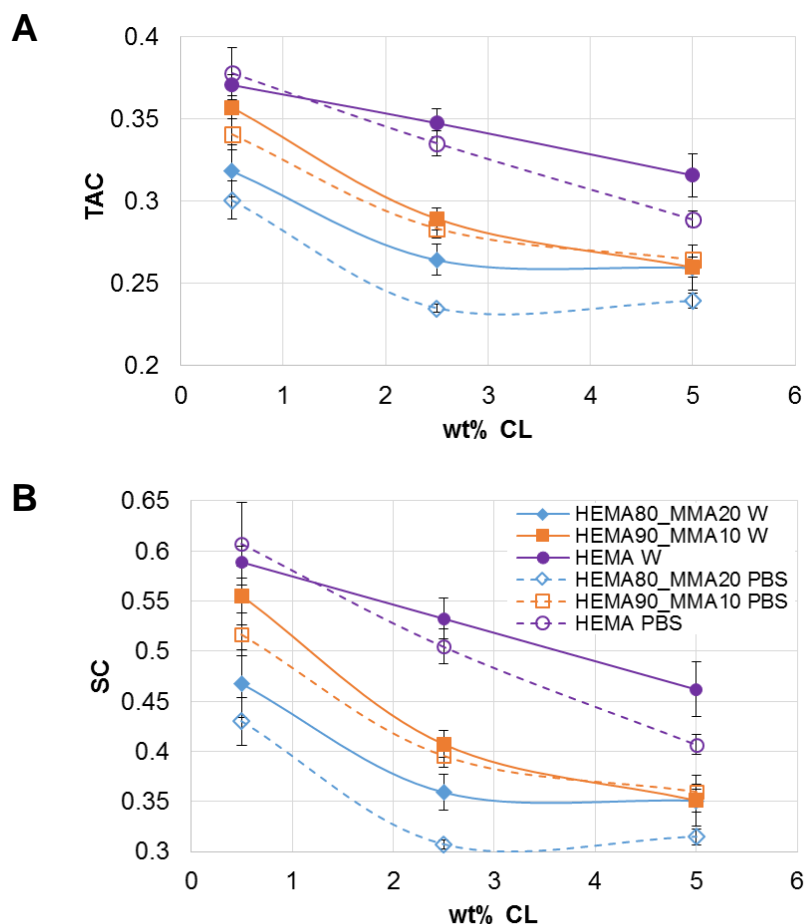

Figure 7.1 – A) Total absorption capacity (TAC) and B) swelling capacity of water (full symbols) or PBS (hallow symbols) of HEMA80_MMA20 (◇), HEMA90_MMA10 (□) and HEMA100 (○) in function of cross-linker (CL) content.

7.3.2 Individual drug release

The partition and effective diffusivity values of MFX and DCF in the hydrogels are presented in Table 7.1. Partition and effective diffusivity values were obtained through Equation 6.1 and experimental data fitting as described in section 6.2.3, respectively.

Table 7.1 – MFX and DCF partition (K) and effective diffusivity (D_e) coefficients.

	wt% CL	Moxifloxacin		Diclofenac	
		K	D_e ($\times 10^{-14}$ m^{2}s^{-1})	K	D_e ($\times 10^{-14}$ m^{2}s^{-1})
HEMA80_MMA20	0.5	3.41 ± 0.04	8.1 ± 0.43	28.76 ± 1.82	10.9 ± 0.12
	2.5	1.70 ± 0.08	4.26 ± 0.06	18.96 ± 1.61	3.49 ± 0.08
	5	1.259 ± 0.003	4.48 ± 0.88	13.95 ± 2.65	3.90 ± 2.06
HEMA90_MMA10	0.5	12.23 ± 0.48	14.2 ± 0.14	25.01 ± 0.48	28.9 ± 0.40
	2.5	9.70 ± 1.78	4.88 ± 0.31	27.26 ± 1.48	10.4 ± 0.40
	5	4.64 ± 0.22	3.62 ± 0.15	19.68 ± 2.30	5.27 ± 0.41
HEMA100	0.5	14.71 ± 0.92	16.7 ± 0.23	25.68 ± 2.47	31.2 ± 0.47
	2.5	10.71 ± 0.32	8.83 ± 1.4	24.26 ± 1.48	22.2 ± 0.15
	5	9.03 ± 1.30	2.96 ± 0.23	17.87 ± 0.25	11.1 ± 0.39

In Figure 7.2 and Figure 7.3 fraction cumulative mass release of MFX and DCF, respectively, are plotted, for all the nine hydrogels herein produced. Model fitting for D_e determination are also presented.

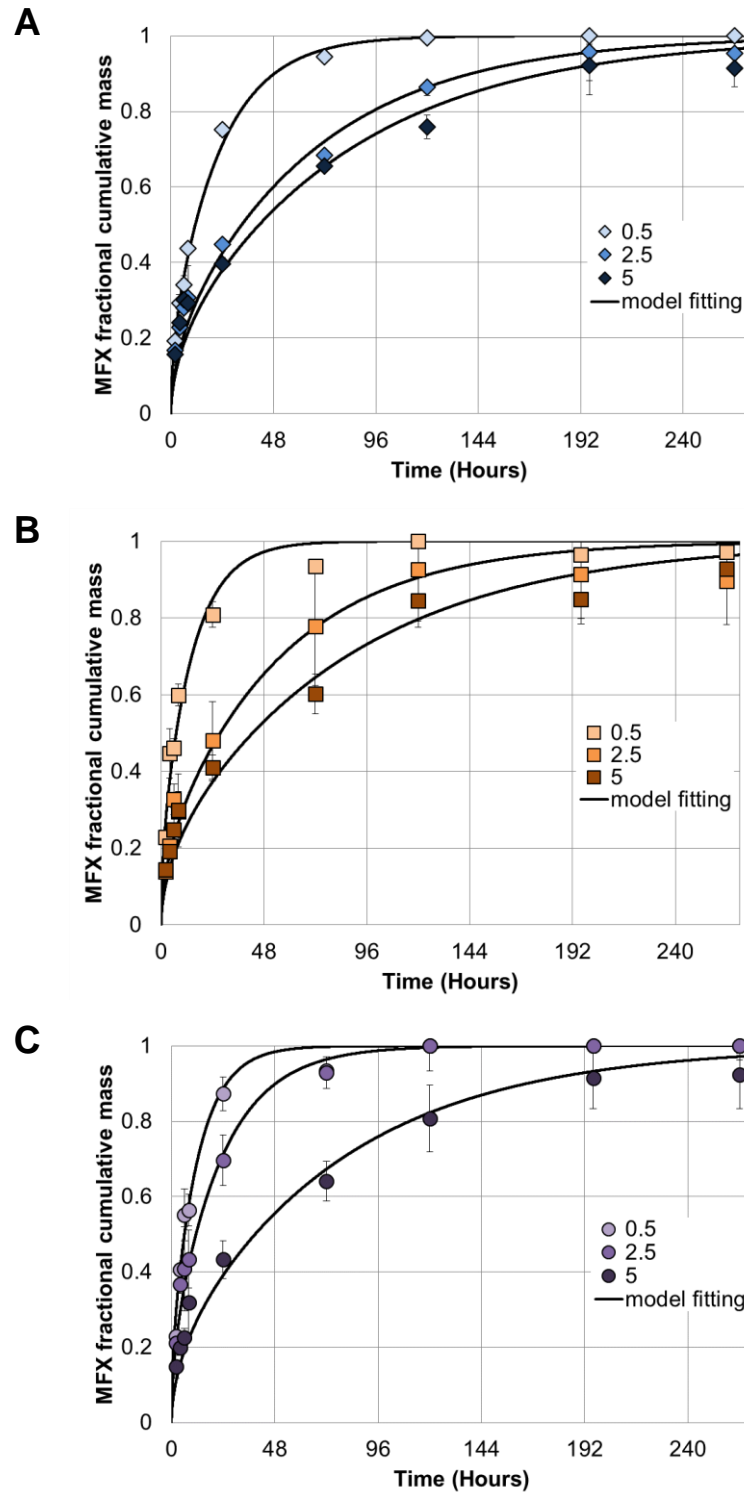**Figure 7.2 – Moxifloxacin fractional cumulative release from A) HEMA80_MMA20 (◇), B) HEMA90_MMA10 (□) and C) HEMA100 (○) with different cross-linker wt% (0.5, 2.5 and 5%).**
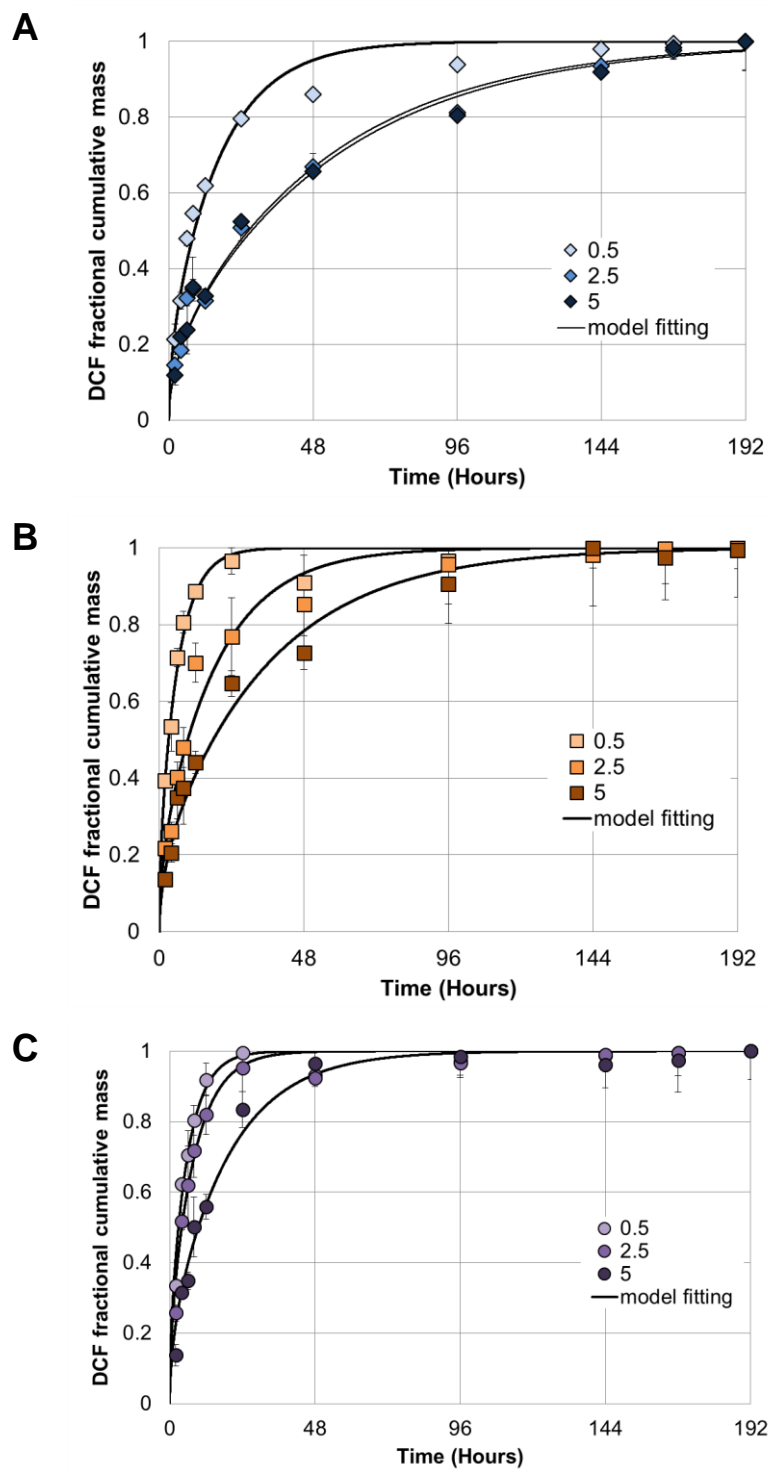
Figure 7.3 – Diclofenac fractional cumulative release from A) HEMA80_MMA20 (◇), B) HEMA90_MMA10 (□) and C) HEMA100 (○) with different cross-linker wt% (0.5, 2.5 and 5%).

As expected, both MFX and DCF release kinetics are affected by the different hydrogel compositions. Partition of moxifloxacin to the hydrogels decreases with increased hydrophobic monomer content, and with increased wt% CL, whereas for diclofenac this relations do not occur for all cases. Dependence of D_e follows the same tendency as TAC or SC (see Figure 7.1 and Figure 7.4), with decrease of D_e as consequence of increased MMA content or increased amount of cross-linker, which could indicate that the aqueous phase plays a decisive role on the mechanism of transport. In general, with increased amount of added cross-linker (CL), lower values of D_e are observed, with smaller D_e values for DCF when compare to those of MFX in the same material, except for the HEMA80_MMA20 when D_e for both drugs present similar values (see Figure 7.4). Since a detailed characterization of the hydrogel-drug interactions, such as in Chapter 2, was not the main focus of this work, no further studies were conducted, and no further conclusions can be drawn.
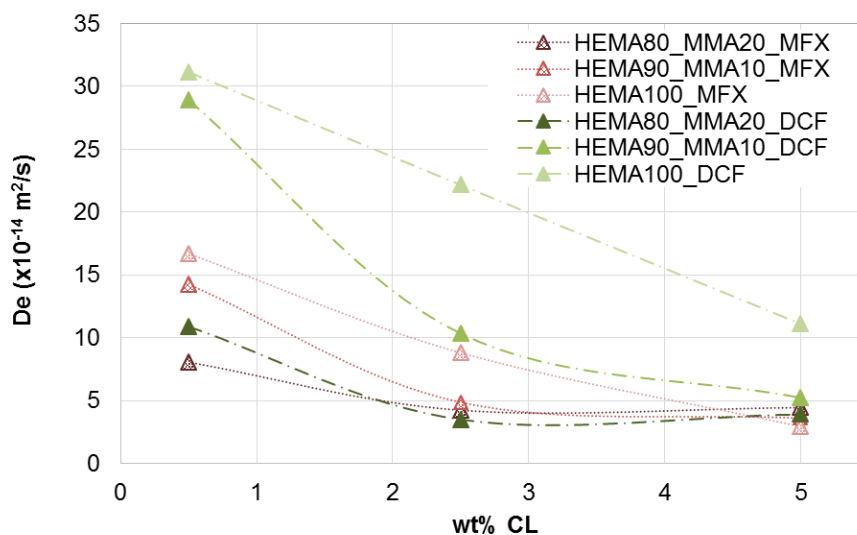
Figure 7.4 – Dependence of D_e on the amount of added cross-linker (CL).

7.3.2.1 Concentration predictions with *in vivo* model

The *in vivo* model described in Chapter 6 was used to predict the *in vivo* efficacy of IOLs (6 mm of diameter and 0.6 mm of height) made from these nine hydrogels, loaded with MFX or DCF. 15 days of loading in 5 mg.mL^{-1} solutions of either MFX or DCF were considered for simulations, since for a 0.6 mm, longer time periods are necessary to attain

equilibrium with loading solutions. As in the previous chapter, specific corneal permeability of MFX or DCF, and an aqueous volume of 0.25 mL and turnover rate of 1%/min were used for simulations.

Results from simulation are presented for MFX and DCF in Figure 7.5 and Figure 7.6, respectively. Following the same reasoning as in Chapter 6, minimum inhibitory concentration (MIC) of MFX against susceptible *Staphylococcus aureus* and *Staphylococcus epidermidis* [15], and DCF half maximal inhibitory concentration (IC$_{50}$) values for the inhibition of the cyclooxygenase (COX) enzyme and the consequential reduction in prostaglandin synthesis [16] were considered to obtain information about the *in vivo* efficacy potential of our hydrogels. Simulation results suggest that for all studied hydrogel compositions, concentration of release MFX from an IOL manufactured with these hydrogels will remain above reference MIC values up to 18 days (see Figure 7.5 B).
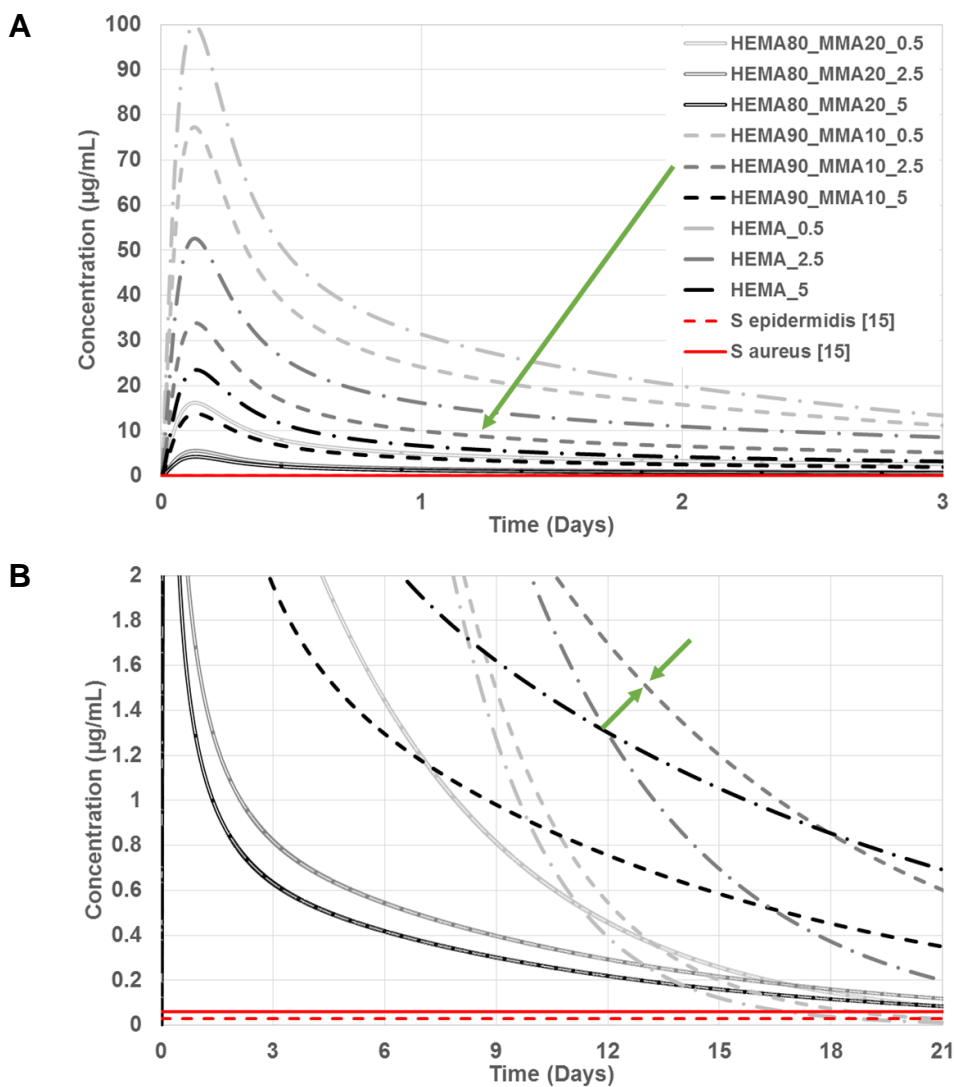
Figure 7.5 - Prediction of moxifloxacin concentration in the aqueous humor released from our hydrogels, and representative bacteria MICs. The release profiles are represented in A and B using different scales for clarity reasons.

Considering the maximum IC_{50} assumed in this work (0.302 µg.mL^{-1}) for DCF, five hydrogel compositions are predicted to release enough DCF to remain above this concentration value up to 3 weeks (see Figure 7.6).
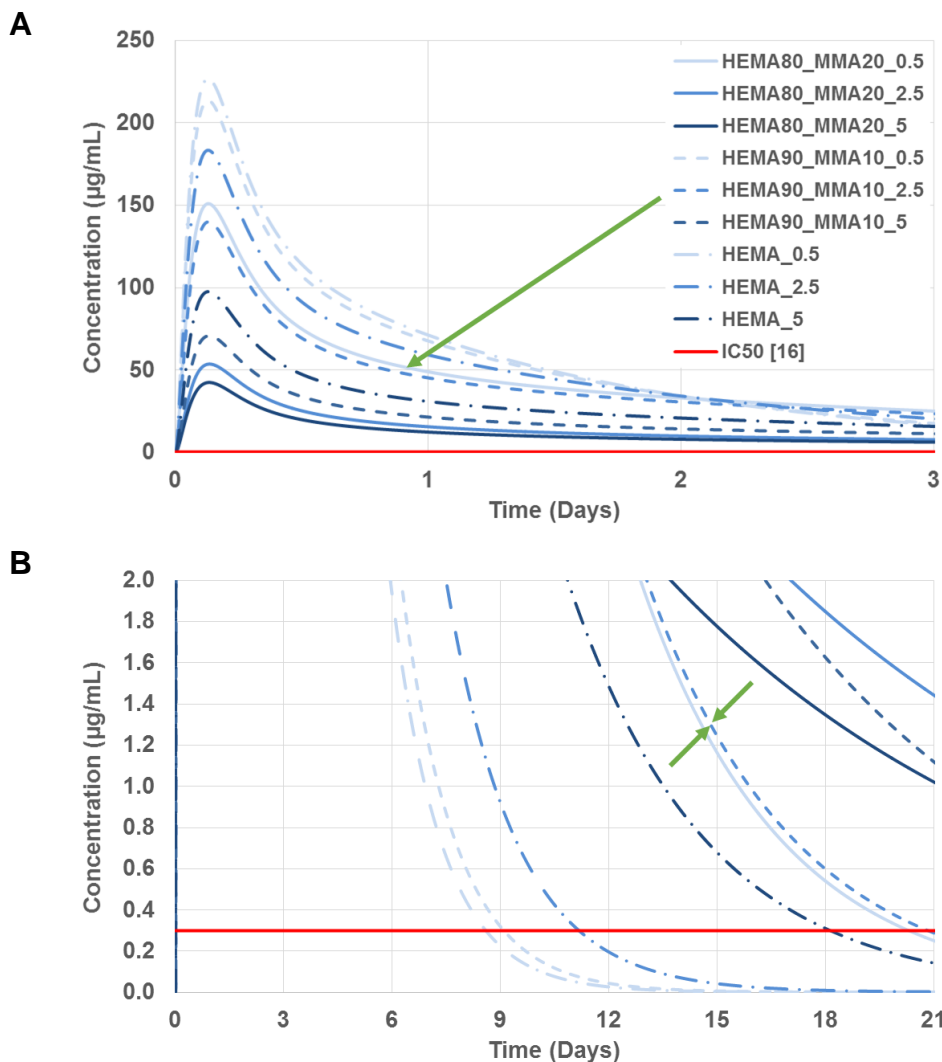
Figure 7.6 - Prediction of diclofenac concentration in the aqueous humor released from our hydrogels, and range between maximum and minimum reported IC$_{50}$ (shaded region). The release profiles are represented in A and B using different scales for clarity reasons.

With the results from individual MFX and DCF release, and the *in vivo* concentration predictions, we chose the HEMA90_MMA10 2.5 wt% CL (indicated in Figure 7.5 and Figure 7.6) as the composition to further study as platform for dual release of MFX and DCF. This was one of the compositions that release both MFX and DCF for 3 weeks above the considered MIC and IC$_{50}$ values.

7.3.3 Simultaneous drug release

Since preliminary tests suggested low solubility of DCF when in presence of MFX in a PBS solution, we decided to follow a sequential loading strategy. Hence, loading through soaking of HEMA90_MMA10 2.5 wt% CL hydrogel samples with DCF was performed first for 6 days. After this period, the hydrogel samples were loaded in MFX solution either for 3, 7 or 10 days (see Table 7.2).

Table 7.2 – Diclofenac and moxifloxacin sequential loading protocol.

Sample	Diclofenac		Moxifloxacin
#1	6 days	➜	3 days
#2	6 days	➜	7 days
#3	6 days	➜	10 days

In Figure 7.7, photographs of hydrogel samples after loading of DCF and MFX, or only MFX are shown. Visible precipitation of drug molecules occurs inside the hydrogels during MFX loading, for samples already loaded with DCF. Visible yellow coloration (characteristic of MFX powder, and solution) of the hydrogels samples occurs after loading with MFX, with a more intense visible yellow color for the 10 days MFX loaded samples, suggesting that higher amount of MFX is present in these samples. When the dual drug loaded samples were placed in fresh PBS for the release experiments, visible transparency was regain after approximately 30 minutes on all samples, indicating that the precipitated drug is solubilized after this period.
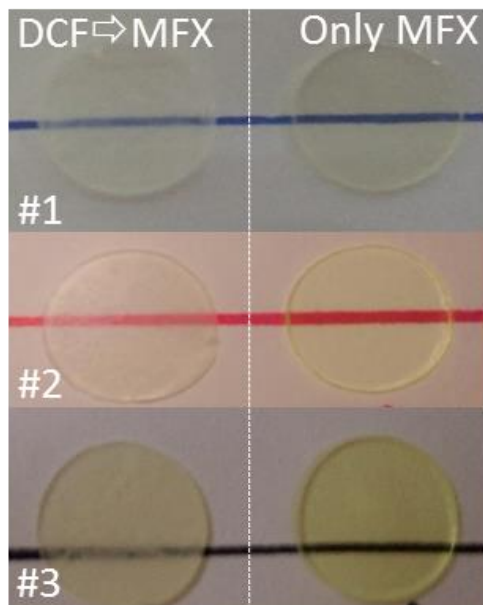
Figure 7.7 – Hydrogels after DCF loading and 3, 7 or 10 days of MFX loading (left side), and after only 3, 7 or 10 days of MFX loading (right side).

Drug release experiments were performed, and quantification of the released drugs was done following the reasoning reported by Kim and Chauhan [17], where the individual drug concentration can be determined by applying the least square fit method.

Release profiles of DCF, and MFX are plotted in Figure 7.8. In Table 7.3 partition and effective diffusivity coefficients of the drugs released simultaneously are presented, and compared to those obtained for individual release from the same hydrogel (HEMA90_MMA10 2.5 wt% CL, Table 7.1).

The total mass of DCF released (see Figure 7.8 A) is independent of the loading period of MFX. Whereas, the total mass of MFX release is dependent on the loading time period: more mass of MFX was released for the longer loading samples. We hypothesize that DCF precipitates inside the lens. DCF release attains a plateau equilibrium after approximately 400 hours (16 days) of release, for the three loading sequential conditions (Figure 7.8 A). While for MFX, a plateau equilibrium difficult to identified, by the 600th hour of release (25 days) it appears to be achieved for all the conditions. When directly compared to the individual DCF and MFX released from HEMA90_MMA10 2.5 wt% CL (Figure 7.2 B and Figure 7.3 B), dual release presents longer time duration. It must be

stressed that the samples sequentially loaded presented double thickness that of the individually loaded, to approximate to the real IOL thickness.
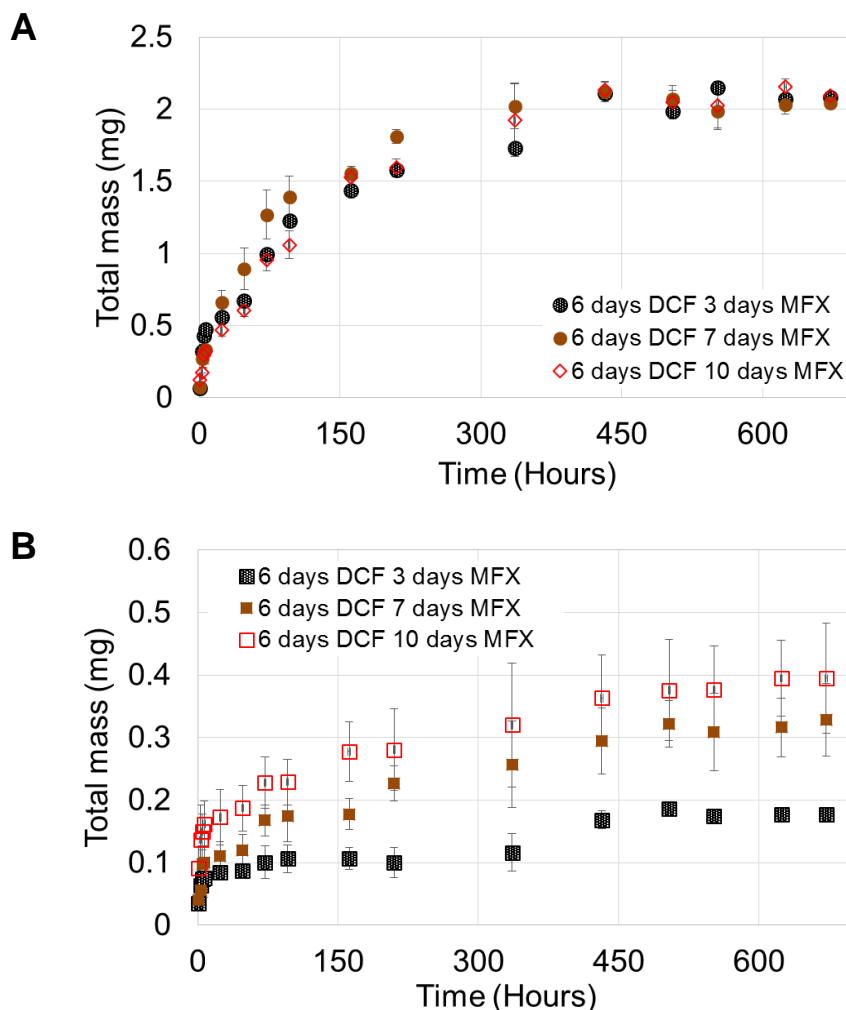
Figure 7.8 – A) Diclofenac and B) moxifloxacin total cumulative mass release from dual loaded HEMA90_MMA10 2.5 wt% CL samples.

Partition coefficient values of DCF for the three sequential loading conditions are similar between themselves, and inferior to that in the individual loading, what could be expected since 6 days are insufficient to attain equilibrium during loading (data obtained through simulation of the loading process, not shown). This DCF loading time was chose as such, since, if as we hypothesize, precipitated molecules are DCF molecules, higher values of DCF inside the hydrogel could compromise MFX loading, afterwards. As for MFX partition values, they slightly increase with MFX loading time increasing, suggesting that, even if already loaded DCF impacts the efficiency of MFX loading, it is still possible to increase

the amount of MFX inside the hydrogel, by extending the loading time period. Effective diffusivity values of DCF are reduced in the dual loaded samples, when compared to the individual loaded, which could be related to drug-drug interactions inside the gel. MFX effective diffusivity does not present such meaningfully variation between the studied conditions.

Table 7.3 – MFX and DCF partition (K) and effective diffusivity (D_e) coefficients from dual loaded HEMA90_MMA10 2.5 wt% CL samples: individual and dual release.

		Moxifloxacin	
		K	D_e $(\times 10^{-14}\ m^2 s^{-1})$
Individual release		9.70 ± 1.78	4.88 ± 0.31
Simultaneous release	#1	1.05 ± 0.06	3.89 ± 1.57
	#2	1.86 ± 0.23	3.75 ± 0.59
	#3	2.19 ± 0.5	5.37 ± 1.28

		Diclofenac	
		K	D_e $(\times 10^{-14}\ m^2 s^{-1})$
Individual release		27.26 ± 1.48	10.4 ± 0.40
Simultaneous release	#1	16.82 ± 0.50	4.31 ± 1.82
	#2	17.55 ± 0.76	7.04 ± 1.12
	#3	17.45 ± 1.55	4.03 ± 0.14

7.3.3.1 Concentration predictions with *in vivo* model

Analogously to the simulations done in section 7.3.2.1, *in vivo* concentration predictions were obtained to estimate the efficacy of dual loaded IOLs made from the hydrogel. Model assumptions were kept, but, since the model does not predict the simultaneous release of two different species, individual loading, and release was simulated for each of the drugs using the parameters in Table 7.3.

In Figure 7.9 simulation results are plotted. Considering the MIC values of MFX for the reference bacteria (*S. aureus* 0.06 µg.mL^{-1} and *S. epidermidis* 0.03 µg.mL^{-1}), and IC$_{50}$ range for DCF (0.038 to 0.302 µg.mL^{-1}), it is possible to estimate the efficacy of our dual drug releasing IOLs. MFX concentrations, for the first loading condition (Figure 7.9 A)

concentration remain above the highest considered MIC of 0.06 µg.mL^{-1} until the 11th day of release. For the second, and third conditions of loading (Figure 7.9 B and C) MFX concentrations are expected to remain above 0.06 µg.mL^{-1} for at least 3 weeks. For the three loading conditions, DCF concentration remains more than 3 weeks always above the maximum value in the IC$_{50}$ range (0.302 µg.mL^{-1}).

Maximum expected concentrations during the initial burst are approximately 70 µg.mL^{-1} for DCF and 8 µg.mL^{-1} for MFX. A report published by Lee and co-workers show that a DCF commercial eye drops formulation (Ofenac®) presented toxic effects against human corneal epithelial cells, which were proportional to the drug concentration and to the exposure time. They report significant differences on cell cytotoxicity between 12 and 24 hours exposure to 20 or 100 µg.mL^{-1}, with no significant toxic effect for the lower DCF concentration [18]. In our case studies, we observe that an expected DCF *in vivo* concentration above 20 µg.mL^{-1} could occur for periods of time of 12 to 24 hours. Nonetheless, Lee *et al* results were obtained with a commercial formulation that contains preservatives, which are associate to toxic effects, particularly in long-term treatments, for the ocular surface [19, 20]. To further infer about the possible toxic effect of DCF released from our preservative free IOL *in vitro* cytotoxicity studies should be conducted. MFX burst concentration is small when compare to the concentration of antibiotic delivered through the use of intracameral antibiotic injection during the surgical procedure [21]. Hence, a toxic effect it is not expected and, in fact, a complementary intracameral antibiotic injection should still be applied to reduce the initial bacterial load present in the eye, since a 8 µg.mL^{-1} concentration value is not projected to be sufficient.
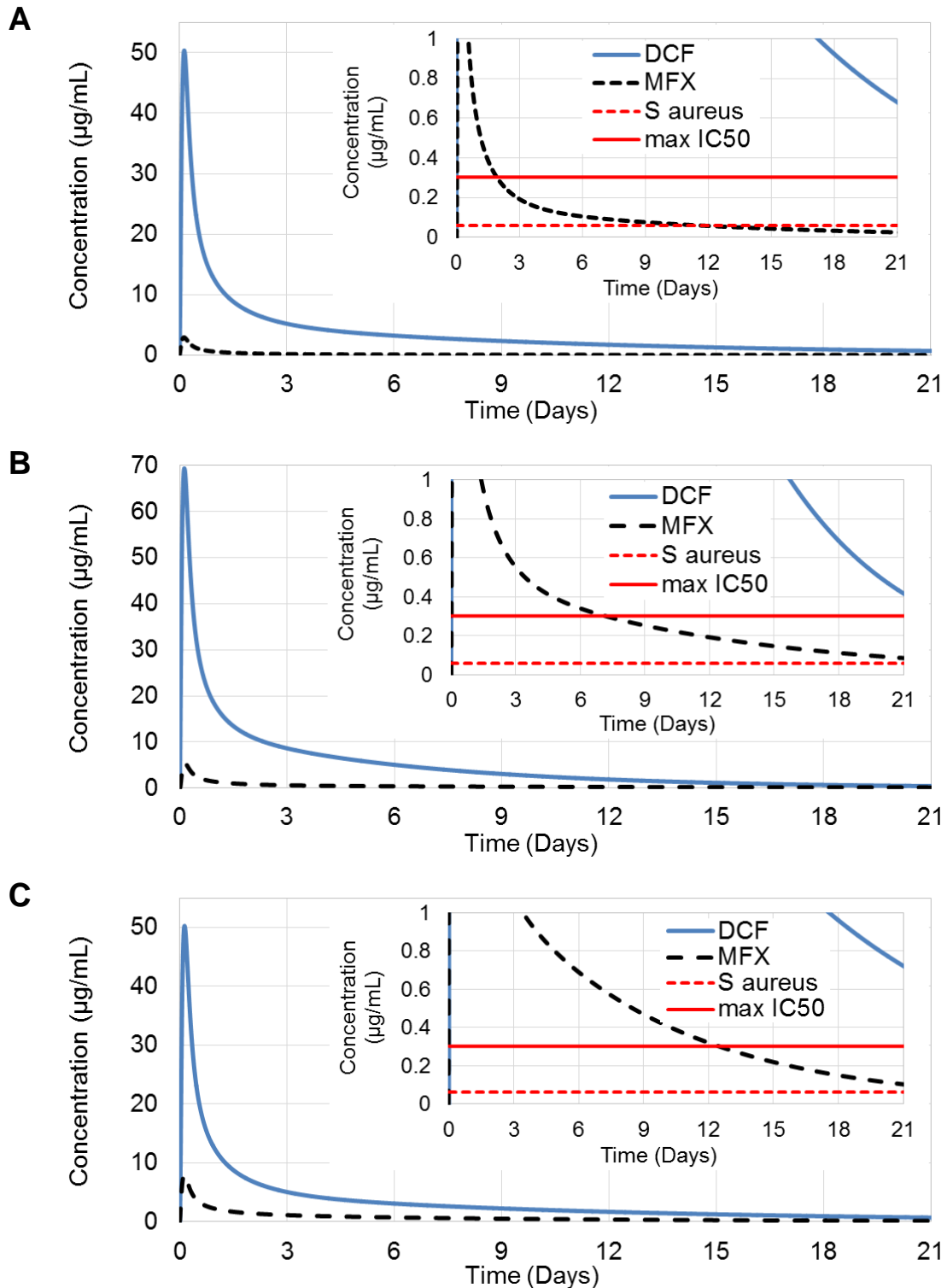
Figure 7.9 - Prediction of DCF and MFX concentration in the aqueous humor released from dual loaded HEMA90_MMA10 2.5 wt% CL for different loading conditions. A) #1, B) #2, and C) #3 (see Table 7.2).

7.4 Conclusions

A system that could simultaneously deliver effective doses of antibiotic, for prevention of post-cataract removal acute endophthalmitis, and an anti-inflammatory over a long period of time, is viewed as an added value for postoperative cataract removal prophylaxis [22]. In the present Chapter, we designed a hydrogel and a dual loading strategy for the delivery of MFX and DCF to meet the described features.

Different hydrogel compositions were produced, and, through individual loading/release of both moxifloxacin and diclofenac, release kinetics were evaluated. The *in vivo* model presented in this thesis was used to screen the prospective efficacy of the hydrogels, and the most promising composition was used as platform for dual drug release.

Our results show that an IOL manufactured with the proper hydrophilic/hydrophobic monomer ratio and amount of cross linker loaded with an antibiotic and an anti-inflammatory, following a sequential drug loading strategy, could be an effective controlled drug delivery system for postoperative cataract surgery removal prophylaxis. Moreover, as showed in the present Chapter and in Chapter 6, it is possible to tailor the loading conditions (e.g. time, concentration) to obtain an *in vivo* concentration profile that meet the desired therapeutic recommendations.

7.5 References

1. Thomas, R. and R. Melton. *Clinical Guide to Ophthalmic Drugs.* [cited 2017 August]; Available from: https://www.reviewofoptometry.com/CMSDocuments/2016/5/dg0516i.pdf.

2. McCulley, J.P., *Fluoroquinolones and postoperative endophthalmitis*: J Cataract Refract Surg. 2009 Feb;35(2):206;.

3. Cheng, C., et al., *Development of a dual drug-loaded hydrogel delivery system for enhanced cancer therapy: in situ formation, degradation and synergistic antitumor efficiency.* Journal of Materials Chemistry B, 2017. **5**(43): p. 8487-8497.

4. Murata, M., et al., *Dual drug release from hydrogels covalently containing polymeric micelles that possess different drug release properties.* Colloids Surf B Biointerfaces, 2017. **153**: p. 19-26.

5. Hsu, K.-H., et al., *Dual drug delivery from vitamin E loaded contact lenses for glaucoma therapy.* European Journal of Pharmaceutics and Biopharmaceutics, 2015. **94**: p. 312-321.

6. Rad, M.S. and S.A. Mohajeri, *Simultaneously Load and Extended Release of Betamethasone and Ciprofloxacin from Vitamin E-Loaded Silicone-Based Soft Contact Lenses.* Curr Eye Res, 2016. **41**(9): p. 1185-91.

7. White, C.J., S.A. DiPasquale, and M.E. Byrne, *Controlled Release of Multiple Therapeutics from Silicone Hydrogel Contact Lenses.* Optometry and vision science : official publication of the American Academy of Optometry, 2016. **93**(4): p. 377-386.

8. Kernt, M. and A. Kampik, *Endophthalmitis: Pathogenesis, clinical presentation, management, and perspectives.* Clinical Ophthalmology (Auckland, N.Z.), 2010. **4**: p. 121-135.

9. Lemley, C.A. and D.P. Han, *Endophthalmitis: a review of current evaluation and management.* Retina, 2007. **27**(6): p. 662-80.

10. Lalwani, G.A., et al., *Acute-onset endophthalmitis after clear corneal cataract surgery (1996-2005). Clinical features, causative organisms, and visual acuity outcomes.* Ophthalmology, 2008. **115**(3): p. 473-6.

11. Miller, J.J., et al., *Acute-onset Endophthalmitis After Cataract Surgery (2000–2004): Incidence, Clinical Settings, and Visual Acuity Outcomes After Treatment.* American Journal of Ophthalmology, 2005. **139**(6): p. 983-987.

12. Chang, D.F., et al., *Antibiotic prophylaxis of postoperative endophthalmitis after cataract surgery: Results of the 2014 ASCRS member survey.* J Cataract Refract Surg, 2015. **41**(6): p. 1300-5.

13. Rossetti, L., et al., *Effectiveness of diclofenac eyedrops in reducing inflammation and the incidence of cystoid macular edema after cataract surgery.* Journal of Cataract & Refractive Surgery, 1996. **22**: p. 794-799.

14. Kessel, L., et al., *Post-cataract Prevention of Inflammation and Macular Edema by Steroid and Nonsteroidal Anti-inflammatory Eye Drops: A Systematic Review.* Ophthalmology, 2014. **121**(10): p. 1915-1924.

15. Lister, P.D., *Pharmacodynamics of moxifloxacin and levofloxacin against Staphylococcus aureus and Staphylococcus epidermidis in an in vitro pharmacodynamic model.* Clin Infect Dis, 2001. **15**(32): p. S33-8.

16. Reddy, R. and S.J. Kim, *Critical appraisal of ophthalmic ketorolac in treatment of pain and inflammation following cataract surgery.* Clinical Ophthalmology (Auckland, N.Z.), 2011. **5**: p. 751-758.

17. Kim, J. and A. Chauhan, *Dexamethasone transport and ocular delivery from poly(hydroxyethyl methacrylate) gels.* Int J Pharm, 2008. **353**(1-2): p. 205-22.

18. Lee, J.S., Y.H. Kim, and Y.M. Park, *The Toxicity of Nonsteroidal Anti-inflammatory Eye Drops against Human Corneal Epithelial Cells in Vitro.* J Korean Med Sci, 2015. **30**(12): p. 1856-64.

19. Baudouin, C., et al., *Preservatives in eyedrops: the good, the bad and the ugly.* Prog Retin Eye Res, 2010. **29**(4): p. 312-34.

20. Vaede, D., et al., *[Preservatives in eye drops: toward awareness of their toxicity].* J Fr Ophtalmol, 2010. **33**(7): p. 505-24.

21. Barry, P., et al., *ESCRS study of prophylaxis of postoperative endophthalmitis after cataract surgery: Preliminary report of principal results from a European multicenter study.* J Cataract Refract Surg, 2006. **32**(3): p. 407-10.

22. Stephenson, M. *New Alternatives in Post-Cataract Pharmacology.* 2016 [cited 2017 14 November]; Available from: https://www.reviewofophthalmology.com/article/new-alternatives-in-postcataract-pharmacology-feb16.

8 Conclusions and future work

Table of Contents

8.1 Conclusions

The general aim of this thesis was to contribute to the development of alternative ocular drug delivery systems as substitute and/or complement for the conventionally used eye drops based on contact and intraocular lenses. A comprehensive knowledge of the eye disorder to be treated or prevented, of the materials and drugs to be used, and of the eye biological and hydrodynamic environment is fundamental for the achievement of a tailored ocular drug delivery system. In this thesis, attention was given to all these aspects, and it was conclusively shown that hydrogels used to produce the lens present the potential to be used as extended ophthalmic drug delivery systems. For intelligibility reasons, the main conclusions will be divided by chapters.

In Chapter 2, the equilibrium partitioning and the diffusion coefficients of several ophthalmic drugs, namely, chlorhexidine, levofloxacin and diclofenac in two hydrogel materials for contact lenses, a PHEMA based hydrogel (HEMA/PVP) and a silicone based hydrogel (TRIS/NVP/HEMA), were measured. The experimental results suggest the existence of specific adsorption and/or attractive electrostatic interactions between the drugs and the polymeric chains. Comparison between the measured effective diffusion coefficients, D_e, with the diffusion coefficients, D, of the same solutes non-adsorbed on the hydrogel chains was done. We concluded that the diffusion coefficients for the nonadsorbing solutes are 2 to 3 orders of magnitude greater than the corresponding effective diffusion coefficients, D_e. Thus, it was demonstrated that the three studied drugs adsorb on the polymeric strands of both hydrogels, independently of its charge or hydrophilicity. The intrinsic properties of both the drug molecules and the polymer influence the release behavior of the system. The design of an optimized controlled release system should start by the understating of these interactions and their impact on the mechanisms of drug release for each particular pair drug/hydrogel.

In Chapter 3, a microfluidic cell was designed to simulate the hydrodynamic conditions of the eye tear fluid, namely the low volume and its continuous renovation, during the *in vitro* drug release experiments. The release of a non-steroid anti-inflammatory commonly used in ocular therapy (diclofenac) from a conventional contact lens HEMA/PVP hydrogel was investigated. The drug release profiles obtained in static conditions and with the

microfluidic cell were compared. The release rate of the drug from the studied hydrogel decreased under flow, suggesting that common static drug release experiments should be providing underestimated release time durations. The eye *in vivo* conditions, here *in vitro* approximated, may not be sufficient to ensure a sink condition that is usually assumed for in-lab static experiments. Hence, a more reliable prediction of the *in vivo* efficacy shall be found with *in vitro* drug release experiments approximated to the hydrodynamic conditions of the eye.

In Chapter 4, a commercially available hydrophilic acrylic intraocular lenses material was explored as a vehicle to deliver an antibiotic (moxifloxacin) to the eye during the recommended endophthalmitis prophylaxis period after the cataract removal surgery. It was found that the surface modification of the material through argon plasma-assisted grafting copolymerization of AMPS (2-acrylamido-2-methylpropane sulfonic acid) in presence of the drug improved the release profile of moxifloxacin (in total released amount and release time) both in static and in hydrodynamic conditions. An electrostatic interaction between the predominant positive electrical charge of moxifloxacin and the negatively ionized AMPS during the coating formation step can confer high affinity for drug molecules during the loading step, therefore increasing the amount of drug loaded by the modified lens. Under hydrodynamic conditions, moxifloxacin was released at effective concentrations against *Staphylococcus aureus* and *Staphylococcus epidermidis* for 12 days. Characterization of the modified samples showed that the coatings did not affect significantly the relevant properties of the lenses.

In Chapter 5, a multi-layered lens approach was explored to minimize the initial burst of the drug released and to achieve a constant target release rate over an adequate time interval. Two drugs, levofloxacin and chlorhexidine, and a PHEMA based hydrogel (HEMA/PVP) hydrogel were used for experimental data collection. The diffusivity of the drug in the material and an interfacial resistance parameter were obtained by fitting a mathematical model to experimental release data. The drug release behavior dependence on different system parameters, namely of the drug diffusion coefficient, the layers thicknesses and the interfacial transport resistance between the layers, was simulated mathematically. It was shown that the initial burst may be minimized, and near zero-order

186

release conditions may be achieved by properly selecting the relative dimensions and characteristics of the multi-layered lens.

In Chapter 6, a mathematical model for estimation of *in vivo* drug concentration in the aqueous humor was developed to be used as a complementary tool to drug release evaluation experimental studies. After validation of the model with reported *in vivo* studies, its potential to predict the efficacy of drug loaded intraocular lens was demonstrated. Data were obtained for four different drugs (moxifloxacin, levofloxacin, diclofenac and ketorolac) released from two commercially available materials (a silicone hydrogel and a hydrophilic acrylic), using only the drugs partition and diffusion coefficients obtained from experiments carried out in static conditions.

In Chapter 7, different HEMA based hydrogel compositions, with variable hydrophobic MMA and cross linker amounts, were produced, and tested as moxifloxacin and diclofenac individual release platforms. The most promising composition (HEMA:MMA 90:10, 2.5 wt% cross linker) then was sequentially loaded with diclofenac and moxifloxacin. The mathematical model presented in Chapter 6 was applied to the simultaneous release of diclofenac and moxifloxacin to predict the effectiveness in the eye. The results suggest that an IOL manufactured with the proper hydrophilic/hydrophobic monomer ratio and amount of cross linker, and loaded with an antibiotic and an anti-inflammatory could be an effective controlled drug delivery system for cataract removal surgery postoperative prophylaxis.

8.2 Future work

This work has revealed some insights for future developments on alternative ocular drug delivery systems based on ophthalmic lenses to substitute and/or complement the conventionally used eye drops. Nonetheless, further future perspectives of work may be suggested, namely:

▪ characterization of other drug/material pairs regarding the partition and effective diffusivity coefficients, and evaluation of their potential *in vivo* with the model presented in Chapter 6;

- additional chemical/physical characterization of the material chose as the most promising in Chapter 7 and cytotoxicity evaluation;

- study of other multi-drug release platforms, with new intra-ocular lenses materials and also contact lenses materials;

- further drug loading strategies investigation, especially for hydrophobic acrylic materials, since they are widely used for intra-ocular lenses manufacturing and loading through soaking does not seems feasible;

- evaluation of the effect of post-production steps (eg. packaging, sterilization, etc.) on the drug eluting ophthalmic lenses herein developed;

- optimization of the intra-ocular lenses microfluidic cell, taking into account the vitreous chamber, since currently it only considerers the aqueous humor volume and renovation;

- *ex vivo* investigation of different drug molecules permeability to the cornea and the vitreous, possibly using a Franz diffusion cell equipment;

- *in vivo* tests for further understanding of the drug eluting ophthalmic lenses behavior and performance, since the eye is a complex system and difficult to reproduced with *in vitro* conditions, aiming their efficacy and safety characterization;

- *scale up* designing of the manufacturing process to develop a commercial product with the best drug-eluting ophthalmic lens systems.